

Diploma Thesis
in the subject of Physics

**Nonequilibrium Phase Transition
in a System with Complex
Dynamics**

submitted by
Andreas Dienst

Supervisor:

Prof. Dr. Rudolf Friedrich

Institute of Theoretical Physics
University of Münster
Münster, Germany

September 2007

Münster, September 2007

I, ANDREAS DIENST, student of Physics at the University of Münster, student ID no. 306473, solemnly declare that I have prepared this thesis independently. Not any other aids than those referred to in this thesis have been employed. This work has not been previously submitted to any other examination board.

ANDREAS DIENST

Contents

Title Page	i
Declaration	iii
Table of Contents	iv
List of Figures	vi
Acknowledgement	viii
Dedication	ix
1 Introduction	1
2 Magnetohydrodynamic Dynamos and the ABCDE Model	4
2.1 Experimental Realizations of Magnetic Dynamo Action	5
2.2 The Lorenz Equations	6
2.3 The ABCDE Model	8
3 Dynamical Systems and Differential Equations	11
3.1 Basics of Dynamical Systems Theory	12
3.2 Linear Homogeneous Differential Equations	14
3.2.1 Equations Exhibiting Periodic Coefficients	15
3.2.2 Equations Exhibiting Real Bounded Coefficients	16
4 Numerical Observation of the Phase Transition	17
4.1 The Characteristic Exponent Λ	18
4.2 Time Series of the Variable r	19
4.3 Phase Space Projections and Moments of the Variable r	20
5 Stability Analysis of Equilibria	23
5.1 Linearization of Dynamical Systems and Stability of Equilibria	24
5.2 Fixed Points of the ABCDE System	25
5.3 Linear Stability Analysis of Stationary Solutions to the ABCDE System	26

5.3.1	Fixed Point No. 1 (\mathbf{X}_1^0)	26
5.3.2	Fixed Points No. 2 and 3 ($\mathbf{X}_2^0, \mathbf{X}_3^0$)	27
5.3.3	Fixed Points No. 4 and 5 ($\mathbf{X}_4^0, \mathbf{X}_5^0$)	28
6	Lyapunov Characteristic Exponents	29
6.1	An Example and the Expected Behavior	30
6.2	Definition and Calculation of Lyapunov Characteristic Exponents	31
6.3	Lyapunov Exponent Spectra of the ABCDE Model	34
6.3.1	Spectrum for the Chaotic Regime	35
6.3.2	Spectrum in Case of Limit Cycles	37
6.3.3	Spectrum for the Chaotic Regime with Respect to Periodic Orbits	41
6.4	Another Approach to Determine the Characteristic Exponent	45
7	Stochastic Treatment of the Transition	48
7.1	Brief Introduction into Stochastic Calculus	49
7.1.1	The Langevin and the Fokker-Planck Equation	50
7.2	Numerical Results of the Stochastic Model	51
7.2.1	Determination of Drift Coefficients	52
7.2.2	Determination of Diffusion Coefficients	53
7.2.3	Discussion of Stochastic Force \mathbf{F}	54
7.2.4	Reconstruction of Variable \mathbf{b} in Terms of Langevin Process	57
8	Conclusion	60
	Bibliography	63
A	Description of Hénon Trick	67
B	Autocorrelation Functions	68
C	Probability Density Estimates	69
D	Stochastic Reconstructions	70

List of Figures

1.1	Qualitative illustration of a bifurcation	2
4.1	Characteristic exponent Λ as function of the control parameter value ϵ	18
4.2	Time series of variable r for different values of ϵ	19
4.3	Projections of attractor onto the Lorenz subspace	21
4.4	Projections of attractor onto the b_1 - b_2 plane	22
4.5	Moments $\langle r \rangle$ and $\langle r^2 \rangle$ in dependence of ϵ	22
5.1	Eigenvalues of the linearized system at fixed point No. 1	27
5.2	Eigenvalues of the linearized system at fixed points No. 2 and 3	27
5.3	Eigenvalues of the linearized system at fixed points No. 4 and 5	28
6.1	Potential of sliding ball in vase	30
6.2	Exemplary exponent Ω as a function of the control parameter	31
6.3	Lyapunov characteristic exponents for the chaotic regime in dependence of ϵ	36
6.4	Phase space projections of limit cycles	37
6.5	Phase space projections indicating the destruction of a limit cycle	38
6.7	Hysteresis of the variable $\langle r \rangle$	38
6.6	Lyapunov characteristic exponents in dependence of ϵ in case of a limit cycle	39
6.8	Construction of solution for \mathbf{b} by means of Floquet's theory (No. 1)	40
6.9	Sketch of the Lorenz mask	41
6.10	Critical Lyapunov exponent with respect to periodic orbits as function of ϵ	42
6.11	Phase space portraits of trajectories associated with periodic orbits	43
6.12	Construction of solution for \mathbf{b} by means of Floquet's theory (No. 2)	44
6.13	Characteristic exponent Λ as function of ϵ (alternative approach)	46
6.14	Local positivity of characteristic exponent Λ	47
7.1	Projection of attractor onto b_1 - b_2 plane together with superimposed grid	52
7.2	Vector field of drift coefficients in the b_1 - b_2 plane	53
7.3	Vector field of drift coefficients in the r - ϕ plane	53
7.4	Eigenvectors and corresponding eigenvalues of the diffusion matrices	54
7.5	Autocorrelation function of the stochastic force \mathbf{F}	56
7.6	Probability density estimates of the stochastic force \mathbf{F}	57

7.7	Reconstruction of deterministic variable \mathbf{b} by stochastic process	58
7.8	Probability density estimates of r and ϕ for $\epsilon = 4.5$	59
7.9	Probability density estimates of r and ϕ for $\epsilon = 2.5$	59

Acknowledgement

I am indebted to Professor R. Friedrich for supporting my studies and providing very intensive and friendly supervision. Many aspects of this thesis are based on work that initially developed out of some of his suggestions.

It goes without saying that I extend my gratitude to the whole working group at the Institute of Theoretical Physics. In particular, I would like to thank M. Tassler, S. Eule and O. Kamps for many helpful discussions and critically reading my manuscript.

I am much obliged for the friendship of K. Ruschmeier, B. Wielens and, in particular, Y.H. Li during my studies in Münster.

Finally, I can only fall short in expressing my deep gratitude towards my parents for their overwhelming support and encouragement.

DEDICATED TO MY PARENTS

Chapter 1

Introduction

Nonlinear dynamical systems play an increasingly important role in various areas of the classical natural sciences as well as in engineering and technology. Systems of this class are, for instance, used to model flows around airplanes or submarines as well as vibrations of mechanical structures as studied in the field of engineering, currents in electrical networks examined in the subject of electronics, and blood flow in the heart as well as neuron activity observed in biology. In the fields of physics, the areas of application range from the description of climate related phenomena over tracer diffusion in flow systems to the modeling of population dynamics in terms of predator-prey interactions. All these systems depend on various parameters, which can partially be controlled or monitored. A practical problem of main importance in studying these models is to predict the critical values of parameters, at which considerable qualitative changes of the dynamical behavior occur. These changes are often denoted as bifurcations. For instance, a long-outstanding physical problem is to predict a description of the transition from laminar to turbulent flows. Similarly, a vibrating structure can bifurcate from quasiperiodic dynamics to chaotic motion, the latter being practically unpredictable and potentially leading to the breakdown of the structure.

Chaotic systems are characterized by deterministic dynamics which are extremely sensitive to initial conditions. Thus, chaotic systems appear to evolve randomly on a large time scale, attributable to the exponential growth of uncertainties concerning the initial conditions. However, deterministic chaos does not include stochastic elements and is uniquely defined in terms of the initial configuration, whereas nonlinearity is one of the main features and criteria for the occurrence of chaotic motion. In the study of chaotic properties of complex dynamical systems, Lyapunov characteristic exponents are of particular interest, being essentially related to the exponential divergence of nearby orbits in the course of time.

Thus far, we have not explicitly mentioned that a system under investigation might be subject to external or internal fluctuations. It has emerged that fluctuations represent an integral feature of real natural systems and play a decisive role in processes, which are close to a critical bifurcation. In this regard, one particular distinguishes between regimes exhibiting either an equilibrium or nonequilibrium state. Fluctuations in systems far away from equilibrium turn the

challenging objective of bifurcations into the even more complex, and thus increasingly sophisticated problem of nonequilibrium phase transitions. There are numerous examples of systems in equilibrium and nonequilibrium states exhibiting transitions between phases of characteristic spatial and spatio-temporal configurations. Observations of physical and chemical systems display transitions between gas, fluid and solid phases of matter. Further prominent examples include turning points in laser between the generation of ordinary and coherent laser light as the supplied energy is changed, or transitions in ferromagnets, giving rise to either vanishing or finite persistent magnetization. In case of the investigation of dynamical systems which are subject to deterministic fluctuations, it is a widely accepted approach to identify a suitable model in terms of a stochastic description. In this context, heavily fluctuating chaotic forces are sometimes treated as stochastic perturbation, coupled to slowly evolving deterministic degrees of freedom. Implementing a suitable stochastic approach for a deterministic system, it is often possible to gain a deeper understanding of the underlying transport processes.

In the further treatment of the subject, we will denote transitions between different characteristic spatio-temporal manifestations of systems far away from equilibrium as nonequilibrium phase transitions. Relevant parameters, which can be used to monitor and control the bifurcations, are hitherto referred to as control parameters. It might be useful to introduce order parameters, denoting quantities which represent the actually changing characteristics of the system in the vicinity of the analyzed phase transition. In this regard, figure 1.1 displays a typical qualitative description of a hypothetical transition. A further useful term in the investigation of complex systems is called self-organization, indicating a process in which the internal organization of a system increases in complexity without being guided by an outside source.

In this document, we are concerned with an investigation of the ABCDE model, a low-dimensional system which was developed to study the magneto-hydrodynamic dynamo effect. Dynamo action is an instability process in which part of the mechanical energy is converted into magnetic energy by the motions of an electrically conducting fluid. This effect, observed for instance in the earth's liquid metal core, or at motions in the convective zones of stars, is believed to be the origin of the magnetic fields of planets and many astrophysical objects.

This manuscript is organized as follows. The chief objective of this thesis is a closer examination of the nonequilibrium phase transition, which can be detected for a certain critical control parameter value. To this end, chapter 2 entails a discussion of the actual model system, which provides the foundation of this work, as well as an introductory presentation of experiments aiming at the generation of dynamo action in a laboratory environment. The chapter opens

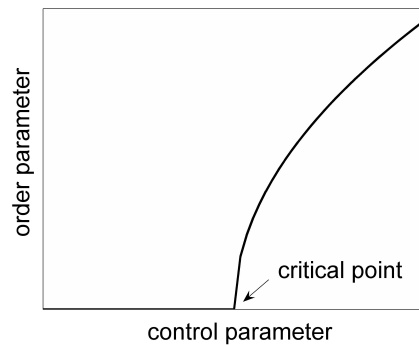


Figure 1.1: Qualitative illustration of a bifurcation (according to (Frank, 2005))

with a reflection of relevant recent publications concerning the dynamo effect. Special attention is devoted to outlining our motivation in the present research topic by presenting relevant experimental realizations of dynamo action. Furthermore, we briefly introduce the pure Lorenz equations, building an integral part of the system under examination. Subsequently, we contemplate the ABCDE model as an approach to study the magnetohydrodynamic dynamo effect by presenting the corresponding set of equations governing the convective system, and sketching the basic structure of the deviation starting with the fundamental hydromagnetic equations. Chapter 3 treats general dynamical systems and their representation by ordinary differential equations. To achieve a basic understanding of deterministic dynamics, the corresponding part opens with a section introducing some basic principles of dynamical systems theory. In the following, we present some technical aspects of ordinary differential equations with periodic and real bounded coefficients, respectively. Both special cases will become relevant in later sections of this thesis.

In the following chapter 4, we present numerical results indicating the existence of a non-equilibrium phase transition in the ABCDE model. Basic characteristics, such as phase space projections, moments of certain relevant degrees of freedom, and characteristic exponents, which govern the asymptotic dynamical behavior, are being examined for varying control parameter values. Subsequently, in chapter 5, we focus on the determination of stationary solutions and briefly introduce the concept of linear stability analysis. Thereafter, we conduct a numerical linear stability analysis of the identified equilibria. In the subsequent chapter 6, we contemplate the dynamical system's behavior by means of analyzing the spectra of Lyapunov characteristic exponents under use of various individual configurations. Firstly, the expected behavior of the critical Lyapunov exponent is deduced from a simple model equation giving rise to a pitchfork bifurcation. Subsequently, the underlying theory of Lyapunov characteristic exponents is being introduced and applied to several different system configurations, including chaotic and periodic behavior, the latter enabling us to develop a description in terms of Floquet's theory. In a final step, an alternative way to determine the dependence of the critical Lyapunov exponent on the control parameter is presented, revealing the actual nature of the observed instability. Chapter 7 reports on a stochastic treatment of the assessed transition. To this end, some aspects of stochastic calculus are briefly outlined. Using techniques of data analysis, we extract drift as well as diffusion coefficients from long time series. Afterwards, we present an approach to reconstruct the deterministic dynamics by means of a suitable stochastic Langevin process. The reliability of our ansatz is scrutinized by examining quantities such as autocorrelation and probability density functions. In a final step, we present numerical results concerning our stochastic reconstruction of the deterministic dynamics, demonstrating the credibility of the chosen approach.

Summa summarum, chapters 2-3 provide an introduction into the general objective, as well as a theoretical foundation. Chapter 4 essentially presents a reproduction of achievements foremost discussed in Ref. (Friedrich and Haken, 1992). This survey serves as a basis and provides vital incentive for further investigation. Chapters 4-8 contemplate novel results concerning the nature of the observed instability and close with a part containing concluding remarks.

Chapter 2

Magnetohydrodynamic Dynamos and the ABCDE Model

The aim of this thesis is to gain knowledge of a nonequilibrium phase transition which is observed in a model describing the magnetohydrodynamic convection of a conducting fluid relevant to the solar dynamo problem. At the center of our research activity is the so called ABCDE model, an extension of the minimal convection system (Lorenz, 1963) to three-dimensional convective motions, which was foremost presented by R.G. Kennett in Ref. (Kennett, 1976). The significance of Kennett's model becomes evident when considering the disclosure of anomalously long-lived magnetic fields, observed around many astronomical objects. One established attempt to describe this remarkable phenomena arises from dynamo theory, which is based on the idea that the motion of a conductive body in the presence of a magnetic field results in a regeneration of the ambient magnetic field. In case a conducting fluid is assumed to regenerate a present magnetic field, the theory employs magnetohydrodynamic equations to investigate the fluid motions and the resulting dynamo action. One considerable phenomena, which has been reported in experimental observations as well as in numerical studies, is the *intermittent* behavior of the magnetic field close to the onset of dynamo activity. We shall remark that we will investigate this feature in detail in later sections and clarify that a process switching abruptly from extended periods of stasis to strong intermittent bursts of large variation manifests intermittency, also often denoted as *on-off intermittency* (Platt *et al.*, 1992).

In recent years, several attempts have been carried out to numerically investigate and model magnetohydrodynamic dynamos by systematic parameter studies of the governing basic hydromagnetic equations. We would like to refer the reader to Ref. (Christensen and Glatzmaier, 1999; Ponty *et al.*, 2005) for extensive information on the numerical study of dynamo action under certain individual conditions. A related bifurcation, denoted by the authors as *blowout bifurcation*, of the underlying hydromagnetic equations at certain parameter values, has been reported in (Sweet *et al.*, 2001). Furthermore, we would like to mention the recent reference (Zhou *et al.*, 2007), presenting a study regarding on-off intermittency in a continuum system driven by the Lorenz equation. Even though the dynamical behavior of the therein examined

model equations shows similarities to the characteristics of the ABCDE system, one main attribute, i.e. the feedback of the additional degrees of freedom onto the Lorenz subsystem, which dramatically influences the system dynamics, is being neglected in the referred case.

The remarkable feature of the ABCDE model consists in the fact that it is able to account for the generation of a convective dynamo by exhibiting linearly stable periodic solutions with a non-zero magnetic field under use of certain parameter values, without assuming rotation (Kennett, 1976). Moreover, R. Friedrich and H. Haken reported intermittent temporal behavior of certain degrees of freedom close to a nonequilibrium phase transition (Friedrich and Haken, 1992). This further characteristic allows for a possible application in the study of magnetic field excitations by chaotic motion of electrically conducting fluids. Experimentalists revealed long-term changes in the level of solar magnetic activity, which shows intermittent behavior and exhibits periods of nearly vanishing magnetic activity. We mention, for instance, the Spörer (1460-1500 AC) as well as the Maunder minimum (1645-1715 AC), denoting time periods where the sun exhibited strongly reduced magnetic activity (Eddy, 1977). Furthermore, investigations of geomagnetic field reversals showed that polarity transitions are characterized by intervals of directional change and reduced field strength. Besides the reversals of the earth's magnetic dipole field, the existence of heavy dynamic fluctuations of the magnetic field strength have been revealed. The reader is referred to the review article (Bogue and Merrill, 1992) for an extensive discussion of geodynamo theory.

2.1 Experimental Realizations of Magnetic Dynamo Action

The basic principle of ordinary mechanical dynamos producing electricity and magnetic fields from mechanical motions can be denoted as one of the main accomplishments, which were achieved in the field of physics during the 19th century. However, since the motions of all constituents composing an ordinary dynamo, such as rotors and generated electric currents, are fixed and almost inflexible, the existence of astrophysical magnetic fields cannot be described by these means. Thus, experiments aiming at the production of dynamo action in laboratory environments evolved towards abolishing further geometric constraints. Experiments based upon solid rotors but unrestrained electric currents have shown to exhibit dynamo action even in case of steep mechanical motion (Loves and Wilkinson, 1963, 1968). Thereby, the dynamo consisted of two solid cylinders spinning at right angles to each other located in a block of metal. However, whereas technical dynamos compose of arrangements of well-separated conductive constructional elements, an astrophysical dynamo operates in a nearly homogeneous medium without ferromagnetic properties. Thus, the dynamo effect, i.e. the generation and regeneration of a magnetic fields by the turbulent motions of a an electrically conducting fluid, is believed to cause the magnetic fields of planets and many other astrophysical objects such as stars or even galaxies. An important achievement concerning the experimental realization of fluid dynamos was achieved in 2000 with the presentation of results from two independent experiments in Karlsruhe and Riga (Stieglitz and Müller, 2001; Gailitis *et al.*, 2000). Both experiments utilize a spiral flow to stir

liquid sodium, but differ in the geometry of the experimental setup as the Karlsruhe experiment is based on a circular "honeycomb" structure in which the liquid metal circulates in a vortex, while the Riga experiment uses a single vortex in the center that flows back through a surrounding tube which is itself embedded in a stationary fluid. In both experimental realizations of dynamo action, the generated self-sustained fields exhibited simple temporal behavior with a stationary field in Karlsruhe and an oscillatory evolution in the Riga approach. Since most of the observations of dynamo processes in nature show a more complex dynamical behavior, experimentalists undertook considerable efforts to implement flows exhibiting a higher degree of turbulence by minimizing geometric constraints. As one example, we would like to mention the Madison dynamo experiment (Nornberg *et al.*, 2006), where the authors examined how turbulence in a stainless steel sphere, filled with liquid sodium, changes the onset conditions of the dynamo activity. Instead of a smooth transition from vanishing to growing fields, as predicted by kinematic as well as mean field dynamo theory, the authors revealed that the transition is characterized by intermittent bursts of the magnetic fields. The transient excitation pinpoints the intermittent nature of a turbulent dynamo transition, whose theoretical understanding, within the framework of a related model system, builds the main objective of this thesis. Recently, the first experimental observation of dynamo field reversals, generated in a laboratory setup which is based on the turbulent flow of liquid sodium, have been reported in (Monchaux *et al.*, 2006; Berhanu *et al.*, 2007). The authors achieved dynamo action in the von Kármán sodium experiment and proved the existence of a self-generating, statistically stationary dynamo, as well as the occurrence of irregular reversals and excursions of the magnetic field. In this context, especially the Kármán sodium experiment shows a high relevancy with respect to this thesis as the geometric setup shows similarity and the experimental observations are in close agreement with the results of our theoretical investigations.

The present introduction into experimental realizations of dynamo action shall give a rough overview about this very active field of research and motivate our interest in a thorough understanding of the instability which we encounter when numerically studying the ABCDE model. As can be concluded from the above description of corresponding experiments, the investigation of instabilities leading to the onset of dynamo action provides a vital and extremely relevant research objective.

2.2 The Lorenz Equations

The Lorenz equations form a significant part of the magnetohydrodynamic model under consideration and shall therefore be introduced briefly in the present section. The Lorenz model was foremost discussed by E.N. Lorenz in 1963 as an idealized model for the description of hydrodynamic systems. Lorenz introduced the system of three coupled ordinary differential equations when studying the flow, which occurs in a bounded layer of fluid with constant depth, when applying a uniform temperature difference in Cartesian direction \mathbf{e}_z between the upper and lower surface. The fluid is assumed to be unbounded in the principal directions orthogonal to the

boundary layers, i.e., in the directions \mathbf{e}_x and \mathbf{e}_y . For a derivation of the model motivated by works of Rayleigh (1916) and based on a treatment of the hydrodynamic convection equations, i.e., the Navier Stokes equations, by Saltzman (1962), we refer the reader to the original article (Lorenz, 1963). Since its discovery, this 3-dimensional set of equations serves as a paradigm for chaotic dynamics and is still being extensively studied nowadays. For an exhaustive discussion of the system dynamics, especially under the change of various parameter values, we refer the reader in particular to Ref. (Sparrow, 1982). The nonlinear system of ordinary differential equations representing the Lorenz model reads

$$\begin{aligned}\dot{x} &= \sigma(-x + y) \\ \dot{y} &= -y + (r - z)x \\ \dot{z} &= -bz + xy \quad ,\end{aligned}\tag{2.1}$$

where the three positive parameters σ , r and b are proportional to the Prandtl number, the Rayleigh number, and some physical properties of the model setup, respectively. The dots in equation (2.1), and further on in this thesis, denote the derivative with respect to the time. The quantity x is proportional to the velocity of the convective motion of the described fluid, and y is proportional to the temperature difference between the descending and ascending currents. The variable z is proportional to the distortion of the vertical temperature gradient from linearity. Congruent signs of x and y indicate that warm fluid is rising and cold fluid is descending. A positive value of z implies that the strongest gradient occurs near the upper and lower boundary. In the following, we employ the vector notation $\mathbf{x} = (x, y, z)$, giving rise to the equivalent representation of the Lorenz equations in the form $\dot{\mathbf{x}} = \mathcal{M}\mathbf{x}$. According to the choice of the free parameters, the Lorenz equations exhibit a variety of characteristic solutions. In particular, it shall be noted that the original parameter values $\sigma = 10$, $r = 28$, and $b = 8/3$ lead to chaotic dynamics.

The Lorenz equations play a vital role in the study of the ABCDE model. However, since a further treatment of the Lorenz system would go beyond the scope of this work, we mention a few characteristics we shall need in the further treatment. a) Symmetry: The Lorenz equations exhibit the natural symmetry $(x, y, z) \rightarrow (-x, -y, z)$. Thus, non-symmetric objects, for instance periodic orbits, occur in pairs. However, this property shall not be mentioned when referring to periodic orbits in the later section 6.3.3. b) Divergence: The divergence of the flow defined by the Lorenz equations reads $\nabla \cdot \mathcal{M} = -(\sigma + b + 1)$. Hence, for positive parameter values, a volume element V_0 is being contracted exponentially fast $\sim V_0 \exp(-(\sigma + b + 1)t)$ in the course of time t . c) Equilibria: For the standard parameter values under investigation, the Lorenz system exhibits three non-stable stationary points given by $\mathbf{x}_1^0 = (0, 0, 0)$ and $\mathbf{x}_{2,3}^0 = (\pm\sqrt{b(r-1)}, \pm\sqrt{b(r-1)}, r-1)$. The flow, linearized around the equilibria, exposes one real, negative eigenvalue, and a pair of complex conjugate eigenvalues with positive real part. c) Strange Attractor: The Lorenz system gives rise to chaotic motion, employing ordinary parameter values. The limit set, which determines the chaotic dynamics, is called strange attractor (see section 3.1). Informally speaking, a strange attractor globally attracts trajectories while

locally inducing mutual exponential divergence (Argyris *et al.*, 1994). d) Lyapunov Spectrum: As will be described in detail in chapter 6, chaotic dynamics can be categorized by means of characteristic Lyapunov exponents. The Lyapunov spectrum of the Lorenz equations has been extensively studied in (Wolf *et al.*, 1984; Frøyland and Alfsen, 1984; Sandri, 1996), while we cite (Ramasubramanian and Sriram, 2000) stating $(\lambda_1, \lambda_2, \lambda_3) = (0.9051, 0.0000, -14.5718)$. e) Periodic Solutions: Under certain circumstances, the Lorenz equations give rise to periodic solutions. We mention the existence of unstable periodic orbits at standard parameter values, as well as the formation of an attracting limit cycle as the parameter r is increased.

2.3 The ABCDE Model

The relevance and topicality of the ABCDE system is given by the fact that it represents a low dimensional model which is capable of generating dynamo action without assuming rotation. Rather than replicating the derivation of the ABCDE equations from the underlying magnetohydrodynamic description in great detail, we prefer to sketch the general approach and outline some important elements of the assertion. Although our main interest is in the chaotic nature of the system's solutions, rather than in the understanding of the corresponding convective motions, we shall briefly introduce the physical background of the ABCDE model. For further information on the derivation of this particular model system, the reader is referred to Kennett's original paper (Kennett, 1976).

Central to the construction of the ABCDE model is, similar to the Lorenz system, the consideration of a layer of fluid with constant depth under the influence of a uniform temperature difference between the upper and lower surface. The most significant differences manifest in the extension of the model to three dimensional motions of an electrically conducting fluid, yielding a convective dynamo which is able to account for stable solutions with non vanishing magnetic amplitudes. The derivation is based on consideration of hydromagnetic and Boussinesq approximations of the underlying basic magnetohydrodynamic equations describing the interaction between the fluid motions and the magnetic field. Useful background information and suitable mode expansions can be reviewed in great detail in Ref. (Chandrasekhar, 1981). Thereby, the equations obtained in this manner, govern the model system by determining the velocity field, the magnetic field, the idealized linear temperature profile and the actual deviation of the temperature profile from this assumed linear form. The first two quantities are vector-valued, three dimensional quantities, while the latter two variables exhibit scalar form. At this point, it shall be mentioned that Kennett, in the subsequent deviation, only considers one component of the actually three dimensional velocity field, and two magnetic field modes of the magnetic field vector, respectively.

All quantities mentioned above are subject to a couple of boundary conditions specific for the physical system under investigation. Taking these constraints into account, a suitable ansatz for each component of the governing set of equations can be found in form of a suitable mode expansion, which, after rearranging and subsequent averaging over the surface layer, leads directly to

the primordial representation of the ABCDE model as contemplated in detail in Ref. (Kennett, 1976). The term ABCDE model stems from the original syntax denoting the five dependent system variables, as specified above, by means of the characters $\{a, b, c, d, e\}$. If one introduces new variables $\{b_1, b_2, x, y, z\}$, by simply rescaling the old coordinates via introduction of constant multiplicative coefficients, the entire set of equations determining the ABCDE model reads in the final, and for our treatment relevant form

$$\begin{aligned} \dot{b}_1 &= -\epsilon a_1 b_1 + \alpha x b_2 \\ \dot{b}_2 &= -\epsilon a_2 b_2 + \alpha x b_1 \end{aligned} \quad (2.2a)$$

$$\begin{aligned} \dot{x} &= \sigma(-x + y) - b_1 b_2 \\ \dot{y} &= -y + (r - z)x \\ \dot{z} &= -bz + xy \quad . \end{aligned} \quad (2.2b)$$

In the following, we will frequently refer to the two nonlinearly coupled subsystems given by the two sets of variables $\mathbf{b} = \{b_1, b_2\}$ and $\mathbf{x} = \{x, y, z\}$. To this end, we denote the two elementary components as \mathbf{b} variables, and \mathbf{x} variables or Lorenz subsystem, respectively. Thereby, the physical meaning of the variables constituting the Lorenz subsystem \mathbf{x} is the same as described in section 2.2 above, whereas b_1 and b_2 are associated with the amplitude of two magnetic field modes, as outlined in Ref. (Kennett, 1976).

Sometimes it turns out to be convenient to utilize the following trivial definitions: the vector $\mathbf{X} = \{b_1, b_2, x, y, z\}$ constitutes the whole set of variables, and further on the ABCDE system can be expressed by

$$\dot{\mathbf{X}} = \mathcal{F}\mathbf{X} \quad , \quad (2.3)$$

where the matrix \mathcal{F} defines the specific dynamical system according to equation (2.2). In a later section, we will investigate solutions for the \mathbf{b} subsystem assuming periodic coefficients, i.e., with the matrix $\mathcal{A}(t)$, defined by

$$\begin{aligned} \dot{\mathbf{b}} &= \mathcal{A}(t)\mathbf{b} \\ \mathcal{A}(t) &= \begin{pmatrix} -\epsilon a_1 & \alpha x(t) \\ \alpha x(t) & -\epsilon a_2 \end{pmatrix} \quad , \end{aligned} \quad (2.4)$$

satisfying the relation $\mathcal{A}(t) = \mathcal{A}(t + T)$, where T denotes the time period. Moreover, in the general case where $\mathcal{A}(t)$ exhibits chaotic dynamics, equation (2.4) clearly illustrates that we are dealing with two degrees of freedom representing magnetic field modes which are driven by the Lorenz set of equations via variable x . Though, one should bear in mind that we encounter a feedback term of the \mathbf{b} on the \mathbf{x} subsystem, as represented in equation (2.2b).

In addition, following the treatment presented in Ref. (Friedrich and Haken, 1992), under certain circumstances it has turned out to be convenient to introduce hyperbolic coordinates (Zeidler, 1996), according to the transformation

$$b_1 = r \cosh(\phi) \quad , \quad b_2 = r \sinh(\phi) \quad . \quad (2.5)$$

The motivation to introduce hyperbolic coordinates stems from the special geometric form of the chaotic attractor when projected onto the b_1 - b_2 plane. As we will contemplate in later sections, the transformation into the new variables also makes sense in terms of numerical stability and accuracy of the computations. Substituting expression (2.5) into the ABCDE model, the subsystem of equations (2.2a) assumes the shape

$$\begin{aligned} \dot{r} &= \epsilon r [-a_1 + (a_2 - a_1) \sinh^2(\phi)] \\ \dot{\phi} &= -\epsilon(a_2 - a_1) \sinh(\phi) \cosh(\phi) + \alpha x \quad . \end{aligned} \quad (2.6)$$

Due to the structure of equations (2.6), it is possible to directly obtain the subsystem's characteristic exponent, as will be discussed in section 4.1. Moreover, it shall be noted that the substitution leads to a formal decoupling of the dependent variables; while b_1 and b_2 in (2.2a) both depend on x , as well as the complementary variable b_2 or b_1 , respectively, ϕ is independent of r , and entirely determined by the evolution of x .

In analogy to the section focussing on the Lorenz equations, we shall make some general statements concerning basic properties of the ABCDE model which will become relevant in the further treatment. a) Symmetry: It is to be noted that due to symmetry properties of equation (2.2), if $\tilde{\mathbf{X}} = (\tilde{b}_1, \tilde{b}_2, \tilde{x}, \tilde{y}, \tilde{z})$ represents a solution, then $\tilde{\mathbf{X}} = (-\tilde{b}_1, -\tilde{b}_2, \tilde{x}, \tilde{y}, \tilde{z})$, $\tilde{\mathbf{X}} = (\tilde{b}_1, -\tilde{b}_2, -\tilde{x}, -\tilde{y}, \tilde{z})$ and $\tilde{\mathbf{X}} = (-\tilde{b}_1, \tilde{b}_2, -\tilde{x}, -\tilde{y}, \tilde{z})$ are also solutions. Thus, any solution of this class might be defined in terms of only one particular solution. In this thesis, we restrict ourselves as a matter of principle to the case where $b_1 > 0$. b) Divergence: The divergence of the flow defined by the ABCDE model reads $\nabla \cdot \mathcal{F} = -(\epsilon(a_1 + a_2) + \sigma + b + 1) = \Sigma(\epsilon)$. For strictly positive parameter values, a volume element V_0 is being contracted exponentially $\sim V_0 \exp(-(\epsilon(a_1 + a_2) + \sigma + b + 1)t)$ in the course of time t . Hence, the ABCDE model ranks among the class of dissipative systems. c) Equilibria: Stationary solutions of the ABCDE model and a linear stability analysis of the fixed points will be discussed in detail in chapter 5. d) Lyapunov Exponents: An extensive study of the spectrum of Lyapunov characteristic exponents is presented in chapter 6. e) Coupling of Subsystems: The response of the \mathbf{b} variables to the Lorenz subsystem leads to a saturation of the magnetic field. Without this feedback term, b_1 and b_2 would grow at an exponential rate.

Summarizing, the ABCDE equations represent an approach to model the enhancement of magnetic fields by chaotic flows, an ansatz originating from the observation of astrophysical bodies, which often exhibit rapidly rotating turbulent atmospheres. Due to the structure of the set of equations given in (2.2), two general physically relevant solutions of the dynamical system can be identified. We either observe $\mathbf{b} = \mathbf{0}$ and $\mathbf{x} \neq \mathbf{0}$, that corresponds to non-magnetic convection, or we perceive $\mathbf{b} \neq \mathbf{0}$ and $\mathbf{x} \neq \mathbf{0}$, indicating self-sustained, dynamo induced magnetic fields. Thereby, dynamo action may be called *subcritical* if dynamo solutions coexist at the same parameter values with non-magnetic convection solutions, which are stable against small magnetic perturbations, while solutions may be denoted as *supercritical*, if a small initial field grows in the course of time.

Chapter 3

Dynamical Systems and Differential Equations

Nonlinear dynamical systems play a central role in modeling complex phenomena, ranging from communities competing for resources in theoretical biology over problems encountered in magnetohydrodynamic systems in the field of physics to mechanical questions discussed in engineering. When dealing with continuous phenomena, a representation by ordinary differential equations, i.e., relations that contain functions of, or derivatives with respect to, only one independent variable, is often possible. The governing differential equations prevalently exhibit nonlinearities, complicating an analytical treatment but being able to account for many properties observed in natural systems, giving rise to, for instance, characteristic spatio-temporal patterns or quasi-periodic and chaotic solutions.

Owing to the complexity of nonlinear dynamical systems, the present chapter shall only be seen as a brief introduction providing essential knowledge, since a more comprehensive discussion of the topic would go beyond the scope of this work. The instant chapter on dynamical systems and differential equations opens with a section containing an introduction into the basic notions concerning complex dynamical systems and their representation by differential equations. In order to be able to understand the complex dynamics represented by nonlinear differential equations, it is instructive to discuss linear dynamical problems in the first place. Unlike nonlinear phenomena where it is, irrespective of some special cases, impossible to derive a general solution for a whole class of systems, linear systems can be treated in a more rigorous and comprehensive way. Given the fact that we will numerously encounter problems involving linear homogeneous ordinary differential equations of first order throughout this thesis, the following section 3.2 will focus on the theory of this particular category of differential equations. Taking into account the special form of (2.4), and the option to explicitly examine periodic solutions of the Lorenz subsystem (2.2b), Floquet theory for ordinary differential equations with periodic coefficients will be introduced. Furthermore, linear differential equations with real bounded coefficients are briefly treated to inaugurate the decisive concept of characteristic exponents, providing an important measure for the stability of a generated solution.

3.1 Basics of Dynamical Systems Theory

From a general point of view, the theory of dynamical systems provides a framework to investigate the evolution of time dependent systems. Due to the fact that nonlinear dynamical systems cannot be treated in a comprehensive way in this thesis, the reader is referred to relevant literature, including an exhaustive theoretical treatment of nonlinear problems and associated differential equations, for instance given in Ref. (Argyris *et al.*, 1994; Hahn, 1967; Hartmann, 1982; Zwillinger, 1989; Kamke, 1967; Sandri, 1996).

Some authors distinguish between stochastic and deterministic dynamical systems, whereby the present contemplation is restricted to deterministic and finite dimensional dynamics. In this case, the actual problem can often be described by sets of coupled ordinary differential equations. Any differential equation of n -th order can be expressed by a system of n first order differential equations. Furthermore, we restrict ourselves to autonomous systems, since any nonautonomous set of n differential equations with explicit time dependence can be represented by a $n + 1$ -dimensional set of equations, as a result of treating the time t as a dependent variable and introducing the additional trivial evolution equation $\dot{t} = 1$. Therefore, in the following we will focus on the class of differential equations which reads

$$\dot{\mathbf{x}} = \mathbf{F}(\mathbf{x}) \quad , \quad (3.1)$$

whereby $\mathbf{x}(t) \in \mathbb{R}^n$ denotes the state variable in dependence of time t . The function $\mathbf{F} : U \rightarrow \mathbb{R}^n$ represents a vector field on an open set $U \subset \mathbb{R}^n$ and can be either linear or nonlinear in its components. The space of the dependent variables $\mathbf{x} = \{x_1, \dots, x_n\}$ is usually referred to as the n -dimensional phase space \mathfrak{S} of the system. A particular solution with initial position $\mathbf{x}_0 \in U$ at time t_0 shall be denoted by $\mathbf{p}(t, \mathbf{x}_0, t_0)$. The set $\{\mathbf{p}(t, \mathbf{x}_0, t_0) : t \in \mathbb{R}^n\}$ is denoted as trajectory of the system in phase space, uniquely defined by the initial condition \mathbf{x}_0 . The whole ensemble of possible motions in phase space is also called flow. Given a distinctive point in phase space, the corresponding system trajectory is fully characterized and its temporal evolution absolutely deterministic.

Due to the complexity of most natural or model systems under investigation, one often focusses the attention on the description of asymptotic evolutions as $t \rightarrow \infty$, rather than on finding a self-contained solution. An important concept for the characterization of asymptotic behavior in phase space is the notion of a limit set. A point P is called an ω -limit point of \mathbf{x}_0 , if the trajectory visits points $\mathbf{p}(t_1, \mathbf{x}_0, t_0), \mathbf{p}(t_2, \mathbf{x}_0, t_0), \mathbf{p}(t_3, \mathbf{x}_0, t_0), \dots$ in phase space, such that $\mathbf{p}(t_i, \mathbf{x}_0, t_0) \rightarrow P$ as $t_i \rightarrow \infty$. The set containing all ω -limit points of \mathbf{x}_0 is henceforth denoted ω -limit set $\Omega(\mathbf{x}_0)$. With the hitherto specified terms, it is possible to define an ω -limit set as being attractive in case there exists an open neighborhood U of $\Omega(\mathbf{x}_0)$ such that $\Omega(\mathbf{x}_0) = \Omega$ for all $\mathbf{x}_0 \in U$. The set of all initial conditions \mathbf{x}_0 that approach Ω as $t \rightarrow \infty$ is called basin of attraction B_Ω . At this stage it shall be mentioned that examples of limit sets include fixed points, periodic orbits, limit cycles and attractors. However, the terms attracting limit set and attractor do not exactly have the same meaning, as every attractor is an attracting limit set but not all attracting limit sets are attractors. An attractor is a set to which a dynamical system

evolves after a sufficiently long time. Trajectories which get close enough to the attractor remain close for all time, even if they are slightly perturbed. Geometrically, an attractor can be a point, a curve, a manifold, or even a complicated set with a fractal structure which is widely-known as a *strange attractor*. The Lorenz equations, which build an integral component of the model system central to this thesis, exhibit such a strange attractor under use of the original parameter values (Lorenz, 1963; Sparrow, 1982).

A differential equation may give rise to only one or several attracting limit sets, each one exhibiting a different basin of attraction. In the latter case, the choice of initial conditions determines which limit set will be approached, i.e., one might encounter qualitatively deviating, coexisting solutions under use of certain fixed parameter values. For observations of real systems and also corresponding numerical simulations, normally only attracting limit sets play an exceptional role. Rather than discussing the wide field of dynamical systems theory in too great detail, we shall list the following aspects which will become crucial to the further investigation. In general, four basic types of limit sets can be identified, giving rise to four different kinds of solutions for the underlying dynamical system (Argyris *et al.*, 1994; Sandri, 1996).

Fixed Points A fixed point or equilibrium is a stationary, i.e., time independent solution $\mathbf{p}^0 = \mathbf{p}(t, \mathbf{x}_0, t_0)$, which fulfills the condition $\mathbf{F}(\mathbf{p}^0) = 0$. Stationary solutions and their stability properties under change of certain control parameter values can often be used to characterize bifurcations of dynamical systems. Fixed points of the ABCDE model and their stability are analytically and numerically investigated in chapter 5

Periodic motions A periodic motion is defined by a solution to equation (3.1) which holds $\mathbf{p}(t, \mathbf{x}_0, t_0) = \mathbf{p}(t + T, \mathbf{x}_0, t_0)$, $\forall t$, whereas $T > 0$ is called period. The analysis of periodic solutions to a nonlinear complex dynamical system provides an opportunity to characterize the coexistent chaotic motions. Periodic orbits and their contribution to the observed instability are treated in detail in chapter 6, where we also employ results derived from Floquet's theory on differential equations exhibiting periodic coefficients

Quasiperiodic motions A quasiperiodic solution \mathbf{p} can be written in the form $\mathbf{p}(t, \mathbf{x}_0, t_0) = \tilde{\mathbf{p}}(\omega_1 t, \dots, \omega_n t, \mathbf{x}_0, t_0)$ with $\tilde{\mathbf{p}}$ being of period 2π in each argument and $n \geq 2$. $\omega_1, \dots, \omega_n$ are real positive numbers that are rationally linearly independent and called base frequencies. For instance, quasiperiodic solutions might arise if a free oscillator is under the influence of a time-dependent force

Chaotic Motions Without stating a formal mathematical definition of chaos it can be said that chaotic dynamics are at hand if the following properties hold: 1) Sensitive dependence of the system on initial conditions 2) Convergence of the system in phase space to a strange attractor 3) The motion exhibits bounded steady state trajectories in phase space, which seem to show random behavior and do not belong to the first three kinds of solutions introduced above. A well-known approach to explore chaotic dynamics is given in terms of Lyapunov characteristic exponents which will be discussed in detail in chapter 6

3.2 Linear Homogeneous Differential Equations

The theory of linear differential equations is well-known and can be reviewed in many books and articles (Hahn, 1967; Hartmann, 1982; Zwillinger, 1989). Many special cases including differential equations with constant, periodic, quasiperiodic, or real bounded coefficients can be treated partly in a considerably rigorous manner. However, in order to keep the focus of this thesis, only the main results and notions which we shall need in the further discussion will be introduced in the following. If necessary for imperative reasons, the reader is explicitly referred to relevant literature.

In the present section on linear homogeneous differential equations, we consider n -dimensional systems of equations exhibiting the general form

$$\dot{\mathbf{x}} = \mathcal{A}(t)\mathbf{x} \quad , \quad (3.2)$$

where it is assumed that the matrix elements a_{ik} composing \mathcal{A} represent continuous functions of time t defined for all $t \geq t_0$, according to the treatment presented in Ref. (Hahn, 1967). A system of n linearly independent solutions $\{\mathbf{x}^{(1)}, \dots, \mathbf{x}^{(n)}\}$ is called fundamental system and forms a basis in the space of solutions. The columns $\mathbf{x}^{(1)}, \dots, \mathbf{x}^{(n)}$ can be assembled to build a matrix \mathcal{X} which satisfies the corresponding matrix equation

$$\dot{\mathcal{X}} = \mathcal{A}(t)\mathcal{X} \quad . \quad (3.3)$$

Owing to the fact that a solution belonging to a particular basis can be expressed as a linear combination of elements of another basis, two distinctive bases \mathcal{X} and \mathcal{Y} can be related by a matrix \mathcal{C} , satisfying $\det \mathcal{C} \neq 0$, according to

$$\mathcal{Y} = \mathcal{X}\mathcal{C} \quad , \quad (3.4)$$

where \det denotes the determinant. The particular basis whose matrix representation resembles the unity matrix for $t = t_0$ is further on denoted by $\mathcal{K}(t, t_0, \mathcal{A}(t))$. From the analytical treatment presented in Ref. (Hahn, 1967), it can be deduced that the general solution of equation (3.2), with respect to a particular initial condition \mathbf{x}_0 at $t = t_0$, takes the form

$$\mathbf{p}(t, \mathbf{x}_0, t_0) = \mathcal{K}(t, t_0, \mathcal{A}(t)) \mathbf{x}_0 \quad . \quad (3.5)$$

Thus far, we have not specified the particular structure of $\mathcal{A}(t)$, which would be necessary to derive a solution for an explicit differential equation by determining $\mathcal{K}(t, t_0, \mathcal{A}(t))$. In general, it is not possible to find a closed analytical solution to a given arbitrary set of equations of the form (3.2). Hence, one often has to resort to numerical treatments of the underlying set of ordinary differential equations. However, if $\mathcal{A}(t)$ exhibits periodicity, a more rigorous treatment becomes possible. The solution matrix $\mathcal{K}(T, t_0, \mathcal{A}(t))$ will play a major role in the investigation of differential equations with periodic coefficients since its eigenvalues determine the stability of the corresponding solutions as will be discussed in the next section.

3.2.1 Equations Exhibiting Periodic Coefficients

One significant special case of (3.2) emerges when \mathcal{A} consists of periodic coefficients. We therefore focus our attention on n -dimensional systems of differential equations in vector notation, which read in the general case

$$\dot{\mathbf{x}} = \mathcal{L}(t)\mathbf{x} \quad , \quad \mathcal{L}(t+T) = \mathcal{L}(t) \quad , \quad (3.6)$$

whereas T is a positive valued quantity denoting the period. Analogous to the proceeding in the general case, one is led to a corresponding matrix equation of solutions given by

$$\dot{\mathcal{X}} = \mathcal{L}(t)\mathcal{X} \quad . \quad (3.7)$$

Hence, employing the periodicity in $\mathcal{L}(t)$ and the general solution (3.5), another solution $\mathbf{p}(t+T, \mathbf{x}_0, t_0) = \mathcal{K}(t+T, t_0, \mathcal{L}(t)) \mathbf{x}_0$ can be obtained by translating the variable t by one period.

Floquet theory, which is discussed for instance in Ref. (Haken, 2004; Hahn, 1967), accomplishes to obtain a generalized solution for differential equations of the form (3.6). The main outcome implies that the solution consists of an exponential constituent, and a component with periodic properties. Following the discussion in Ref. (Hahn, 1967), one is led to the following final statement.

Theorem 1 (Floquet's theorem) *The general solution of a differential equation with periodic coefficients exhibiting the form of equation (3.6) therefore is given by a linear combinations of solution vectors*

$$\mathbf{p}^j(t, \mathbf{x}_0, t_0) = \exp(\sigma_j t) \mathbf{q}^{(j,i)}(t) \quad , \quad (3.8a)$$

whereby

$$j = 1, \dots, r \quad , \quad i = 1, \dots, n_j \quad \text{and} \quad \sigma_j = \frac{\ln \mu_j}{T} \quad . \quad (3.8b)$$

The characteristic exponents σ_j are called Floquet exponents and the numbers μ_1, \dots, μ_r denote the distinct characteristic roots of the matrix $\mathcal{K}(T, 0, \mathcal{L}(t))$, whereby $r \leq n$. The multiplicity of the elementary divisor associated with one particular μ_j is represented by the number n_j . The components of the vector-valued functions $\mathbf{q}^{(j,i)}(t)$ are given by polynomials in time t with periodic coefficients. $\mathbf{q}^{(j,i)}(t)$ takes the general form

$$\mathbf{q}^{(j,i)}(t) = \mathbf{q}_0^{(j)}(t) + \mathbf{q}_1^{(j)}(t)t + \mathbf{q}_2^{(j)}(t)t^2 + \dots \quad , \quad (3.8c)$$

with the degree of each polynomial being at most equal to $n_i - 1$.

In conclusion, the Floquet exponents determine the stability of the corresponding dynamical system. It shall be noted that in general, equation (3.7) cannot be solved analytically, and one has to resort to computer calculations in order to determine the solution matrix $\mathcal{K}(t, 0, \mathcal{L}(t))$. The numerical determination of $\mathcal{K}(T, 0, \mathcal{L}(t))$ is straightforward and will be described in the corresponding sections. In various paragraphs of chapter 6, Floquet's theory is applied to obtain explicit solutions for the \mathbf{b} variables of the ABCDE model, when the Lorenz subsystem exhibits periodicity. In this periodic regime, the equations defining the temporal evolution of the \mathbf{b} subsystem apparently can be treated in terms of Floquet's theory.

3.2.2 Equations Exhibiting Real Bounded Coefficients

As another particular class of differential equations, this subsection treats linear homogeneous differential equations with real bounded coefficients according to Ref. (Haken, 2004). In order to characterize the asymptotic behavior of solutions to the corresponding dynamical system in the limit $t \rightarrow \infty$, the concept of generalized characteristic exponents shall be introduced. To this end, we consider the one-dimensional differential equation

$$\dot{x} = \alpha(t)x \quad , \quad (3.9)$$

whereas $\alpha(t)$ represents an arbitrary continuous function of time, under the constraint that the quantity α is bounded for $0 \leq t < \infty$ such that $|\alpha(t)| \leq B$, while B represents a positive valued constant. Assuming that $\alpha(t)$ is real, the general solution therefore is given by an expression of the form

$$p(t, x_0, t_0) = p(t_0, x_0, t_0) \exp \left(\int_{t_0}^t d\tau \alpha(\tau) \right) \quad , \quad (3.10)$$

so that the temporal evolution of the integral in (3.10) determines the asymptotic behavior. From a simple estimate, taking into account the boundary conditions as sketched in Ref. (Haken, 2004), it follows immediately that the limit

$$\lim_{t \rightarrow \infty} \sup \left(\frac{1}{t} \int_{t_0}^t d\tau \alpha(\tau) \right) = \Lambda \quad , \quad (3.11)$$

exists, satisfying $|\Lambda| < \infty$. Thereby, \sup denotes the supremum (least upper bound), while Λ is called generalized characteristic exponent and provides information on the behavior of solutions as time approaches infinity. The existence of the limit (3.11) immediately implies that the solution to (3.9) possesses an upper bound at each time t , given by

$$|p(t, x_0, t_0)| \leq |C| \exp(\Lambda t + f(t)) \quad , \quad C = \text{const.} \quad , \quad (3.12)$$

whereas $\lim_{t \rightarrow \infty} \sup \left(\frac{1}{t} f(t) \right) \rightarrow 0$. Hence, the generalized characteristic exponent has the same significance regarding the stability of solutions of equation (3.9) as the Floquet exponent for differential equations with periodic coefficients, treated in section 3.2.1. Like we have noted in the introduction of this chapter, nonlinear systems exhibiting chaotic dynamics cannot be treated in a comparably generalized way as the problems discussed above. However, there are ways of categorizing solutions according to their stability behavior. To this end, the concept of Lyapunov exponents will be introduced in chapter 6. Lyapunov characteristic exponents represent a special case of generalized characteristic exponents and provide a framework to understand the instability, which is detected in the ABCDE model for a critical control parameter value. A direct application of the results stated in this section follows in parts 4.1, and 6.4, respectively, where the critical generalized characteristic exponent for the **b** subsystem is being investigated in detail, revealing the nature of the intermittent bursts of magnetic activity close to the transitional state.

Chapter 4

Numerical Observation of the Phase Transition

The present chapter contains a detailed numerical investigation of the ordinary differential equations associated with the ABCDE model (2.2). Thereby, special attention is paid to the examination of an instability, which is being encountered under use of certain parameter values. The findings discussed in the present chapter constitute a reproduction of results which have foremost been reported by R. Friedrich and H. Haken in Ref. (Friedrich and Haken, 1992), and provide an important fundament of this thesis; the outcome and conclusions of the investigation presented in Ref. (Friedrich and Haken, 1992) serve as chief motivation to contemplate the nonequilibrium phase transition in more detail. Throughout the discussion and the following chapters presenting numerical computations, the classical parameter values $r = 28$, $\sigma = 10$, and $b = 8/3$, which were used by Lorenz in his original work (Lorenz, 1963), are being employed. Under exceptional circumstances, when for instance the Rayleigh number r is varied for the examination of limit cycles in subsection 6.3.2, the temporary deviation from the basic convention is explicitly indicated. The remaining parameter values are independently chosen and read $a_1 = 0.1$, $a_2 = 0.2$, as well as $\alpha = 0.2$. The system parameter ϵ is assigned a special status, since it serves as control parameter. As a matter of principle, ϵ is chosen to be larger than zero. For large values of the above defined quantity ϵ , the Cartesian norm of \mathbf{b} vanishes in the course of time as the linear dumping terms in (2.3) dominate the system's behavior. When ϵ is reduced and approaches a certain critical boundary, $\|\mathbf{b}\|$ starts fluctuating strongly in time. The critical parameter value for which this instability arises shall be called ϵ_c in the following.

The present chapter is organized as follows. First, we will numerically examine the system's characteristic exponent that determines the onset of dynamo action as the control parameter ϵ is varied. Second, we demonstrate the temporal evolution of some degrees of freedom close to the transition, exhibiting strongly intermittent behavior. Finally, we assess the dependence of suitable order parameters, represented by first and second moments of relevant degrees of freedom, on the control parameter ϵ , and depict projections of exemplary trajectories in the five dimensional phase space on several separable subspaces.

4.1 The Characteristic Exponent Λ

The special structure of (2.6) allows an estimate of ϵ_c , denoting the critical parameter value modeling the observed instability. By neglecting the back reaction of the newly introduced variables r and ϕ on the Lorenz subsystem, an analytic expression for the behavior of r in the course of time can be found. If one denotes the solution of the pure Lorenz system by $\mathbf{x}_0(t)$, and the solution of the angular variable by $\phi_0(t)$, respectively, one is led to

$$\begin{aligned} r(t) &= r(0) \exp[\Lambda(t)t] \\ \Lambda(t) &= \epsilon \left(-a_1 + (a_2 - a_1) \frac{1}{t} \int_0^t d\tau \sinh^2(\phi_0(\tau)) \right) \quad , \end{aligned} \quad (4.1)$$

as has been shown in (Friedrich and Haken, 1992). Thereby, it is assumed that the time limit $\Lambda = \lim_{t \rightarrow \infty} \Lambda(t)$ exists. Together with the equations (4.1), this assumption implies that the limit

$$\langle \sinh^2(\phi^0) \rangle = \lim_{t \rightarrow \infty} \frac{1}{t} \int_0^t d\tau \sinh^2(\phi_0(\tau)) \quad , \quad (4.2)$$

is well-defined. From equation (4.1), one can conclude that $r(t)$ vanishes in the course of time for an characteristic exponent $\Lambda < 0$. Otherwise, the corresponding variable grows at an exponential rate while fluctuating heavily, since the integral in (4.1), and therewith $\Lambda(t)$, is a fluctuating quantity. It should be mentioned at this point that for $\epsilon < \epsilon_c$, the back reaction of the \mathbf{b} variables onto the Lorenz subsystem \mathbf{x} cannot be neglected in general. Hence, if one considers the actual set of equations including back coupling, the unlimited growth of r is being inhibited due to the dominating dumping terms.

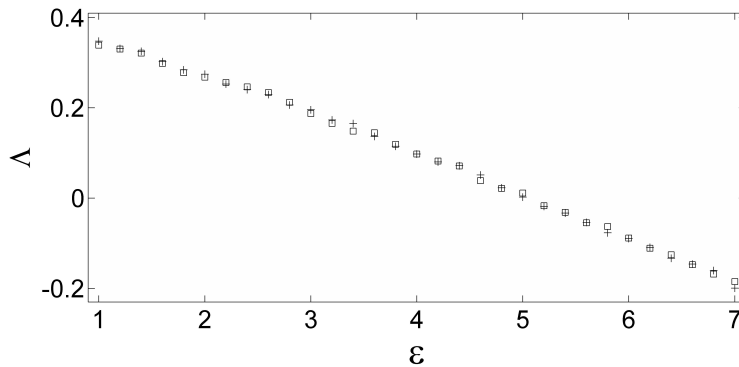


Figure 4.1: Characteristic exponent Λ as function of the control parameter value ϵ for two different arbitrary initial conditions denoted by (+, □)

In the following, the characteristic exponent Λ has been determined numerically for various control parameter values ϵ to assess the onset of instability. To this end, at first the Lorenz subsystem $\mathbf{x}(t)$ has been integrated numerically together with the angular variable ϕ , using a Runge-Kutta (4,5) integration routine with appropriate step size. Having obtained the evolution of ϕ^0 by this means, the characteristic exponent has been calculated according to equation

(4.1). To exclude significant influences of initial conditions for the five dimensional system on the calculation of the characteristic exponent, the same computation has been performed for various starting conditions. For the sake of clarity, figure 4.1 shows only the result of the computation for two randomly chosen initial conditions. The characteristic exponent Λ appears to be a continuous function of ϵ . The critical parameter value is estimated to be approximately $\epsilon_c = 5$, indicated by the zero-crossing of the characteristic exponent. As can be reasoned from the outcome of the computation, the basic properties of the characteristic exponent do not depend on the choice of initial conditions for the integration of the underlying differential equations. The findings confirm the numerically obtained critical parameter value that leads to the onset of instability, as has foremost been reported in Ref. (Friedrich and Haken, 1992).

4.2 Time Series of the Variable r

The present section focuses on the surveillance of time series of the variable r . According to the observations presented in the previous section 4.1, one expects to perceive a qualitative change of behavior when ϵ approaches the characteristic threshold ϵ_c . In accordance with the

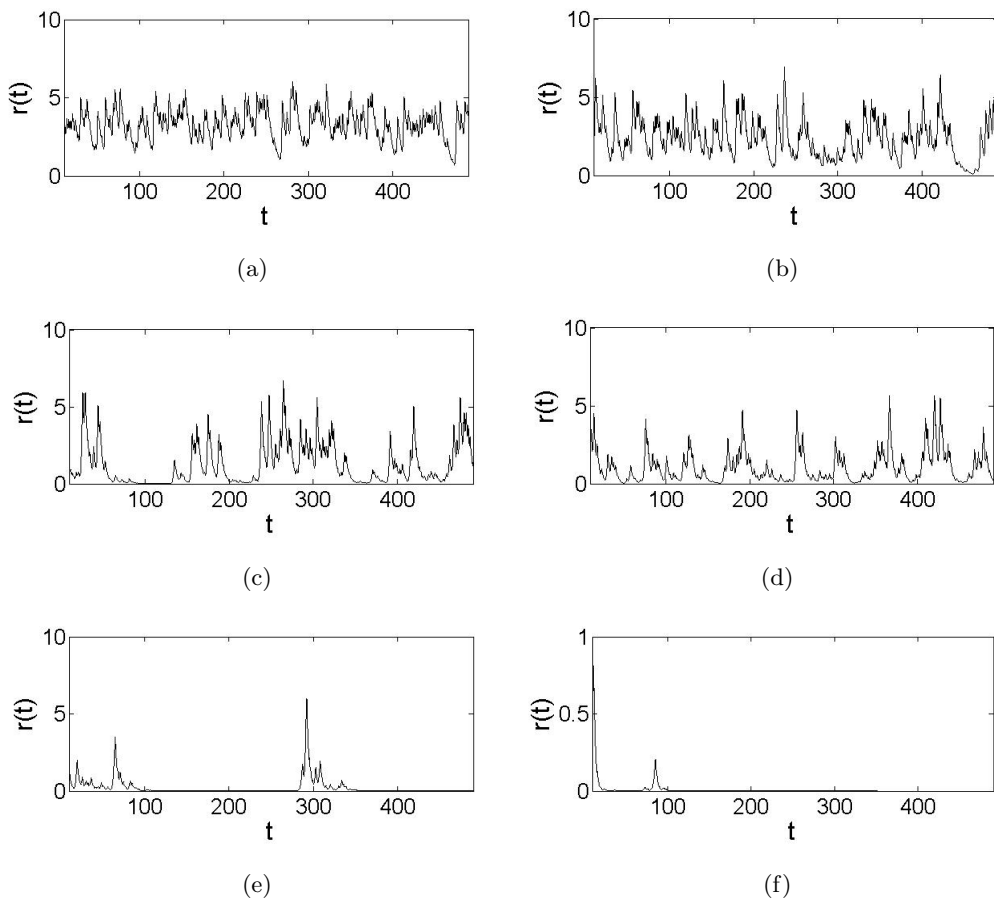


Figure 4.2: Time series of variable $r(t)$ for different values of ϵ . (a) $\epsilon = 2$, (b) $\epsilon = 3$, (c) $\epsilon = 4$, (d) $\epsilon = 4.5$, (e) $\epsilon = 5$, (f) $\epsilon = 6$. Close to the onset of magnetic dynamo action, intermittent temporal behavior can be identified

expectation, examining time series of the variable r for different values of the order parameter ϵ , an instability of the system can be observed for a characteristic value of $\epsilon_c = 5$. To this end, the set of nonlinear ordinary differential equations expressed in hyperbolic coordinates (r, ϕ) has been numerically integrated. Figure 4.2 presents time series of the system variable r for various values of the control parameter ϵ . Apparently, $r(t)$ fluctuates heavily around a certain mean value as long as the control parameter is chosen to hold $\epsilon < \epsilon_c$. In this regime, the back reaction of the $\{r, \phi\}$ variables on the Lorenz subsystem cannot be neglected and results in a prevention of the unlimited growth of the variables $\{r, \phi\}$, or $\{b_1, b_2\}$, respectively. When ϵ approaches its critical value ϵ_c from below, intermittent behavior of $r(t)$ can be monitored. Strong chaotic bursts of activity alternate with periods of vanishing activity. The closer ϵ approaches its critical value from below, the longer these periods of evanescent activity become. However, r vanishes rapidly in the course of time as the control parameter exceeds the critical threshold and takes a value above ϵ_c . At this point, we would like to highlight that, as addressed in section 2.1, several experimental observations have revealed intermittent temporal behavior of magnetic field modes close to the onset of hydromagnetic dynamo action and magnetic field reversals. Clearly, a qualitative change of behavior is witnessed in the ABCDE model for varying control parameter values, while the system shows strong intermittency close to the transitional point. Using the denotation introduced in chapter 1, we thus encounter a process of self-organization when crossing the threshold to dynamo action.

4.3 Phase Space Projections and Moments of the Variable r

Supplemental information about the nature of the observed transition might be found by examining projections of phase space trajectories onto miscellaneous subspaces. One outstanding feature in this regard is the robustness of the Lorenz attractor for the regime $\epsilon < \epsilon_c$. In this domain, the back reaction of the \mathbf{b} variables onto the Lorenz subsystem cannot be neglected, and intuitively might lead to a destruction of the pure strange Lorenz attractor. However, taking note of figure 4.3 illustrating a projection of the attractor onto the Lorenz subspace and the x - y plane, respectively, the topology persists and only marginal perturbations of the pure Lorenz attractor can be discovered. As ϵ takes on its critical value, the perturbations cease to exist and vanish entirely for a value significantly larger than ϵ_c due to the increasing back coupling.

Analogous to figure 4.2 monitoring the intermittency of the variable $r(t)$, projections of the attractor onto the b_1 - b_2 plane in figure 4.3 clearly indicate dramatic behavioral changes as the control parameter ϵ is varied. When choosing $\epsilon < \epsilon_c$, the persistent structure of the attractor becomes evident. Near the critical value ϵ_c , one can anticipate the regime of intermittency which becomes evident when examining r in the course of time. However, investigating the characteristic temporal evolution for control parameter values $\epsilon > \epsilon_c$, the order parameter $\|\mathbf{b}(t)\|$ vanishes as the time t approaches infinity.

Apart from the examination of phase space characteristics, the behavior of moments of the hyperbolic variable r in dependence of the control parameter ϵ can be assessed via numerical

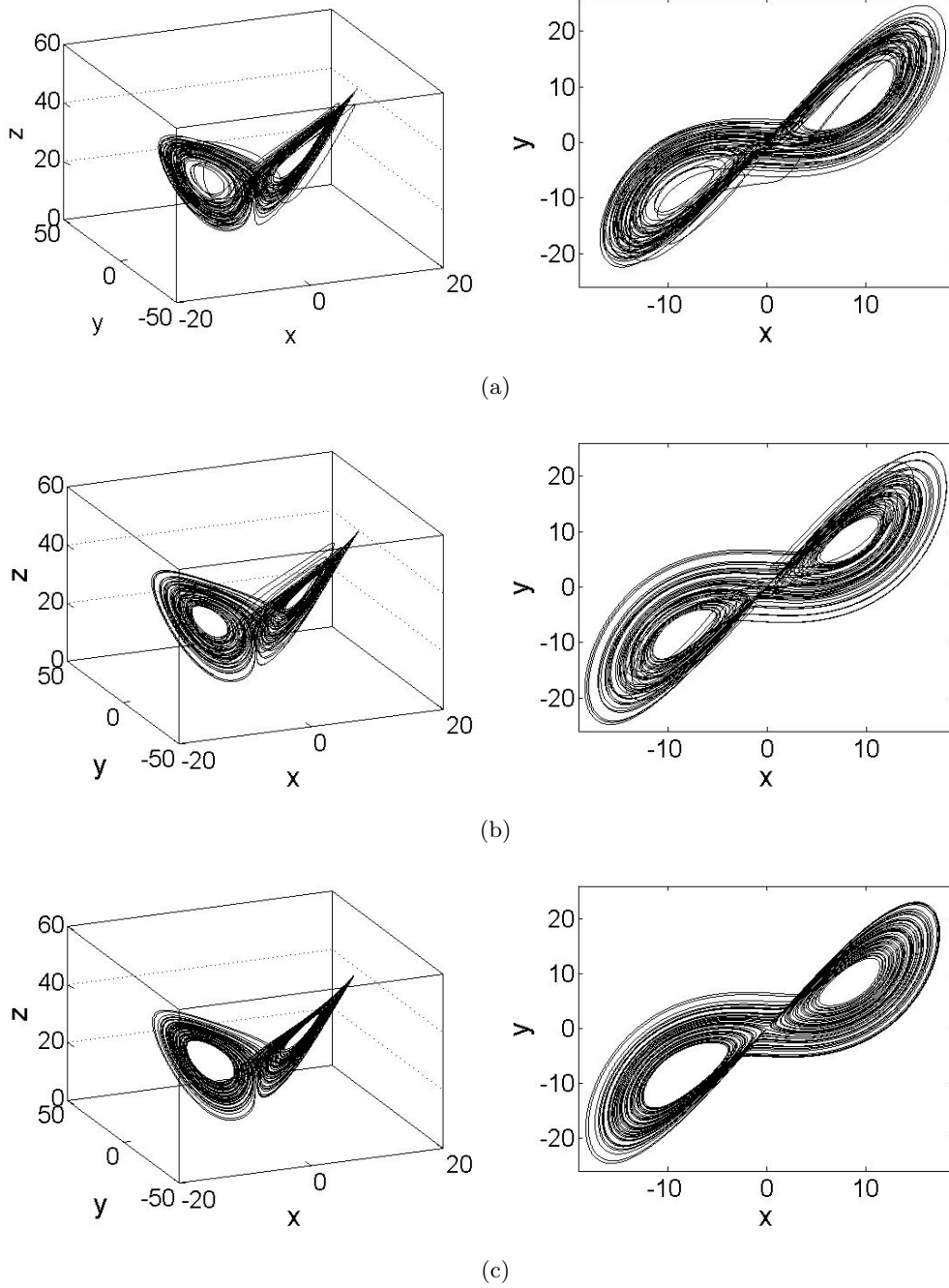


Figure 4.3: Projection of five dimensional phase space on the Lorenz subspace (first column) and projection onto the $x - y$ plane (second column). Thereby, the control parameters read (a) $\epsilon = 2$, (b) $\epsilon = 4.5$, (c) $\epsilon = 7$

integration of the ABCDE equations. Figure 4.5 shows the moments $\langle r(t) \rangle$ and $\langle r^2(t) \rangle$ as a function of ϵ . Apparently, both moments decrease smoothly as the order parameter approaches its critical value from below. This observation indicates the existence of a nonequilibrium phase transition according to the definitions given in Ref. (Frank, 2005; Haken, 2004). Comparing the graphs with figure 1, the attribution of control and order parameters, respectively, becomes evident. Moreover, the onset of magnetohydrodynamic dynamo action is directly reflected in

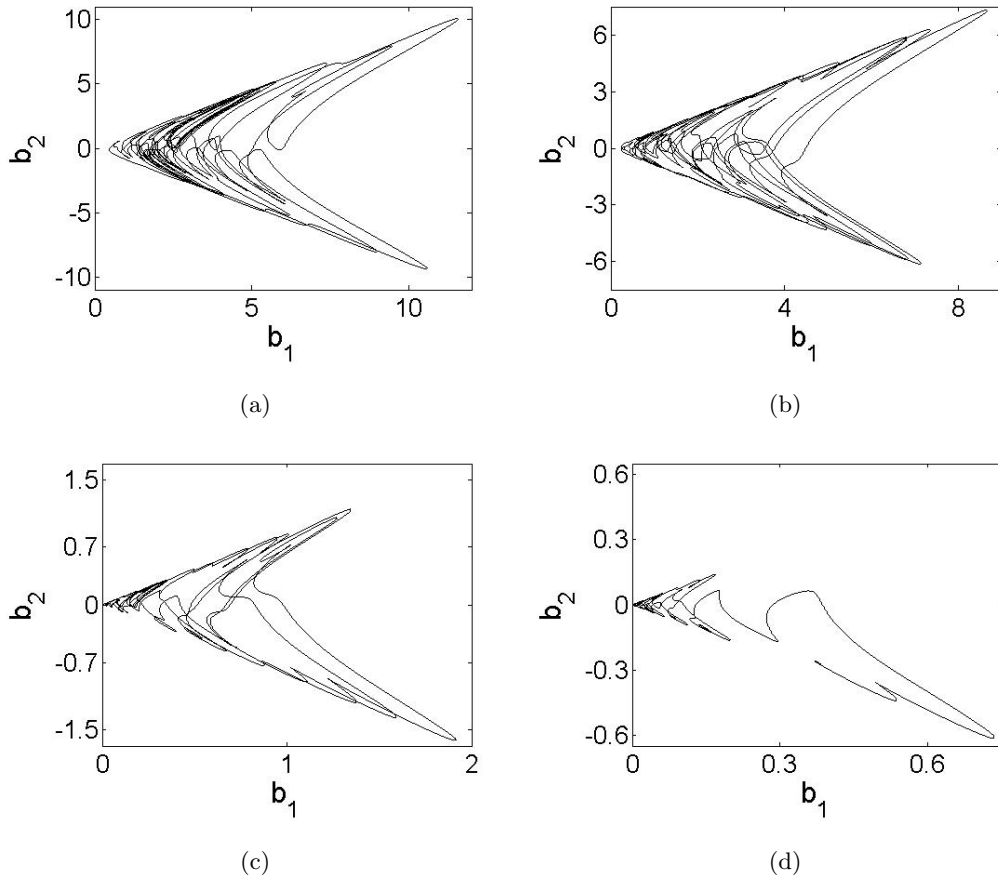


Figure 4.4: Projection of attractor onto the b_1 - b_2 plane for (a) $\epsilon = 2$, (b) $\epsilon = 4.5$, (c) $\epsilon = 5.2$, (d) $\epsilon = 7$

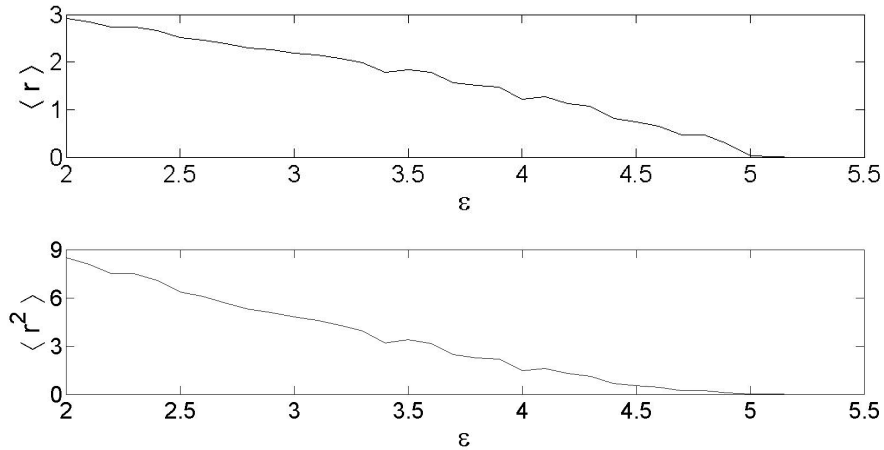


Figure 4.5: Smoothly decreasing moments $\langle r(t) \rangle$ and $\langle r(t)^2 \rangle$ in dependence of the control parameter ϵ

figure 4.5. Given the numerical study presented in this chapter, it is alluring to investigate the nature and immediate origin of the encountered nonequilibrium phase transition. The remaining chapters are being devoted to a detailed analysis of the underlying dynamical processes, as well as a stochastic treatment of the instability. However, the next chapter discusses stationary solutions of the ABCDE equations and their stability properties.

Chapter 5

Stability Analysis of Equilibria

A conventional approach to study qualitative macroscopic changes of complex systems is given by the assessment of stability properties of the governing solutions. An orbit in phase space, describing the temporal evolution of the underlying dynamical process, is said to be stable if nearby orbits remain in a neighborhood of the reference trajectory. Assuming that all adjacent trajectories within some small initial distance, $\xi(t_0) \rightarrow 0$, are repelled from the reference trajectory for $t > t_0$, the dynamics are referred to as unstable. A generalized method to study nonlinear dynamical systems based on the investigation of Lyapunov characteristic exponents is discussed in detail in chapter 6. However, at this point, we shall focus on the examination of stability properties with respect to stationary solutions. The analysis is straightforward and provides first impressions of the nature of the perceived instability. We utilize the well-known result stating that the stability of nonlinear dynamical systems can sometimes be disclosed by consulting the corresponding linearized system of differential equations. Hence, we first have to evaluate the fixed points of the five-dimensional system of differential equations employing simple analysis. Subsequently, we have to explore the linearization of the basic relevant differential equations (2.2) and apply a linear stability analysis regarding the system's stationary solutions.

The present chapter is organized as follows. To characterize the nature of the potential equilibrium solutions in a more precise manner, several different definitions of stability are briefly introduced in the following section. Furthermore, we outline the basic concepts of linear stability analysis of stationary solutions, and highlight its significance with respect to the disclosure of stability properties of hyperbolic fixed points. Subsequently, the stability of the equilibrium points of the set of equations defining the ABCDE model, given in equations (2.3), is being examined. As far as possible, analytic expressions for the eigenvalues of the correlative linearized system, evaluated at all identified equilibria, are being presented. In addition, numerical calculations of the eigenvalues of the corresponding Jacobian matrix allow conclusions concerning the stability of equilibria of the dynamical system under investigation as the control parameter ϵ is varied. We show that the analytically derived results fully correspond to the numerically determined eigenvalues. However, we disclose that the stability of neither fixed point alters when the control parameter is varied within the relevant predefined interval.

5.1 Linearization of Dynamical Systems and Stability of Equilibria

In the following, systems of first order ordinary differential equations without explicit time dependence, i.e. autonomous systems, are being considered. The set of equations (2.3), building the foundation of this thesis, ranks among this type of systems of coupled nonlinear ordinary differential equations. For extensive information on the stability analysis of dynamical systems, as well as on the linearization of nonlinear problems and the assessment of stability of equilibria, the reader is referred to Ref. (Haken, 2004; Argyris *et al.*, 1994; Hahn, 1967). Expressed in vector notation, a first order n -dimensional system exhibits the form

$$\dot{\mathbf{x}} = \mathbf{f}(\mathbf{x}) \quad \text{whereas} \quad \mathbf{f}(\mathbf{x}) = \begin{pmatrix} f_1(x_1, \dots, x_n) \\ \vdots \\ f_n(x_1, \dots, x_n) \end{pmatrix}, \quad \mathbf{x} = \begin{pmatrix} x_1 \\ \vdots \\ x_n \end{pmatrix}. \quad (5.1)$$

The vector-valued function $\mathbf{f}(\mathbf{x})$ thereby can be linear or nonlinear in its components. A particular solution to (5.1) shall be consecutively denoted by $\mathbf{x}(t)$. Fixed points or equilibria \mathbf{x}^0 are constant solutions, which therefore satisfy the characteristic equation $0 = \mathbf{f}(\mathbf{x}^0)$. To characterize how trajectories behave in the vicinity of these stationary solutions \mathbf{x}^0 , the following definitions of stability shall be introduced.

Definition 1 (Lyapunov Stability) *An equilibrium \mathbf{x}^0 is stable in the sense of Lyapunov, if for every open neighborhood V of \mathbf{x}^0 there exists another open neighborhood $U \subseteq V$ of \mathbf{x}^0 , such that $\mathbf{x}(0) \in U$ implies that $\mathbf{x}(t) \in V$ for all $t > 0$. Thereby, the trajectory $\mathbf{x}(t)$ does not necessarily need to approach \mathbf{x}^0 in the course of time.*

If the fixed point \mathbf{x}^0 is not stable, it is called unstable.

Definition 2 (Asymptotic Stability) *An equilibrium \mathbf{x}^0 is denoted as asymptotically stable if it is Lyapunov stable and the open neighborhood U can be chosen such that $\|\mathbf{x}(t) - \mathbf{x}^0\| \rightarrow 0$ as $t \rightarrow \infty$ for all $\mathbf{x}(0) \in U$.*

Definition 3 (Exponential Stability) *The fixed point \mathbf{x}^0 is regarded as exponentially stable in case there is an open neighborhood U of \mathbf{x}^0 , and a constant $d > 0$, such that $\|\mathbf{x}(t) - \mathbf{x}^0\| < \exp(-dt)$ as $t \rightarrow \infty$ for all $\mathbf{x}(0) \in U$. Since all exponentially stable equilibria are asymptotically stable, they are also stable in the sense of Lyapunov.*

One useful attempt to investigate the stability of a particular dynamical system's equilibria is given by a linearization of the governing system of equations. Supposing that \mathbf{x}^0 is an equilibrium of (5.1), let $\mathbf{x}(t) = \mathbf{x}^0 + \boldsymbol{\xi}(t)$. Thereby, $\boldsymbol{\xi}(t)$ represents a small perturbation of the stationary solution obeying $\|\boldsymbol{\xi}(t)\| \ll 1$. Substitution of this ansatz into (5.1) yields, after expansion of the function \mathbf{f} in a vector valued Taylor series

$$\dot{\mathbf{x}}^0 + \dot{\boldsymbol{\xi}} = \mathbf{f}(\mathbf{x}^0 + \boldsymbol{\xi}) = \mathbf{f}(\mathbf{x}^0) + \mathcal{J}\mathbf{f}(\mathbf{x}^0)\boldsymbol{\xi} + \mathcal{O}(\|\boldsymbol{\xi}\|^2) \quad , \quad (5.2)$$

whereas $\mathcal{J}\mathbf{f}(\mathbf{x}^0)$ denotes the $n \times n$ Jacobian matrix of the differential equations evaluated at the fixed point \mathbf{x}^0 . $\mathcal{O}(\|\boldsymbol{\xi}\|^2)$ represents terms of second and higher order in the components of the vector $\boldsymbol{\xi}$. Therefore, choosing $\|\boldsymbol{\xi}\| \rightarrow 0$, the first term in the Taylor expansion dominates the behavior of the series, and one obtains the linearization of (5.1) at the equilibrium point \mathbf{x}^0 as

$$\dot{\boldsymbol{\xi}} = \mathcal{J}\mathbf{f}(\mathbf{x}^0)\boldsymbol{\xi} \quad . \quad (5.3)$$

When λ is a real eigenvalue of the Jacobian $\mathcal{J}\mathbf{f}(\mathbf{x}^0)$ with the corresponding eigenvector \mathbf{u} , the general solution of (5.3) can be expressed in the form

$$\boldsymbol{\xi}(t) = c\mathbf{u}\exp(\lambda t), \quad c = \text{const.} \quad . \quad (5.4)$$

In case of a pair of conjugate complex eigenvalues $\lambda_{1,2} = \alpha \pm i\beta$ with complex eigenvectors $\mathbf{g} = \mathbf{v} \pm i\mathbf{w}$, the general solution to (5.3) exhibits the form

$$\boldsymbol{\xi}_1(t) = \exp(\alpha t)(\mathbf{v} \cos(\beta t) - \mathbf{w} \sin(\beta t)), \quad \boldsymbol{\xi}_2(t) = \exp(\alpha t)(\mathbf{v} \sin(\beta t) + \mathbf{w} \cos(\beta t)) \quad . \quad (5.5)$$

Hence, in both cases the real parts of the Jacobian matrices' eigenvalues, $\Re(\lambda)$, determine the asymptotic behavior of the solutions. In the following, the stability of equilibria is being treated in the case of non degenerate fixed points, i.e., when neither of the eigenvalues of the corresponding Jacobian has zero real part. In this case, the corresponding fixed point is named hyperbolic equilibrium, and subsequent to the computation of the eigenvalues of the Jacobian matrix evaluated at the stationary solution, one can state whether the equilibrium is stable.

Proposition 1 (Stability of hyperbolic fixed points) *Let \mathbf{x}^0 be a fixed point of the inertial differential equation (5.1) and all eigenvalues of $\mathcal{J}\mathbf{f}(\mathbf{x}^0)$ be strictly negative, then the equilibrium is exponentially, and therefore asymptotically and Lyapunov stable. If at least one eigenvalue is observed to have positive real part, then the equilibrium \mathbf{x}^0 is unstable.*

5.2 Fixed Points of the ABCDE System

In this section, the fixed points of the ABCDE model, i.e. the equilibria of the underlying set of ordinary differential equations (2.3), are being investigated. Stationary solutions of the five dimensional system can be obtained by finding solutions $\mathbf{X}^0 = (b_1^0, b_2^0, x^0, y^0, z^0)$ of the equation $\mathcal{F}(\mathbf{X}^0) = 0$. Hence, under the assumption that $b_1 > 0$, the five stationary points are given by

$$\mathbf{X}_1^0 = \begin{pmatrix} 0 \\ 0 \\ 0 \\ 0 \\ 0 \end{pmatrix}, \quad \mathbf{X}_{2,3}^0 = \begin{pmatrix} 0 \\ 0 \\ \pm \sqrt{b(R-1)} \\ \pm \sqrt{b(R-1)} \\ R-1 \end{pmatrix}, \quad \mathbf{X}_{4,5}^0 = \begin{pmatrix} \sqrt{\frac{\frac{a_2 \epsilon \sigma}{\alpha} \left(\frac{R}{1 + \frac{\epsilon^2 a_1 a_2}{\alpha^2 b}} - 1 \right)}{\alpha}} \\ \pm \sqrt{\frac{\frac{a_1 \epsilon \sigma}{\alpha} \left(\frac{R}{1 + \frac{\epsilon^2 a_1 a_2}{\alpha^2 b}} - 1 \right)}{\alpha}} \\ \pm \frac{\epsilon}{\alpha} \sqrt{a_1 a_2} \\ \pm \frac{\sqrt{a_1 a_2} \epsilon R}{\alpha \left(1 + \frac{\epsilon^2 a_1 a_2}{\alpha^2 b} \right)} \\ \frac{R}{1 + \frac{\alpha^2 b}{\epsilon^2 a_1 a_2}} \end{pmatrix}. \quad (5.6)$$

The first three fixed points \mathbf{X}_1^0 , \mathbf{X}_2^0 , and \mathbf{X}_3^0 emerge from the trivial partial solution $b_1^0 = b_2^0 = 0$, and represent the three equilibria of the unperturbed Lorenz system (Sparrow, 1982). The remaining stationary solutions \mathbf{X}_4 and \mathbf{X}_5 depend on the critical control parameter ϵ . For the notable value of $\epsilon = \alpha^2 b(R - 1)/(a_1 a_2)$, which yields $\epsilon = 12$ for the standard parameter values under investigation, $\mathbf{X}_{4,5}$ pass into the stationary solutions $\mathbf{X}_{2,3}$. Reminiscing the relevant phase space diagrams presented in figure 4.4, one can, admittedly vigorously evaluating, state that the corresponding unstable stationary points roughly enframe the projection of the attractor onto the b_1 - b_2 plane.

5.3 Linear Stability Analysis of Stationary Solutions to the ABCDE System

Having computed the stationary solutions of the ABCDE system, the stability properties of the fixed points shall be examined subsequently according to the theoretical framework presented in section 5.1. If a critical change of characteristics occurs for a parameter value close to ϵ_c , this observation would shed new light on the kind of bifurcation which constitutes the main motivation of this work. The eigenvalues of the linearized ABCDE system are evaluated at arbitrary position in phase space $\mathbf{X} = (b_1, b_2, x, y, z)$ and can be calculated, using the Jacobian of \mathcal{F} , as the roots of the characteristic polynomial $k(\lambda)$, which is defined by the expression

$$k(\lambda) = \left| \begin{pmatrix} -\epsilon a_1 - \lambda & \alpha x & \alpha b_2 & 0 & 0 \\ \alpha x & -\epsilon a_2 - \lambda & \alpha b_1 & 0 & 0 \\ -b_2 & -b_1 & -\sigma - \lambda & \sigma & 0 \\ 0 & 0 & R - z & -1 - \lambda & -x \\ 0 & 0 & y & x & -b - \lambda \end{pmatrix} \right| = 0 \quad , \quad (5.7)$$

where $|\dots|$ denotes the determinant. Since it is in general not possible to factorize the above polynomial to find an expression for the characteristic roots in analytic form, the stability of the five stationary points are addressed individually in the following subsections.

5.3.1 Fixed Point No. 1 (\mathbf{X}_1^0)

In the first case, the characteristic polynomial can be calculated easily by inserting \mathbf{X}_1^0 into (5.7). Utilizing the Laplace expansion of a matrix determinant, the resulting polynomial reads

$$(\epsilon a_1 + \lambda)(\epsilon a_2 + \lambda)(b + \lambda) (\lambda^2 + \lambda(\sigma + 1) + \sigma(1 - R)) = 0 \quad , \quad (5.8)$$

which, due to the factorization property, directly yields the five eigenvalues of the linearized system evaluated at the fixed point \mathbf{X}_1^0 , given by the expressions

$$\lambda_1 = -\epsilon a_1 \quad , \quad \lambda_2 = -\epsilon a_2 \quad , \quad \lambda_3 = -b \quad , \quad \lambda_{4,5} = -\frac{\sigma + 1}{2} \pm \sqrt{\left(\frac{\sigma + 1}{2}\right)^2 + \sigma(R - 1)} \quad . \quad (5.9)$$

Hence, for the ordinary parameter values and the relevant interval from which to choose the control parameter ϵ , there are five real eigenvalues, while one is positive, and the rest is negative.

Therefore, taking into account the statements made in section (5.1), \mathbf{X}_1^0 is an unstable fixed point and does not change its stability properties when varying the control parameter within the predefined bounds. For the sake of completion, figure 5.1 shows a numerical calculation of the above analytically determined eigenvalues in dependence of the control parameter ϵ . As can be concluded easily, the numerical calculations are consistent with the results of the exact treatment. Thus, the first fixed point does not seem to have an influence on the detected phase transition, as its instability property persists when varying ϵ .

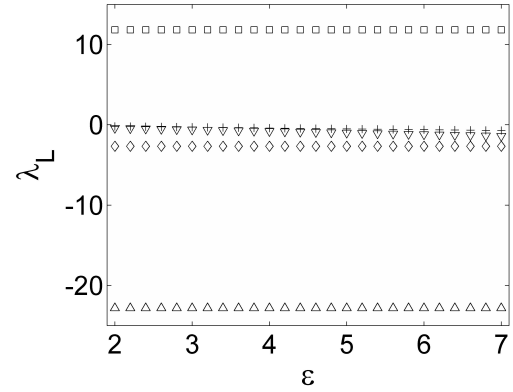


Figure 5.1: Eigenvalues of the linearized system at fixed point X_1^0 in dependence of ϵ . The notation is as follows: λ_1 (+), λ_2 (∇), λ_3 (\diamond), λ_4 (\square), λ_5 (\triangle)

5.3.2 Fixed Points No. 2 and 3 (\mathbf{X}_2^0 , \mathbf{X}_3^0)

Analogous to subsection (5.3.1), and succeeding the substitution of $\mathbf{X}_{2,3}^0$ into equation (5.7), the resulting expression can be simplified by Laplace expansion, giving rise to

$$((\epsilon a_1 + \lambda)(\epsilon a_2 + \lambda) - (\alpha x_{2,3}^0)^2) \left| \begin{pmatrix} -\sigma - \lambda & \sigma & 0 \\ R - z_{2,3}^0 & -1 - \lambda & -x_{2,3}^0 \\ y_{2,3}^0 & x_{2,3}^0 & -b - \lambda \end{pmatrix} \right| = 0 \quad . \quad (5.10)$$

Replacing $x_{2,3}^0$ by the corresponding stationary solution component stated in equation (5.6), the first factor of (5.10) immediately leads to the two real eigenvalues

$$\lambda_{1,2} = -\frac{\epsilon(a_1 + a_2)}{2} \pm \sqrt{\left(\frac{\epsilon(a_1 - a_2)}{2}\right)^2 + \alpha^2 b(R - 1)} \quad . \quad (5.11)$$

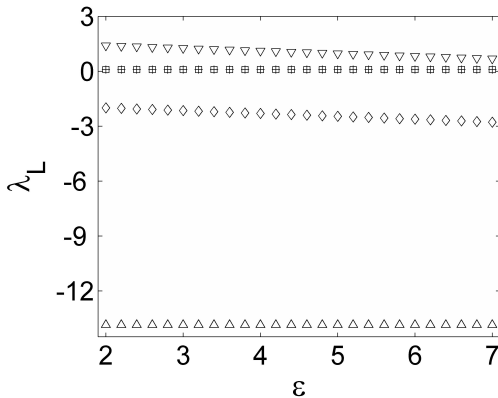


Figure 5.2: Eigenvalues of the linearized system at fixed points $X_{2,3}^0$ in dependence of ϵ . The notation is as follows: λ_1 (∇), λ_2 (\diamond), λ_3 (\triangle), λ_4 (\square), λ_5 (+)

Evaluating the right hand side of expression (5.11), we obtain $\lambda_1 > 0$ and $\lambda_2 < 0$ in case the control parameter fulfills the condition $\epsilon < \sqrt{\alpha^2 b(R - 1)/a_1 a_2}$, i.e. if $\epsilon < 12$. Otherwise, one would observe two real, negative eigenvalues. The second factor in equation (5.10) is independent of the control parameter ϵ , and characterizes the eigenvalues of the linearized ordinary Lorenz system, evaluated at the corresponding fixed points. Citing the results stated in Ref. (Sparrow, 1982), the third eigenvalue is found to be real and to hold $\lambda_3 < 0$, while the two other eigenvalues $\lambda_{4,5}$ are complex conjugate and satisfy $\Re(\lambda_{4,5}) > 0$. Figure 5.2 depicts the numerically computed set of

eigenvalues determined at the stationary points \mathbf{X}_2^0 and \mathbf{X}_3^0 . In conclusion, three eigenvalues of the linearized ABCDE system at the equilibria $\mathbf{X}_{2,3}^0$ exhibiting positive real part can be identified (note that only the real parts of the eigenvalues are plotted). For the relevant values of the control parameter ϵ , there exists no eigenvalue which crosses the imaginary axis. Since none of the eigenvalues discloses a vanishing real part, it can be concluded that the equilibria $\mathbf{X}_{2,3}^0$ remain unstable when varying the control parameter ϵ .

5.3.3 Fixed Points No. 4 and 5 (\mathbf{X}_4^0 , \mathbf{X}_5^0)

After substituting $\mathbf{X}_{4,5}^0$ into equation (5.7), the obtained expression can be simplified by elementary row operations on the matrix, and subsequent Laplace expansion of the matrix determinant to yield

$$k(\lambda) = -\sigma x_{4,5}^0 \left| \begin{pmatrix} -\epsilon a_1 - \lambda & \alpha x_{4,5}^0 & \alpha b_{2,4,5}^0 \\ \alpha x_{4,5}^0 & -\epsilon a_2 - \lambda & \alpha b_{1,4,5}^0 \\ b_{2,4,5}^0 c_2 / \sigma & b_{1,4,5}^0 c_2 / \sigma & c_1 + (\sigma + \lambda) c_2 / \sigma \end{pmatrix} \right|, \quad (5.12)$$

whereas c_1 and c_2 take the values

$$c_1 = \left(y_{4,5}^0 + \frac{(r - z_{4,5}^0)(b + \lambda)}{x_{4,5}^0} \right) \quad c_2 = \left(x_{4,5}^0 + \frac{(1 + \lambda)(b + \lambda)}{x_{4,5}^0} \right).$$

However, the resulting characteristic polynomial (5.12) cannot be factorized without difficulty, and thus, as a result, gives rise to a fifth-order polynomial equation in the variable λ . The roots of the characteristic polynomial have been calculated numerically, and figure 5.3 displays the resulting eigenvalues in dependence of the control parameter ϵ . Notice that only the real parts of the eigenvalues are plotted, and that there exist two positive conjugate complex eigenvalues. Hence, the plot shows three negative real-valued, and two conjugate complex eigenvalues with positive real part on the ϵ interval under investigation. Therefore, it can be concluded that $\mathbf{X}_{4,5}^0$ are unstable fixed points and do not change their stability behavior when the control parameter ϵ is varied.

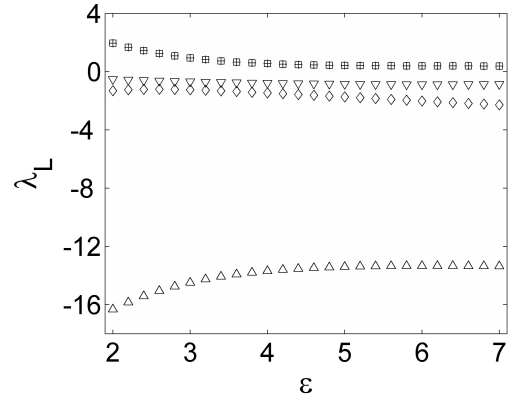


Figure 5.3: Eigenvalues of the linearized system at the fixed points $X_{4,5}^0$ in dependence of ϵ , denoted by (+), (\square), (∇), (\diamond), (\triangle)

In summary, we have shown that under the assumption $b_1 > 0$, the ABCDE system gives rise to five stationary fixed points. Carrying out a linear stability analysis of the obtained equilibria, it has emerged that no qualitative change can be detected for control parameter values close to the characteristic threshold ϵ_c , indicating the onset of hydromagnetic dynamo action. Hence, the following section will focus on the mighty concept of Lyapunov characteristic exponents to reveal the nature of the nonequilibrium phase transition.

Chapter 6

Lyapunov Characteristic Exponents

Tremendous sensitivity of solutions on initial conditions is one of the main properties commonly consulted when defining chaotic dynamical systems. The concept of Lyapunov characteristic exponents provides a commensurate measure for the average divergence or convergence of nearby trajectories in phase space. Since the orientation of the initial separation vector in \mathfrak{S} is arbitrary and can lead to different separation rates, one can observe a whole spectrum of Lyapunov exponents. Thereby, quite frequently the largest exponent is of utmost importance, since it determines the stability, and thereby the predictability of the investigated dynamical system. Thus, a positive characteristic exponent also serves as a measure for the apparent stochasticity of actually deterministic chaotic motion. In summary, it is possible to define a criterion for chaos with the help of Lyapunov exponents, since it can be shown that chaotic systems need to expose at least one positive-valued exponent. Hence, a positive Lyapunov exponent usually serves as an indicator, notifying that a system under investigation exhibits chaotic dynamics. In the context of the whole thesis, the present section plays a major role since the observed nonequilibrium phase transition can be characterized in terms of the dependence of the largest Lyapunov characteristic exponent on the control parameter ϵ .

The present chapter comprises the following topics. The first section of this part contains an example, designed to describe the expected behavior of the critical characteristic exponent, when a related bifurcation which can be examined under investigation of a trivial model equation, occurs. Section 6.2 provides general information on the algorithm used to compute the whole spectrum of Lyapunov characteristic exponents for the five-dimensional ABCDE system. In part 6.3, various explicit numerical results concerning the calculation of the Lyapunov exponent spectrum are being presented. Moreover, the distinctive contribution of various periodic orbits of the Lorenz subsystem up to period four, and the effect of high Rayleigh numbers r , on the onset of dynamo action is being clarified. Besides, explicit analytical solutions to the variable \mathbf{b} are being derived by means of Floquet's theory on differential equations with periodic coefficients. The present chapter closes with an alternative approach to compute the critical characteristic exponent by a suitable coordinate transformation, resulting in a sound description of the nature of the observed nonequilibrium phase transition in the ABCDE model.

6.1 An Example and the Expected Behavior

Before introducing the theoretical concept of Lyapunov characteristic exponents, and computing the leading as well as the whole spectrum of exponents, it might be helpful to recall well-known results from related trivial model systems, exhibiting bifurcations as a control parameter is varied. One famous example for the change of structural instability is to be briefly introduced in the following. Since the back reaction of the \mathbf{b} variables onto the Lorenz subsystem prevents the unlimited growth of $\|\mathbf{b}\|$ in the course of time, it is intuitive to consider an equation of the form (Friedrich and Haken, 1992)

$$\dot{x} = \epsilon x - |\gamma| x^3 = F(x) \quad . \quad (6.1)$$

Equation (6.1) also serves as a description of the sliding motion of a ball in vase (Haken, 2004). The corresponding stationary solutions, x^0 , read $x_1^0 = 0$ in case $\epsilon < 0$, and $x_1^0 = 0$, as well as $x_{2,3}^0 = \pm\sqrt{\epsilon/|\gamma|}$, for a control parameter value $\epsilon > 0$. Thus, we obtain one equilibrium for negative ϵ , while two additional stationary fixed points arise when ϵ becomes positive. This outcome can also be followed easily by visualizing the behavior of the corresponding potential when ϵ changes sign, as displayed in figure 6.1. In order to investigate the stability of the fixed points more formally, one makes use of results from linear stability analysis and renders the hypothesis

$$x(t) = x^0 + \delta x(t) \quad , \quad (6.2)$$

where $\delta x(t)$ is assumed to represent a small perturbation. Substitution of ansatz (6.2) into equation (6.1), and subsequent expansion of the differential equation's right hand side in a Taylor series leads to the linearized differential equation given in the form

$$\delta \dot{x} = \mathcal{J}F(x^0)\delta x \quad , \quad (6.3)$$

where only the zeroth and first order terms are kept, and $\mathcal{J}F(x^0) = \frac{\partial F}{\partial x} |_{x_0}$. Evaluating (6.3) for the three fixed points therefore yields one stable solution, x_1^0 , for $\epsilon < 0$, as well as one unstable solution, x_1^0 , and two stable solutions, $x_{2,3}^0$, in the case $\epsilon > 0$. Considering only the stable fixed points, one is led to the following representation of equation (6.3)

$$\delta \dot{x} = \begin{cases} \epsilon \delta x & \epsilon < 0 \\ -2\epsilon \delta x & \epsilon > 0 \end{cases} \quad . \quad (6.4)$$

The exponent Ω , which determines the stability of the corresponding solutions, becomes immediately evident, and we directly retrieve

$$\Omega = \begin{cases} \epsilon & \epsilon < 0 \\ -2\epsilon & \epsilon > 0 \end{cases} \quad . \quad (6.5)$$

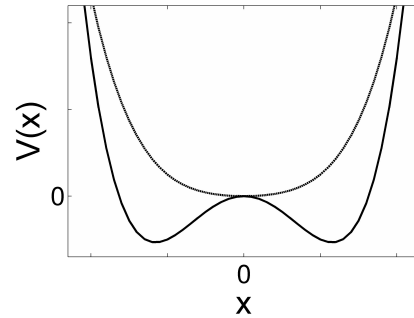


Figure 6.1: Potential of sliding ball in vase for $\epsilon > 0$ (dashed line) and $\epsilon < 0$ (solid line)

A graphical representation of (6.5), such as shown in figure 6.1, clarifies the expected dependence of the exponent Ω on the control parameter ϵ . Apparently, the exponent exhibits a characteristic behavior close to the transitional point at $\epsilon = 0$, when Ω approaches zero.

6.2 Definition and Calculation of Lyapunov Characteristic Exponents

A n -dimensional dynamical system possesses a spectrum of n Lyapunov exponents, corresponding to all principal directions in phase space. The reader is referred to Ref. (Parker and Chua, 1989; Pesin, 1977; Haken, 2004) for an exhaustive introduction and continuative information on the numerical computation of Lyapunov characteristic exponents.

For the investigation of nearby trajectories in phase space, one might consider a small n -dimensional hyper-sphere of initial conditions. The hyper-sphere can be characterized by a set of principal directions e_1, \dots, e_n . After a suitably short period of time, the chaotic dynamics will have deformed the hyper-sphere into a hyper-ellipsoid, contracted along some axes, while stretched along the others. Thereby, the average asymptotic exponential rate of convergence in any principal direction defines the Lyapunov spectrum $\lambda_1, \dots, \lambda_n$. Arranging the characteristic exponents, as well as the deformed principal directions defining the hyper-ellipsoid according to their value in decreasing order $(\lambda_1, \dots, \lambda_n; e_1, \dots, e_n)$, every Lyapunov exponent λ_i can be assigned to one particular axis e_i . Therefore, the largest Lyapunov exponent, corresponding to the most rapidly expanding direction in phase space, dominates the dynamical system's behavior.

At this point it shall be outlined that for the sake of computational efficiency, the algorithm discussed later in this section is based on the temporal evolution of an hyper-parallelepiped in phase space. The algorithm, which has been applied to obtain the results presented in the present chapter, follows the program code developed in Ref. (Wolf *et al.*, 1984), and will be contemplated in the following. Furthermore, the reader is referred to Ref. (Sandri, 1996; Benettin *et al.*, 1980) for supplementary information regarding the determination of Lyapunov spectra based on the Gram-Schmidt orthonormalization procedure.

In order to formulate the above idea in a formal manner, one considers a n -dimensional continuous-time dynamical system

$$\dot{\mathbf{x}} = \mathbf{F}(\mathbf{x}) \quad , \quad (6.6)$$

together with the same notation as established in section 3.1. Before discussing the computation of the whole spectrum of Lyapunov exponents, we focus on the investigation of the largest

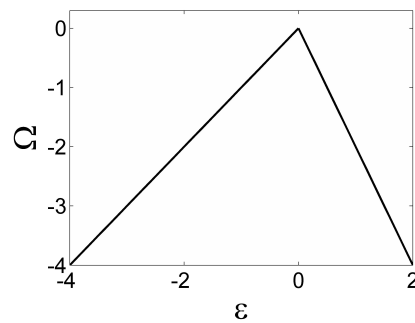


Figure 6.2: Exponent Ω as a function of the control parameter ϵ close to the bifurcation

Lyapunov exponent λ . Thus, consider two trajectories in phase space \mathfrak{S} , which initial positions are given by two nearby points \mathbf{x}_0 and $\mathbf{x}_0 + \mathbf{u}_0$, where \mathbf{u}_0 represents a small perturbation. In the course of time, the initial perturbation in tangent space will evolve according to

$$\mathbf{u}(t) = \mathbf{p}(t, \mathbf{x}_0 + \mathbf{u}_0, t_0) - \mathbf{p}(t, \mathbf{x}_0, t_0) = \mathcal{J}_{\mathbf{x}_0} \mathbf{p}(t, \mathbf{x}_0, t_0) \mathbf{u}_0 \quad , \quad (6.7)$$

whereby the solution \mathbf{p} has been linearized to obtain the last term. Hence, $\mathcal{J}_{\mathbf{x}_0} \mathbf{p}(t, \mathbf{x}_0, t_0)$ denotes the Jacobian of the solution vector, evaluated at the position \mathbf{x}_0 . As the time t approaches infinity, two trajectories starting at \mathbf{x}_0 , and $\mathbf{x}_0 + \mathbf{u}_0$, respectively, will diverge or converge exponentially. Thus, the largest Lyapunov characteristic exponent is defined as

$$\lambda(\mathbf{x}_0, \mathbf{u}_0) = \lim_{t \rightarrow \infty} \frac{1}{t} \ln \left(\frac{\|\mathbf{u}(t)\|}{\|\mathbf{u}_0\|} \right) = \lim_{t \rightarrow \infty} \frac{1}{t} \ln (\|\mathcal{J}_{\mathbf{x}_0} \mathbf{p}(t, \mathbf{x}_0, t_0) \mathbf{u}_0\|) \quad . \quad (6.8)$$

If $\lambda(\mathbf{x}_0, \mathbf{u}_0) > 0$ we observe divergence, while two nearby trajectories exhibiting $\lambda(\mathbf{x}_0, \mathbf{u}_0) < 0$ converge with the average exponential rate defined in (6.8). Oseledec showed that the limit (6.8) exists for almost all initial points $\mathbf{x}_0 \in \mathfrak{S}$, and that it is equal to the largest Lyapunov exponent λ of the dynamical system for almost all perturbation vectors \mathbf{u}_0 (Oseledec, 1968).

As has been contemplated in detail in Ref. (Parker and Chua, 1989), it can be shown by substituting $\mathbf{p}(t, \mathbf{x}_0, t_0)$ into (6.6) and subsequent derivation with respect to \mathbf{x}_0 , that the temporal evolution of the perturbation vector $\mathbf{u}(t)$ follows the so called variational equation,

$$\dot{\mathcal{V}}(t, \mathbf{x}_0, t_0) = \mathcal{J}_{\mathbf{x}} \mathbf{F}(\mathbf{p}(t, \mathbf{x}_0, t_0)) \mathcal{V}(t, \mathbf{x}_0, t_0) \quad , \quad \mathcal{V}(t_0, \mathbf{x}_0, t_0) = \mathcal{I}_n \quad , \quad (6.9)$$

whereas $\mathcal{V}(t, \mathbf{x}_0, t_0)$ is the Jacobian matrix of $\mathbf{p}(t, \mathbf{x}_0, t_0)$, evaluated at \mathbf{x}_0 , i.e., $\mathcal{V}(t, \mathbf{x}_0, t_0) = \mathcal{J}_{\mathbf{x}_0} \mathbf{p}(t, \mathbf{x}_0, t_0)$. Moreover, we have $\mathbf{x} \equiv \mathbf{p}(t, \mathbf{x}_0, t_0)$, $\mathcal{J}_{\mathbf{x}} \mathbf{F}$ denotes the Jacobian of \mathbf{F} evaluated at \mathbf{x} , and \mathcal{I}_n is the n -dimensional identity matrix. The variational equation represents a time-varying matrix-valued linear homogeneous differential equation. It can be interpreted as a linearization of the vector field along the trajectory $\mathbf{p}(t, \mathbf{x}_0, t_0)$. Since the coefficients in the variational equation depend on the evolution of the original system (6.6), the variational equation changes if the trajectory does. Hence, to calculate the maximum Lyapunov exponent, we append the variational equation to the original system and simultaneously solve the combined system

$$\begin{Bmatrix} \dot{\mathbf{x}} \\ \dot{\mathcal{V}} \end{Bmatrix} = \begin{Bmatrix} \mathbf{F}(\mathbf{x}) \\ \mathcal{J}_{\mathbf{x}} \mathbf{F}(\mathbf{x}) \mathcal{V} \end{Bmatrix} \quad , \quad (6.10)$$

where the initial conditions $\mathbf{x}(t_0) = \mathbf{x}_0$, and $\mathcal{V}(t_0, \mathbf{x}_0, t_0) = \mathcal{I}_n$ have to be implemented. Carrying out the above sketched numerical integration for a sufficiently long time period with an appropriate step size using the standard Runge-Kutta integration routine, it is straightforward to directly obtain the maximum Lyapunov characteristic exponent defined by equation (6.8) taking into account Oseledec's theoretical results mentioned above.

The above definition (6.8) only pertains the largest among the whole spectrum of Lyapunov characteristic exponents. To understand complex chaotic dynamical systems in greater depth, it might sometimes be useful to compute estimates for the whole spectrum of Lyapunov exponents.

To this end, definition (6.8), which refers to the evolution of a perturbation vector between two initial positions in phase space, can be generalized, taking up the initially introduced idea of observing the temporal evolution of a p -dimensional volume in the tangent space, whereas $1 \leq p \leq n$. To this end, consider a parallelepiped U_0 , spanned by the p linearly independent vectors u_1, \dots, u_p in tangent space. The Lyapunov exponent of order p is then defined by

$$\lambda^p(\mathbf{x}_0, U_0) = \lim_{t \rightarrow \infty} \frac{1}{t} \ln(\text{Vol}^p(\mathcal{J}_{\mathbf{x}_0} \mathbf{p}(t, \mathbf{U}_0, t_0))) \quad . \quad (6.11)$$

Thereby, Vol^p denotes the p -dimensional volume in tangent space. One main result stated in Ref. (Oseledec, 1968) says that

$$\lambda^p(\mathbf{x}_0, \mathbf{U}_0) = \lambda_1 + \dots + \lambda_p = \sum_{i=1}^p \lambda_i(\mathbf{x}_0, \mathbf{u}_i) \quad , \quad (6.12)$$

whereas each Lyapunov characteristic exponent λ_i corresponds to one of p linearly independent vectors u_i . Thus, λ^p equals the sum of the p maximum Lyapunov exponents of order $p = 1$. Analogous to the calculation of the largest Lyapunov exponent, the combined system (6.10) has to be numerically integrated to track the evolution of the parallelepiped of initial conditions in phase space. In an attempt to compute the matrix \mathcal{V} for large times t , one encounters serious numerical problems, since the columns of \mathcal{V} rapidly align with the dominating, i.e., largest Lyapunov exponent. One well-known solution to this problem is the successive implementation of a Gram-Schmidt orthonormalization procedure, executed after sufficiently short integration periods. The method has foremost been discussed in (Benettin *et al.*, 1980; Wolf *et al.*, 1984) and will be shortly introduced in the following.

Consider the set of linearly independent vectors $U_0 = \{\mathbf{u}_1, \dots, \mathbf{u}_p\}$ of initial conditions in phase space. The Gram-Schmidt orthonormalization generates an orthonormal set $V_0 = \{\mathbf{v}_1, \dots, \mathbf{v}_p\}$ of p vectors, with the property that V_0 spans the same subspace as U_0 . The formulae following Gram and Schmidt read

$$\begin{aligned} \mathbf{w}_1 &= \mathbf{u}_1 \\ \mathbf{v}_1 &= \mathbf{w}_1 / \|\mathbf{w}_1\| \\ \mathbf{w}_2 &= \mathbf{u}_2 - \langle \mathbf{u}_2, \mathbf{v}_1 \rangle \mathbf{v}_1 \\ &\vdots \\ \mathbf{w}_p &= \mathbf{u}_p - \langle \mathbf{u}_p, \mathbf{v}_1 \rangle \mathbf{v}_1 - \dots - \langle \mathbf{u}_p, \mathbf{v}_{p-1} \rangle \mathbf{v}_{p-1} \\ \mathbf{v}_p &= \mathbf{w}_p / \|\mathbf{w}_p\| \quad , \end{aligned} \quad (6.13)$$

where $\|\dots\|$ denotes the Euclidean norm of a vector, and $\langle \dots \rangle$ defines the corresponding scalar product. Furthermore, it is shown in linear algebra that the volume of the parallelepiped spanned by $\{\mathbf{u}_1, \dots, \mathbf{u}_p\}$ can be calculated according to

$$\text{Vol}^p(\mathbf{u}_1, \dots, \mathbf{u}_p) = \|\mathbf{w}_1\| \|\mathbf{w}_2\| \dots \|\mathbf{w}_p\| \quad . \quad (6.14)$$

With all necessary quantities introduced, we turn to the actual numerical computation of the Lyapunov spectra which can be described as follows. We start with determining the initial

condition of the $n \times n$ matrix $\mathcal{U}_0 \equiv (\mathbf{u}_1^0, \dots, \mathbf{u}_n^0)$ representing the n -dimensional volume in phase space as $\mathcal{U}_0 = \mathcal{I}_n$. The initial condition \mathbf{x}_0 for the original system (6.6) is chosen in the basin of attraction of the limit set under study. Furthermore, equation (6.10) is integrated for a sufficiently short time interval dt to obtain

$$x_1 = \mathbf{p}(t_0 + dt, \mathbf{x}_0, t_0) \quad \text{and} \quad \mathcal{U}_1 \equiv (\mathbf{u}_1^1, \dots, \mathbf{u}_n^1) = \mathcal{V}(t_0 + dt, \mathbf{x}_0, t_0) \mathcal{U}_0 \quad . \quad (6.15)$$

Subsequently, the set of vectors $U_1 = \{\mathbf{u}_1^0, \dots, \mathbf{u}_n^0\}$ is being orthonormalized using the above prescription to obtain $V_1 = \{\mathbf{v}_1^0, \dots, \mathbf{v}_n^0\}$. In the following, we construct the matrix $\mathcal{V}_1 = (\mathbf{v}_1^0, \dots, \mathbf{v}_n^0)$ and repeatedly integrate the combined system (6.10) for the short time period dt under the new initial conditions $\{\mathbf{x}_1, \mathcal{V}_1\}$ to obtain $\{\mathbf{x}_2, \mathcal{V}_2\}$. This orthonormalization-integration procedure can now be reapplied to the system k times. During the k -th step, the p -dimensional parallelepiped increases its volume Vol^p according to (6.14) by a factor $\|\mathbf{w}_1^k\| \|\mathbf{w}_2^k\| \dots \|\mathbf{w}_p^k\|$. Hence, the definition of the p -th order Lyapunov exponent (6.11) leads to the expression

$$\lambda^p(\mathbf{x}_0, \mathcal{U}_0) = \lim_{k \rightarrow \infty} \frac{1}{k dt} \sum_{j=1}^k \ln \left(\|\mathbf{w}_1^j\| \|\mathbf{w}_2^j\| \dots \|\mathbf{w}_p^j\| \right) \quad . \quad (6.16)$$

Since we are interested in the n first-order Lyapunov exponents, under consideration of expression (6.12), one can obtain the p -th first order Lyapunov characteristic exponent by subtracting λ^{p-1} from λ^p . Thus, the whole spectrum of Lyapunov exponents can be obtained according to

$$\lambda_p(\mathbf{x}_0, \mathbf{u}_p) = \lim_{k \rightarrow \infty} \frac{1}{k dt} \sum_{j=1}^k \ln (\|\mathbf{w}_p^j\|) \quad , \quad (6.17)$$

where one has to choose $1 \leq p \leq n$. Thereby, of course the limit $k \rightarrow \infty$ cannot be reached, but the plausibility of the quantities can be easily assessed by checking the convergence of λ_p for large time scales $k dt$.

It shall be mentioned that the approach presented above represents just one methodology out of many attempts to tackle the problem of numerically determining the whole spectrum of Lyapunov characteristic exponents. A comparative study of computation of Lyapunov spectra, utilizing different algorithms, can be found in Ref. (Ramasubramanian and Sriram, 2000).

6.3 Lyapunov Exponent Spectra of the ABCDE Model

After introducing the theoretical basis for the computation of the whole spectrum of Lyapunov characteristic exponents, some preliminary statements about the properties of the spectrum can be made before explicit results are being presented. (a) The ABCDE system ranks among the class of dissipative systems, as can be easily verified by showing that $\nabla \cdot \mathcal{F} = \Sigma(\epsilon) < 0$ where \mathcal{F} is defined in (2.3), and Σ is called phase space contraction rate, as determined explicitly in section 2.3. Thus, provided that $p = n$, the sum in (6.12) will be equal to Σ , and therefore negative since dissipation implies a contraction of phase space. In contrast, for a Hamiltonian system the sum of Lyapunov exponents would yield zero since in this case the volume in phase space

is invariant. (b) Moreover, it can be stated that at least one Lyapunov exponent will vanish, since the ABCDE model represents a continuous time dependent dynamical system exhibiting an attractor and basin of attraction whose trajectories do not contain a fixed point (Haken, 1983). The zero exponent corresponds to the slowly changing magnitude of a principal axis in phase space tangent to the direction of the flow.

In the following subsections, a generalized investigation of Lyapunov characteristic exponent spectra will be presented together with a treatment of some special cases including periodicity.

6.3.1 Spectrum for the Chaotic Regime

The results of a numerical computation of the Lyapunov characteristic exponent spectrum is presented below. Thereby, the original parameter values (Lorenz, 1963) have been applied together with $a_1 = 0.1$, $a_2 = 0.2$ and $\alpha = 0.2$. Implementing the algorithm which has been discussed in section 6.2, the five Lyapunov exponents have been computed in dependence of the control parameter ϵ . The corresponding plot is displayed in figure 6.3. The spectrum has been calculated with and without back coupling of the \mathbf{b} variables onto the Lorenz subsystem \mathbf{x} in equation (2.2). For the sake of clarity, both cases are treated independently in the following. However, in the domain $\epsilon > \epsilon_c$, the exponents of both cases merge into each other since the back reaction can be neglected due to the evanescent magnitude of b_1 and b_2 . Moreover, in both cases, one can clearly identify the zero exponent λ_2 , as predicted a priori following Haken's argumentation (Haken, 1983). It shall be noted that $\sum_{i=1}^5 \lambda_i = \Sigma(\epsilon)$ corresponds to the phase space contraction rate, and thus constitutes another possibility to re-examine the implemented algorithm's numerical accuracy. One can distinguish the following characteristics of the two Lyapunov spectra which have been superimposed printed in figure 6.3.

(a) Lyapunov characteristic exponents without back coupling If one considers only the exponents which were obtained by neglecting the back reaction, clearly the three Lyapunov exponents λ_1 , λ_2 and λ_5 , which are associated with the pure Lorenz system, can be identified. Since the Lorenz equations do not exhibit a dependence on ϵ , the exponents remain constant when the control parameter ϵ is varied. Furthermore, the computed values for the pure Lorenz subsystem are in close agreement with literature values reported in Ref. (Ramasubramanian and Sriram, 2000)(see also section 2.2). Besides the exponents which are associated to the Lorenz equations, λ_3 and λ_4 can be assigned to the \mathbf{b} variables. The exponent λ_4 remains negative on the whole interval of ϵ values, and does not contribute to the instability. The behavior of λ_3 as a function of ϵ is entirely identical to the characteristic exponent of the \mathbf{b} subsystem, which has been determined in section 4.1, and in turn, in section 6.4. The results of the present numerical calculation have therefore been validated by various independent sources.

(b) Lyapunov characteristic exponents with back coupling Considering the case when the response is turned on, in the domain $\epsilon < \epsilon_c$, the exponents that can be related to the Lorenz subsystem, as anticipated, also show a dependence on the control parameter ϵ . Moreover, all Lyapunov exponents decrease in absolute value, $|\lambda_i|$, compared to the case when the feedback is neglected, indicating a saturation of the system. As has been observed in chapter 4, the back

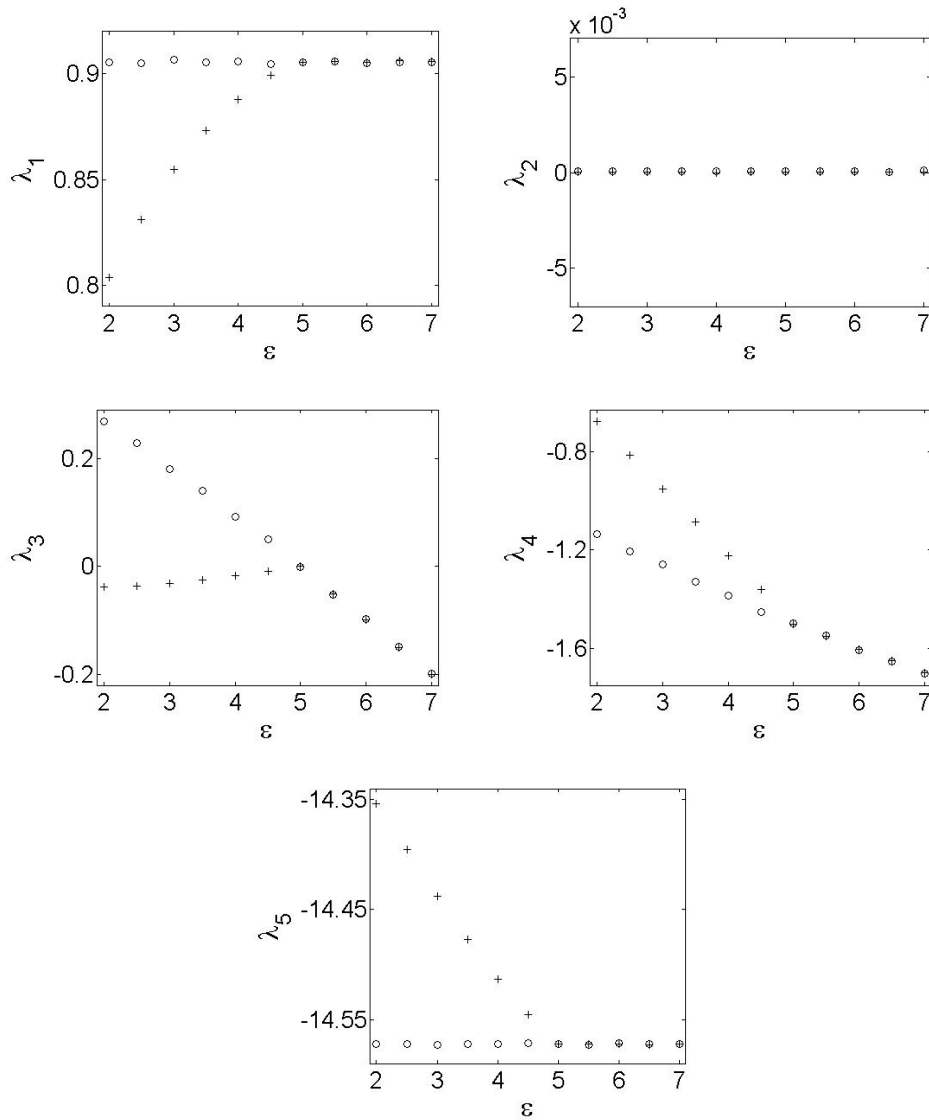


Figure 6.3: The five Lyapunov exponents in dependence of the control parameter ϵ . (a) \circ signals no back coupling of the \mathbf{b} onto the \mathbf{x} variables. (b) $(+)$ denotes results obtained when considering back coupling. Special attention should be paid to the influence of the back reaction on the behavior of the critical exponent λ_3

reaction of the \mathbf{b} variables onto the \mathbf{x} subsystem prevents the unlimited growth of $\|\mathbf{b}\|$. The same characteristic behavior is represented by the nature of λ_3 in dependence of the control parameter; for $\epsilon < \epsilon_c$, the exponent λ_3 retains a negative value due to the back coupling onto the Lorenz subsystem. For $\epsilon = \epsilon_c$ the characteristic exponent λ_3 approaches zero. Since the Lyapunov characteristic exponents presented above represent a time average, or more precisely, an asymptotic limit value (see equation (6.17)), the explicit temporal evolution of the largest characteristic exponent associated with the \mathbf{b} variables in the vicinity of ϵ_c is being treated in detail in section 6.4.

In conclusion, apparently the instability reported in chapter 4 is closely connected to the behavior of λ_3 in the vicinity of the critical control parameter value $\epsilon = \epsilon_c$. The critical Lyapunov exponent shows a dependence on ϵ , which is very similar to the case we encountered when

investigating the related trivial model system that has been discussed in section 6.1. To fully understand the nature of the intermittent bursts of activity, one has to focus its attention on the explicit temporal evolution and fluctuation of the Lyapunov characteristic exponent λ_3 . To this end, an alternative way to calculate the critical Lyapunov exponent is being presented in section 6.4. However, at first, the following subsections investigate the contribution of periodic orbits to the instability and underline an explicit application of Floquet's theory on ordinary differential equations with periodic coefficients.

6.3.2 Spectrum in Case of Limit Cycles

Chapter 2, presenting the ABCDE model, opens with an introduction of the Lorenz equations. The set of coupled ordinary differential equations, which was developed by Lorenz in 1963 when simplifying a system of fluid convection equations, serves as a paradigm for nonlinear deterministic systems exhibiting chaotic dynamics. As has been addressed in section 2.2, the Lorenz equations may give rise to stable knotted periodic orbits if the Rayleigh number r is increased. Via a sequence of Feigenbaum-type period doubling bifurcations, together with symmetry breaking bifurcations for increasing values of r , the strange attractor which is observed for $r = 28$ evolves into a limit cycle (Sparrow, 1982).

Figure 6.4 shows phase space portraits of two different limit cycle. It shall be noted that the whole ABCDE system, including the back coupling term, has been integrated for the present investigation. The feedback of the \mathbf{b} variables onto the Lorenz subsystem does not destroy the structure of the attractor for high Rayleigh numbers. However, for realizable values of the order parameter ϵ , numerical simulations show that for $r < 100.5$, the limit cycle might be destroyed as displayed in figure 6.5. The goal of the present section is to investigate an exemplary Lyapunov spectrum for a high Rayleigh number r . In this case, due to the periodicity of the \mathbf{x} variables, analytic solutions for \mathbf{b} can be found by means of Floquet's theory. Applying the algorithm for the general calculation of Lyapunov exponents in case of the explicit Rayleigh number $r = 147.5$, the spectrum displayed in figure 6.6 has been obtained. In this case, a bifurcation occurs for a critical value of $\epsilon_c \approx 0.4$. Above the threshold $\epsilon > \epsilon_c$,

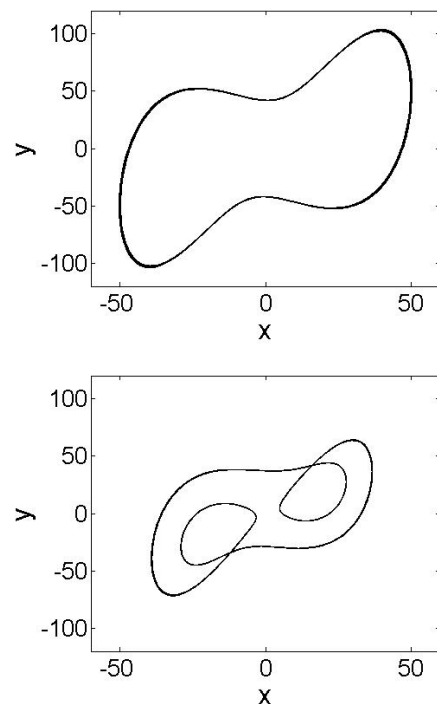


Figure 6.4: Projection of attractor onto x-y plane in the case of high Rayleigh numbers ($r = 350$ for upper, and $r = 148.5$ in case of lower diagram)

we observe one zero, and four negative characteristic Lyapunov exponents. This observation is in agreement with the expected behavior of Lyapunov exponents in presence of an attractive

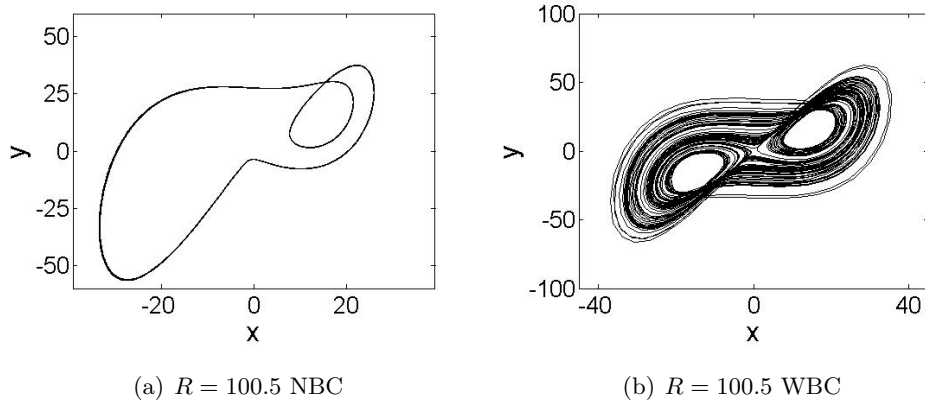


Figure 6.5: Projection of attractor onto x-y plane for $r = 100.5$. Comparison of computation with (WBC) and without back coupling (NBC) of the \mathbf{b} variables onto the \mathbf{x} subsystem

limit cycle (Argyris *et al.*, 1994). The characteristic exponents behave discontinuously at the critical value ϵ_c , and for parameters $\epsilon < \epsilon_c$, we monitor one positive (λ_1), two zero (λ_2, λ_3), and two negative (λ_4, λ_5) Lyapunov characteristic exponents. Thus, the bifurcation of the ABCDE system of differential equations encountered for $r = 147.5$ gives rise to hyper-chaotic dynamics closely below the critical control parameter value $\epsilon = \epsilon_c$.

Bifurcations of the kind observed in the present section are often accompanied by *hysteretic behavior* (Haken, 2004). The investigation of the first moment $\langle r \rangle$ clearly shows a hysteresis when increasing and subsequently decreasing the value of ϵ , as displayed in figure 6.7. The observed hysteretic behavior allows the conclusion, that we encounter *subcritical dynamo action*, since non-magnetic convection solutions coexist at the same parameter values together with hydromagnetic solutions, and are stable against small magnetic perturbations. For a numerical investigation of a subcritical dynamo bifurcation in the Taylor Green flow and further information, we refer the reader to (Ponty *et al.*, 2007).

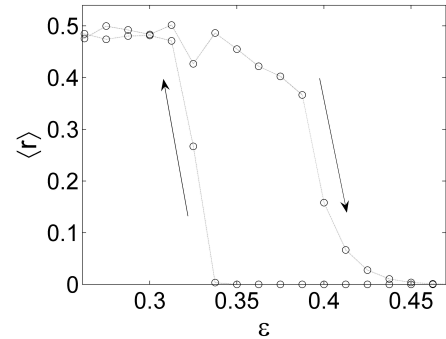


Figure 6.7: Hysteresis of the variable $\langle r \rangle$, which is shown in dependence of the control parameter ϵ whereby $r = 147.5$

Construction of a Solution by Means of Floquet's Theory

Together with the theoretical framework presented in section 3.2.1, it is possible to find solutions to the variables b_1 and b_2 by applying Floquet's theory. If we consider the general solution of a system of ordinary differential equations with periodic coefficients according to equation (3.8), it becomes evident that, to this end, we have to determine the characteristic Floquet exponents σ_1 and σ_2 by computing the period T of $\mathcal{L}(t)$, as well as the eigenvalues μ_1 and μ_2 of the matrix $\mathcal{K}(T, 0, \mathcal{L}(t))$. Apart from theorem 1, Floquet theory does not make any further specification

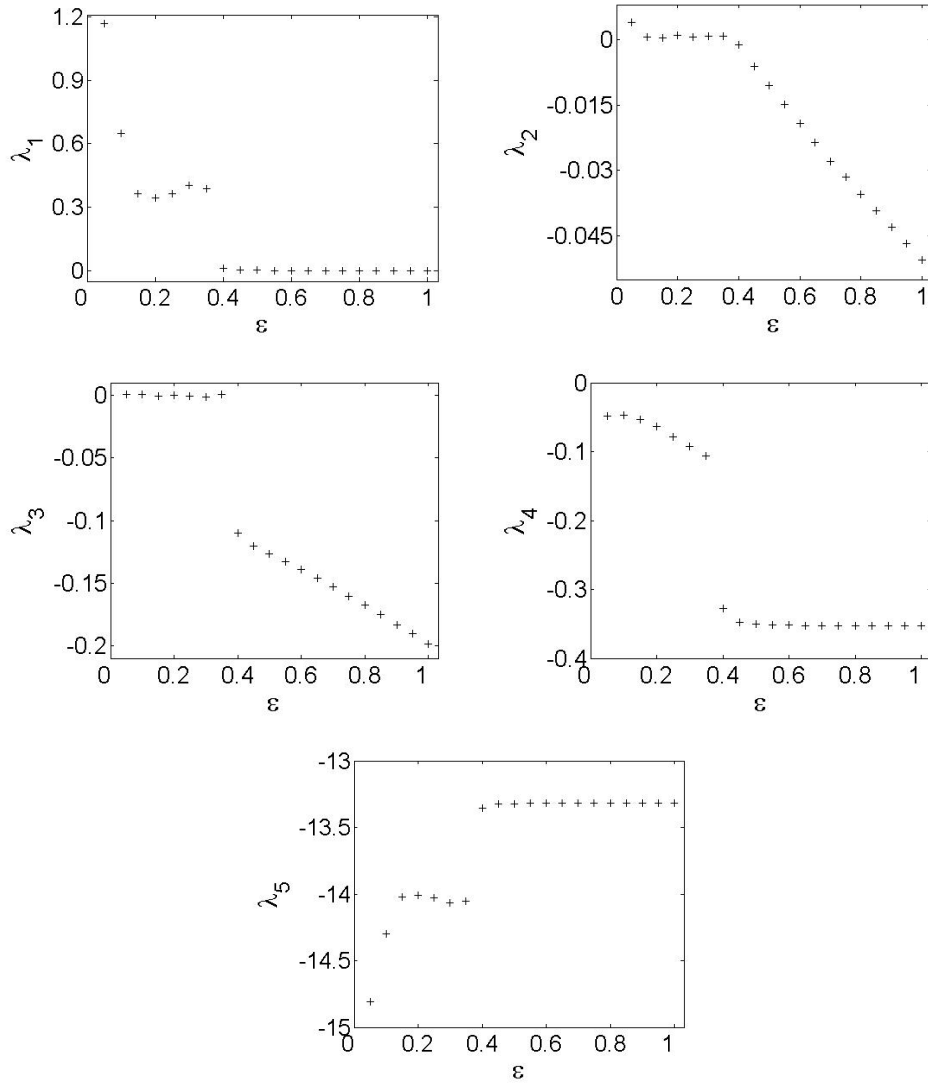


Figure 6.6: Lyapunov exponents in case of a limit cycle ($r = 147.5$) as functions of the control parameter ϵ

concerning the coefficients $\mathbf{q}^{j,i}(t)$ of the exponential functions. Therefore, a suitable ansatz for the polynomials with periodic coefficients has to be conjectured. In the following, we shall give an outline of the technical procedure to determine a particular solution in terms of Floquet's theory. In order to construct a particular solution in presence of a limit cycle, let us start with the computation of the period T . Different Rayleigh numbers r lead to various limit cycles with deviating periodicity, as can be reviewed in Ref. (Sparrow, 1982). To calculate the period T for a given limit cycle with high accuracy, the so called Hénon trick, which was foremost discussed in Ref. (Hénon, 1982), has been applied to the system of differential equations. Thereby, the basic theoretical framework is briefly addressed in appendix A.

Having obtained a precise value for the period T , one has to focus on the construction of the matrix $\mathcal{K}(T, 0, \mathcal{L}(t))$. To this end, it is very convenient to integrate the full ABCDE system for the preassigned time interval T , using the two initial conditions $\mathbf{b}_0^1 = (1, 0)$ and $\mathbf{b}_0^2 = (0, 1)$

for the \mathbf{b} variables, while choosing \mathbf{x}_0 arbitrarily, to obtain $\mathbf{b}^1(T)$ as well as $\mathbf{b}^2(T)$. Hence, this approach immediately yields the result $\mathcal{K}(T, 0, \mathcal{L}(t)) = (\mathbf{b}^1(T), \mathbf{b}^2(T))$. Subsequently, the eigenvalues $\mu_{1,2}$ of the matrix $\mathcal{K}(T, 0, \mathcal{L}(t))$ can be obtained numerically, in order to determine the characteristic Floquet exponents σ_1 and σ_2 . In the following, an appropriate approach for the polynomials that exhibit periodic coefficients $\mathbf{q}^{(j,i)}(t)$, which meets the requirements to simulate the numerically obtained temporal evolution of \mathbf{b} , can be found.

The Floquet exponents have been explicitly computed for $r = 350$. The corresponding limit cycle can be reviewed in figure 6.4, while figure 6.8 shows the projection of a numerically determined trajectory onto the b_1 - b_2 plane, together with an approximation of the solution by means of Floquet's theory. The approximative solution is not scaled appropriately but shall

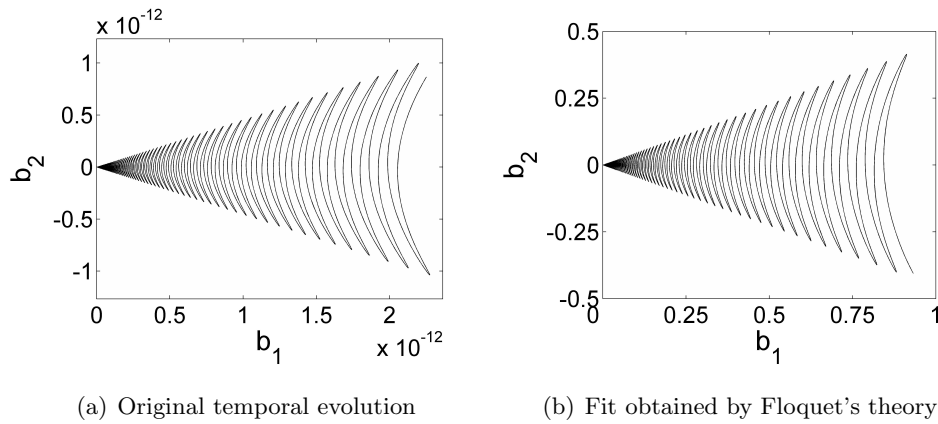


Figure 6.8: Approximation of solution for the variable \mathbf{b} by means of Floquet's theory. r is chosen to hold $r = 350$, so that the Lorenz subsystem exhibits a limit cycle

qualitatively approve the claim that solutions for the \mathbf{b} variables can be found with the help of Floquet formalism in presence of periodic solutions, which are evoked by the existence of a limit cycle. The full expression, leading to the solution which is plotted in figure 6.8 (b), reads

$$\mathbf{b}_f(t) = \mathbf{q}^{1,1}(t) \exp(\ln(\sigma_1)t/T) + \mathbf{q}^{1,2}(t) \exp(\ln(\sigma_2)t/T) \quad , \quad (6.18a)$$

whereby

$$\mathbf{q}^{1,1}(t) = \begin{pmatrix} c_1(\sin^2(2\pi t/T) + 1) \\ c_2 \sin(2\pi t/T) \end{pmatrix} \quad \mathbf{q}^{1,2}(t) = \begin{pmatrix} c_3(\sin^2(2\pi t/T) + 1) \\ c_4 \sin(2\pi t/T) \end{pmatrix} \quad . \quad (6.18b)$$

The constants c_1, \dots, c_2 have to be chosen appropriately to recover the dynamics. Since the multiplicity of the elementary divisor associated with both eigenvalues μ_1 and μ_2 is given by $n_j = 1, j = 1, 2$, the degree of each polynomial is at most zeroth-order.

In conclusion, considering the behavior of the ABCDE model under the assumption that the Lorenz subsystem exhibits a limit cycle for $r = 147.5$, we have found evidence that the bifurcation, encountered at the critical parameter value ϵ_c , gives rise to hysteretic behavior, hyper-chaotic dynamics and subcritical dynamo action. Moreover, we have showed that an explicit solution to the \mathbf{b} variables can be found by application of Floquet's theory.

6.3.3 Spectrum for the Chaotic Regime with Respect to Periodic Orbits

After switching temporarily to higher Rayleigh numbers, the present subsection again treats the original parameter values used by Lorenz (Lorenz, 1963). After examining the case of periodic solutions when the Lorenz subsystem exhibits a limit cycle, it is tempting to also investigate periodic orbits of the Lorenz attractor in the chaotic regime employing $r = 28$. The significance of this examination becomes immediately clear when considering the widely-spread, albeit mathematically naive, definition of an attractor, identifying an attracting or repelling set as a collection of periodic orbits. It has to be noted that the periodic orbits of the Lorenz attractor are unstable in the chaotic regime, and therefore the computation is numerically not stable either. Thus, unlike in the previously treated case of limit cycles, the back reaction of the \mathbf{b} variables onto the Lorenz subsystem has to be neglected. Furthermore, the accuracy of the numerical calculation has to be increased, and the integration period, as well as the Runge-Kutta step size, shortened to ensure reliability of the results.

Various methods have been developed to identify and find periodic orbits in dynamical systems, especially in case of the Lorenz system's strange attractor (Letellier *et al.*, 1994; Eckhardt and Ott, 1994; Franceschini *et al.*, 1992). However, for the sake of efficiency and to keep the focus of this thesis, we have resorted to another method to study the dynamics of periodic solutions by implementing literature values, defining periodic orbits, as initial conditions of our calculations. To this end, we have consulted results stated in Ref. (Letellier *et al.*, 1994) to identify and proof the existence of periodic solutions of the pure Lorenz system. Figure 6.10 shows the Lyapunov spectrum, which we have obtained by applying the above presented algorithm taking into account the special initial conditions, up to fundamental period $m = 4$. The notation used to explicitly identify certain m -periodic orbits thereby follows Ref. (Letellier *et al.*, 1994). To clarify the notation, one might consider the two symmetric wing Lorenz mask displayed in figure 6.9. According to the dynamics of the system on the Lorenz mask or the corresponding template, one can identify each symmetric and asymmetric periodic orbit of period m . Thereby, each periodic orbit is uniquely determined by an encoding partition given by the letter 0 if the system remains on the same wing, and letter 1 if it changes to the other one. Since symmetric orbits return to their initial conditions after the period T , their encoding sequence exhibits an odd number of 1's, while one should bear in mind that asymmetric orbits always occur in pairs.

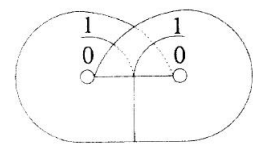


Figure 6.9: The Lorenz mask according to (Letellier *et al.*, 1994)

As can be concluded from figure 6.10, the basic periodic cycle, i.e. orbit 1, does not contribute to the instability. The critical value for the control parameter ϵ shifts rapidly from close to zero to higher values and approaches $\epsilon_c = 5$ with increasing period m of the corresponding unstable orbits. Furthermore, when comparing two orbits with same period m but different symmetry, it becomes evident that the characteristic exponent in case of asymmetric orbits shows a slightly different behavior than in case of symmetric orbits; even though the critical point ϵ_c seems to be identical in any case, the slope of the characteristic exponent in dependence of ϵ is apparently larger in the

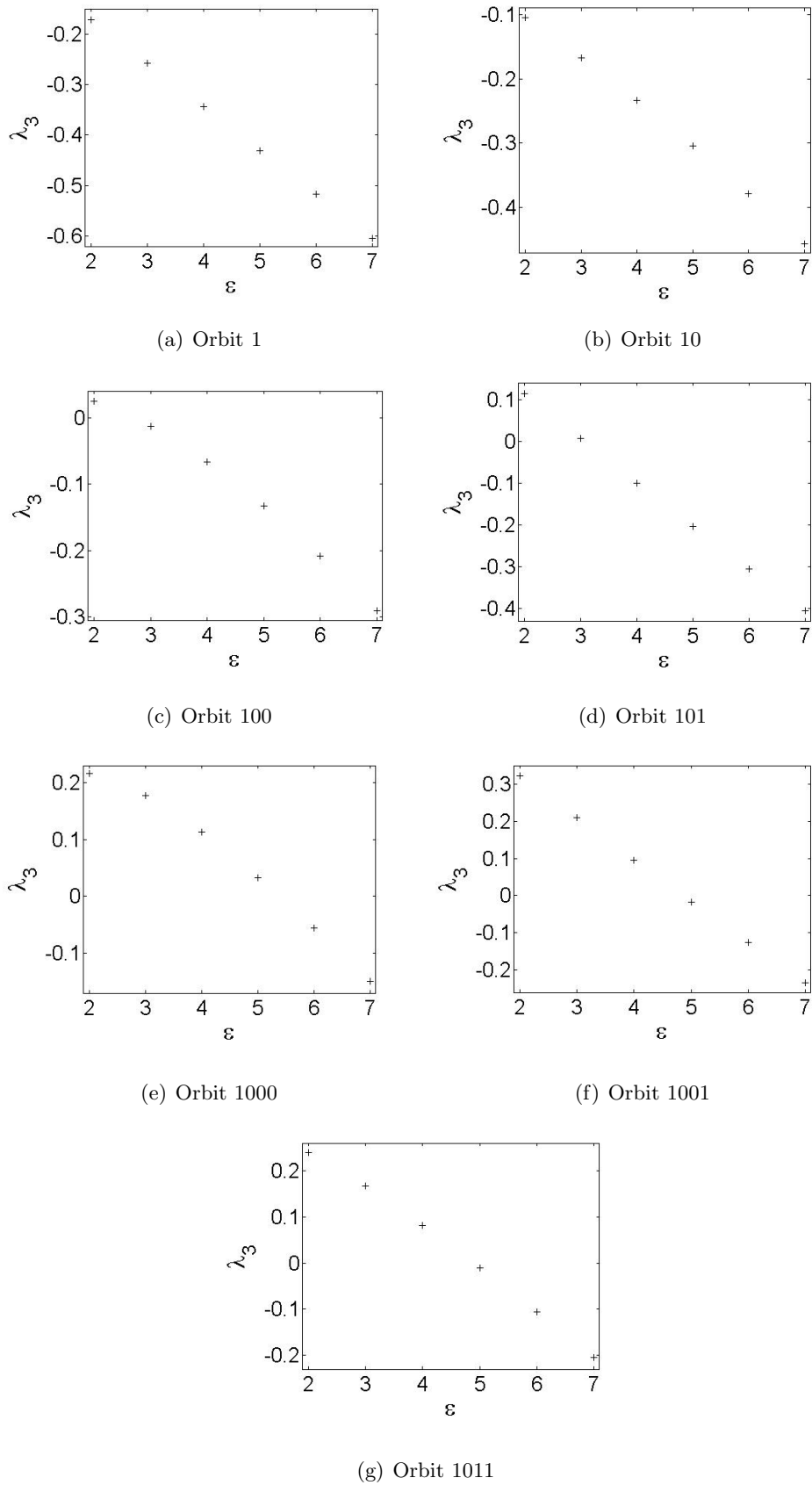


Figure 6.10: The critical Lyapunov characteristic exponent λ_3 for periodic orbits up to period $m = 4$ as a function of the control parameter value ϵ . Clearly one can observe the shift of onset with increasing periodicity T

asymmetric case. To visualize the denotation of periodic orbits and to verify the results above, figure 6.11 displays projections of three different periodic orbits on the x - y plane, together with corresponding phase space projections on the b_1 - b_2 subspace. The control parameter $\epsilon = 2$ is fixed to monitor either exponentially decreasing or growing solutions of \mathbf{b} . If the characteristic Lyapunov exponent is positive for a certain periodic orbit assuming $\epsilon = 2$, one should observe an exponentially increasing solution, while \mathbf{b} should decrease in an exponential manner otherwise. Hence, taking the correspondent characteristic exponents in figure 6.10 under consideration, the results shown in diagram 6.11 correspond very well with our theoretical expectations.

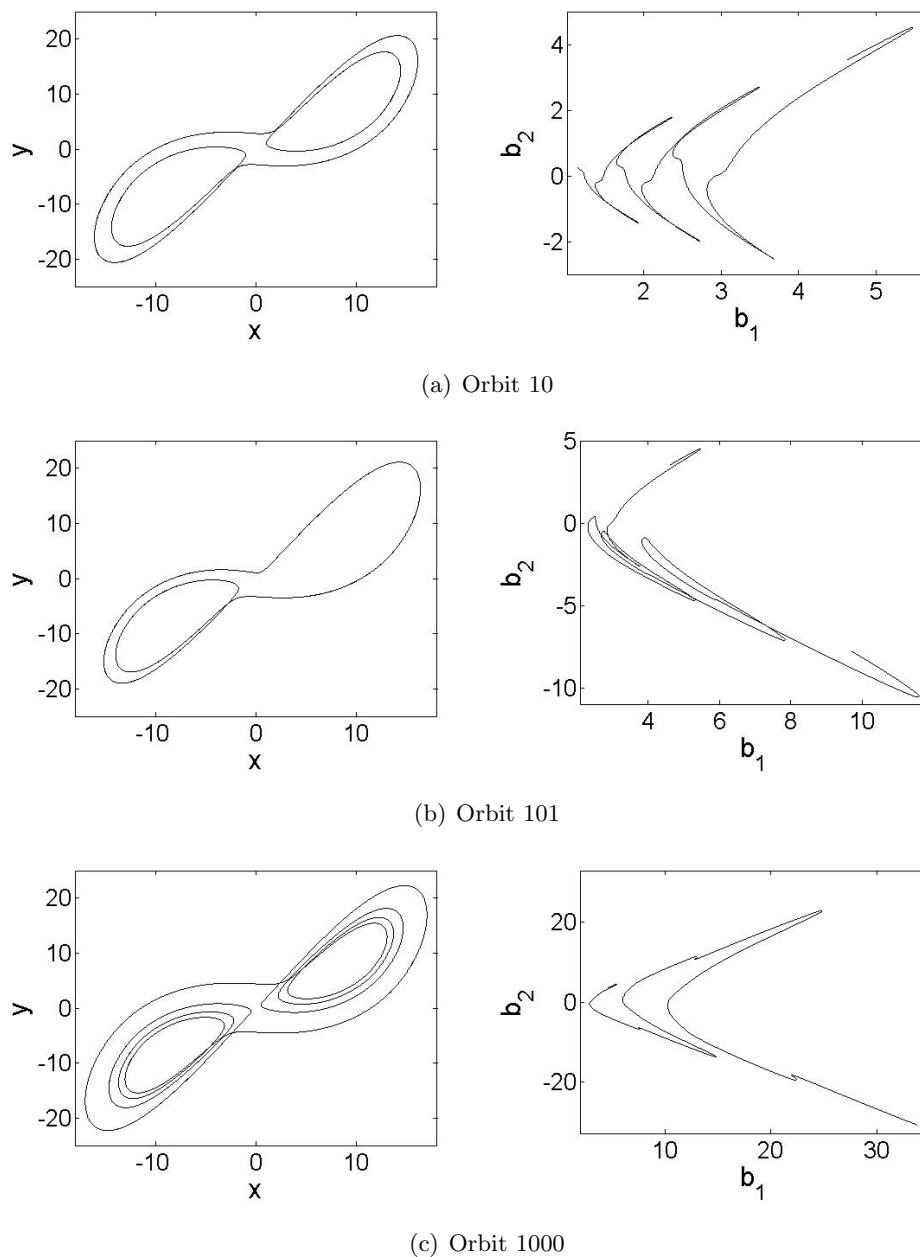


Figure 6.11: Projections of trajectory onto the x - y plane (first column) and b_1 - b_2 plane (second column). Shown are three different periodic orbits evaluated under use of the initial conditions $\mathbf{b}(0) = (4.5, 3.5)$ while $\epsilon = 2$ is fixed

Construction of a Solution by Means of Floquet's Theory

Corresponding to the construction of a solution to the \mathbf{b} variables as discussed in the previous section, one can also investigate the case when the Lorenz equations exhibit unstable periodic solutions in the chaotic regime. In this particular case, a special solution for b_1 and b_2 can also be found by applying Floquet's theory on differential equations with periodic coefficients. According to the theoretical framework presented in section 3.2.1, at first the period T has to be calculated, utilizing the Henon-trick as described in appendix A. Subsequently, the matrix $\mathcal{K}(T, 0, \mathcal{L}(t))$ is being assembled in order to numerically determine its characteristic roots by standard methods. In a final step, a suitable ansatz for the polynomial $\mathbf{q}^{(j,i)}(t)$ possessing periodic coefficients is to be conjectured. Figure 6.12 shows a projection of the directly computed trajectory onto the b_1 - b_2 plane, as well as the corresponding qualitative fit, which has been derived by means of Floquet's theory. Since we investigate the periodic orbit 1000 while $\epsilon = 2$ is fixed, we obtain an exponentially increasing solution due to a positive Floquet exponent, as can be verified when consulting the corresponding Lyapunov spectrum as depicted in figure 6.10. The full model equation leading to the reconstructed solution in figure 6.12 reads

$$\mathbf{b}_f(t) = \mathbf{q}^{1,1}(t) \exp(\ln(\sigma_1)t/T) + \mathbf{q}^{1,2}(t) \exp(\ln(\sigma_2)t/T) \quad , \quad (6.19a)$$

whereas

$$\mathbf{q}^{1,1}(t) = \begin{pmatrix} c_1 |\sin(2\pi t/T)|^{3/2} + c_2 \\ c_3 \sin(2\pi t/T) \end{pmatrix} \quad \mathbf{q}^{1,2}(t) = \begin{pmatrix} c_4 |\sin(2\pi t/T)|^{3/2} + c_5 \\ c_6 \sin(2\pi t/T) \end{pmatrix} \quad . \quad (6.19b)$$

The constants c_1, \dots, c_6 have to be chosen in a suitable manner to recover the intrinsic motion. The directly obtained phase space portrait in graph 6.12 is in very close agreement with the corresponding constructed solution represented by equations (6.19).

As can be concluded when comparing the trajectory with the model solution plotted in figure 6.12, we are able to find a solution to simulate the qualitative behavior of b_1 and b_2 when the back coupling of the \mathbf{b} variables on the Lorenz system is turned off, and when the \mathbf{x} subsystem exhibits periodic solutions. Thus, the present section sets another example for the successful application of Floquet's theory. Furthermore, we have been able to reveal the individual contribution of various symmetric and asymmetric periodic orbits of the chaotic Lorenz attractor to the onset of the observed nonequilibrium phase transition.

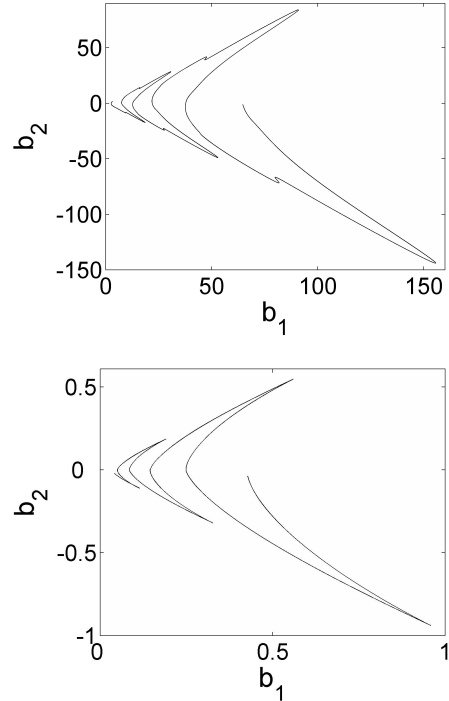


Figure 6.12: Construction of solution for Orbit 1000, while $\epsilon = 2$ is kept constant

6.4 Another Approach to Determine the Characteristic Exponent

In section 4.1, we have already discussed one possible attempt to investigate the critical characteristic exponent in dependence of the control parameter ϵ . This particular approach was foremost introduced in Ref. (Friedrich and Haken, 1992) and is based on a coordinate transformation which leads to a first order differential equation for one of the new variables. The resulting expression thereafter can be solved formally by an exponential ansatz. Thereby, the back reaction of the \mathbf{b} variables on the Lorenz subsystem is being neglected. The method presented in section 4.1 certainly leads to reliable results; however due to the transformation into hyperbolic coordinates and the particular form of equation (4.1) comprising hyperbolic functions, it is difficult to gain a deeper descriptive understanding.

The present section aims at discussing an alternative approach to determine the characteristic exponent of the \mathbf{b} subsystem as a function of the control parameter ϵ . Considering the special form of the \mathbf{b} equations (2.2a), it is tempting to define a new independent variable $w(t)$ according to

$$w(t) = \frac{b_2(t)}{b_1(t)} \quad , \quad (6.20)$$

which is well-defined since $b_1(t) \neq 0$ for all t . Substituting (6.20) into the differential equations determining the \mathbf{b} subsystem (2.2a), we derive a first order nonlinear differential equation for b_1

$$\dot{b}_1 = (-\epsilon a_1 + \alpha x w) b_1 \quad , \quad (6.21)$$

as well as a Riccati-type differential equation for the newly introduced variable $w(t)$ reading

$$\dot{w} = -\epsilon(a_2 - a_1)w - (\alpha x)w^2 + \alpha x \quad . \quad (6.22)$$

It shall be mentioned that equation (6.22) represents a special case of the generalized Riccati equation. For further details concerning this type of nonlinear ordinary differential equations, the reader is referred to Ref. (Reid, 1972; Bittanti, 1991; Zwillinger, 1989). The new variable $w(t)$ is expected to be a strongly fluctuating quantity, since $x(t)$ apparently represents a rapidly varying degree of freedom. Taking into account the results of phase space projections gained in chapter 4, we immediately can identify the constraint $|w(t)| < 1$ for sufficiently large times t . Numerical observations confirm the above statements, and $w(t)$ is observed to fluctuate heavily between the values $+1$ and -1 , while the mean value in time depends on the control parameter ϵ . It shall be noted that $w_{1,2}^0 = \pm 1$ represent two stationary solutions in the limiting case $\epsilon = 0$.

A general solution to equation (6.21) can be obtained by direct integration, yielding

$$b_1(t) = b_1(0) \exp \left(\int_{t_0}^t d\tau [-\epsilon a_1 + \alpha x(\tau)w(\tau)] \right) \quad . \quad (6.23)$$

Allowing for the results presented in section 3.2.2 concerning ordinary differential equations with real bounded coefficients, the solution (6.23) might be written as

$$b_1(t) = b_1(0) \exp(\Lambda(t) t) \quad , \quad (6.24a)$$

whereas

$$\Lambda(t) = \frac{1}{t} \int_{t_0}^t d\tau [-\epsilon a_1 + \alpha x(\tau)w(\tau)] \quad . \quad (6.24b)$$

Apparently, this result only holds true under the assumption that the time limit $\Lambda = \lim_{t \rightarrow \infty} \Lambda(t)$ exists. Expression (6.24b) provides an insight into the behavior of the critical characteristic exponent Λ as a function of the control parameter ϵ . The temporal evolution of the variables w and x can be determined by integrating the ABCDE system in its transformed variables, while the back reaction of w and b_1 onto the Lorenz subsystem is being neglected. Subsequently, equation (6.24b) can be evaluated for various values of the control parameter ϵ . Figure 6.13 shows the numerically determined characteristic exponent Λ in dependence of the control parameter ϵ . The transition at about

$\epsilon_c = 5$ is again being confirmed, and the result recovers the same behavior of Λ as encountered in section 4.1. However, equation (6.24b) sheds new light on the transition pathway, since the slope of Λ in figure 6.13 can be identified as being mainly

determined by the first summand in (6.24b), i.e. by $-a_1 = -0.1$. The second summand in (6.24b), even though also slightly dependent on ϵ , mainly determines the intercept with the y-axis. Thus, the behavior of the critical Lyapunov exponent in the case of different periodic orbits, as presented in section 6.3.3, becomes comprehensible in terms of the above results.

Λ itself is of course also a strongly fluctuating quantity in time. This conclusion is not contradictory to (6.24) since the approach only requires $\lim_{t \rightarrow \infty} \Lambda(t)$ to exist. Therefore, it is tempting to explicitly examine the temporal evolution of the exponent Λ when the system is near the transitional state. If the chaotic bursts of the characteristic variables \mathbf{b} or r are unmistakably associated with the intermittent positivity of the characteristic exponent Λ , an exhaustive description of the transition leading to dynamo action in the ABCDE model would have been revealed. To this end, a function $\sigma(z)$ with $z \in \mathbb{R}$ is being defined, obeying

$$\sigma(z) = \begin{cases} 1 & z > 0 \\ 0 & \text{else} \end{cases} \quad . \quad (6.25)$$

The mapping $\sigma(z)$ can now be applied to a time series of the quantity $\Lambda(t)$, which is obtained by evaluating the right hand side of equation (6.24b). Thereby, $\Lambda(t)$ fluctuates heavily around a certain mean value depending on the control parameter ϵ . Closely

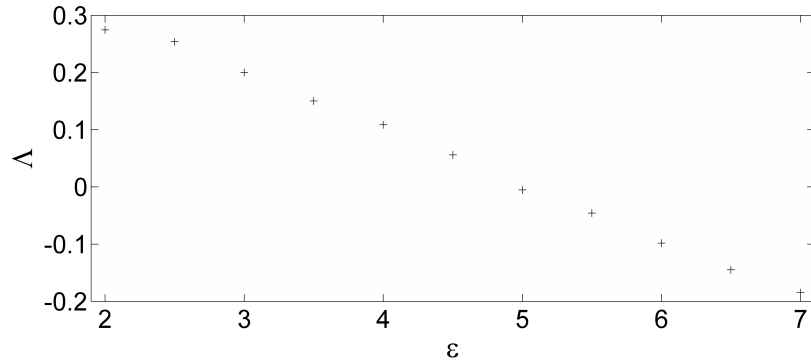


Figure 6.13: Characteristic exponent as function of order parameter ϵ

above the threshold ϵ_c , the mean takes a slightly negative value close to zero and becomes positive on intermittent temporal intervals. Figure 6.14 monitors a time series of the variable b_1 obtained by direct integration of the underlying differential equations, together with a bar plot of the mapping $\sigma(\Lambda)$ as a function of the time t . A strong correlation between chaotic bursts of activity and a locally positive characteristic exponent becomes apparent when comparing the time dependent graphs. In a final conclusion, the intermittent temporal evolution of the characteristic exponent $\Lambda(t)$ can be identified as the direct cause of the instability which builds the foundation of this thesis.

In summary, the present chapter focuses on the investigation of Lyapunov characteristic exponents as a measure of chaoticity in the ABCDE system. Apart from the expected behavior of the critical characteristic exponent, we have provided an introduction into the theoretical framework. Moreover, we have presented results regarding the determination of the spectrum of Lyapunov characteristic exponents in the chaotic regime, as well as in the case of high Rayleigh numbers. In the latter regime, we have recorded hysteretic behavior resulting in subcritical dynamo action and hyperchaotic dynamics. Utilizing results obtained from Floquet's theory, we have derived explicit solutions to reconstruct the evolution of the \mathbf{b} variables. Furthermore, employing standard parameter values, we have clarified the contribution of individual periodic orbits of the strange Lorenz attractor to the observed instability. Corresponding solutions for the \mathbf{b} variables have been identified using Floquet's theory. In a final step, we have revealed the immediate fundamental cause for the observation of intermittent bursts of magnetic activity, in terms of the disclosure of a locally positive characteristic exponent.

The following section shall introduce a stochastic treatment of the fundamental instability. In general, the description of deterministic dynamical systems by means of suitable stochastic processes is a widely accepted approach to reveal characteristic properties of the underlying dynamics. Having extensively scrutinized the concept of Lyapunov characteristic exponents to reveal the nature of the nonequilibrium phase transition, the modeling of chaotic dynamics in terms of an appropriate stochastic process bares a further extremely relevant field of interest.

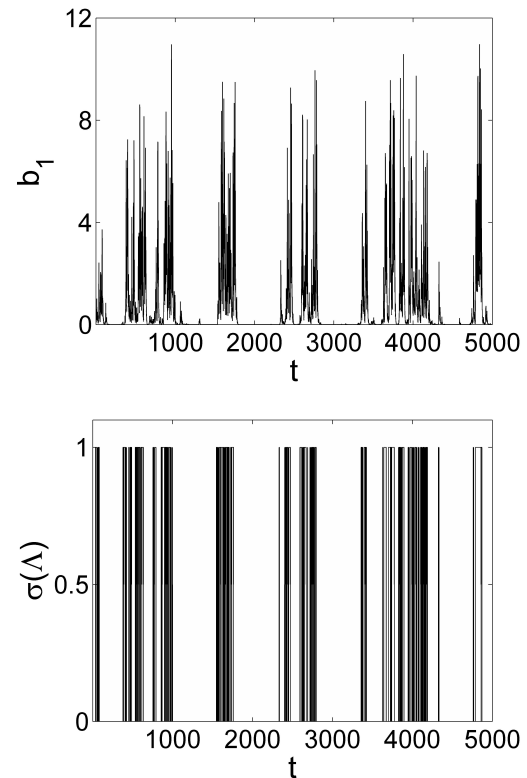


Figure 6.14: Directly obtained time series of variable b_1 (upper diagram) and mapping $\sigma(\Lambda)$ as a function of the time t (lower diagram)

Chapter 7

Stochastic Treatment of the Transition

As has been addressed in previous chapters, chaotic dynamics can be related to exponential divergence of nearby trajectories in phase space, giving rise to paramount sensitivity on uncertainties in initial conditions; a fact that intuitively suggests a stochastic description of the underlying deterministic dynamics. Modeling certain degrees of freedom, which correspond to dynamical systems, by stochastic processes is a widely discussed subject in theoretical as well as experimental physics. Research on the simulation of chaotic dynamics by suitable stochastic model equations has, for instance, been extensively discussed in the area of hydrodynamics (Friedrich and Peinke, 1997a), in the increasingly popular field of climate models (Majda *et al.*, 2006), in the study of tremor data from patients suffering from Parkinson's disease (Gradišek *et al.*, 2000), in stock market data analysis (Friedrich *et al.*, 2000), as well as in experiments on electronic circuits (Stemler *et al.*, 2007). Many of the approaches are based on time scale separation through the introduction of a small parameter, allowing to describe fast chaotic degrees of freedom in terms of noise acting on slow relevant variables.

The present chapter aims at modeling certain degrees of freedom of the ABCDE model, which is represented by the system of nonlinear ordinary differential equations given in (2.2), by suitable stochastic processes. To this end, in the following we present some important stochastic model equations for nonlinear dynamical systems and various applications to chaotic time series. The stochastic treatment discussed in this chapter comprises the computation of drift and diffusion coefficients, as well as the setup for a suitable stochastic description of the dynamical system under investigation. Furthermore, the reliability of the approach is being addressed since it is crucial to check whether the results obtained by a stochastic treatment of a dynamical system remain meaningful, owing to the fact that most methods are based on far-reaching mathematical idealizations. In a final step, the deterministic dynamics of the ABCDE model are being reconstructed by means of suitable stochastic differential equations. Probability density estimates for the \mathbf{b} variables are computed and compared for a final verification. However, we shall start with a brief introduction into the basic theory of a class of stochastic differential equations.

7.1 Brief Introduction into Stochastic Calculus

In the present section, some basic and essential properties of stochastic differential equations shall be presented. The reader is referred to (Frank, 2005; Haken, 2004; Gardiner, 2004; Risken, 1989; Horsthemke and Lefever, 1984) for a detailed discussion and further information. The motivation to treat dynamical systems by means of suitable stochastic approaches is often given by the observation of microscopic and macroscopic processes within a given system. Microscopic degrees of freedom often manifest themselves in form of heavy fluctuations, while the corresponding macroscopic degrees of freedom evolve on a much longer time scale. Even though the macroscopic processes are a direct result of many, sometimes coherent, microscopic mechanisms themselves, it is a generally prevalent approach to describe the entire system by adding additional terms, which account for the fluctuations, to the otherwise deterministic equations governing the macroscopic quantities. Within the theory of stochastic differential equations, being able to account for many properties of chaotic dynamical systems, the fluctuations are often treated in a mathematically idealized way, which is discussed in the following.

Consider a single, time-dependent variable $x(t)$, whereby out of the continuous flux of time t , a discrete set of times t_i is chosen. It is assumed that the time intervals $\Delta t = t_{i+1} - t_i$ remain constant. The influence of deterministic and fluctuating forces on the variable x might then be described by

$$\Delta x(t_i) = K(x(t_{i-1}))\Delta t + \Delta w(t_i) \quad , \quad (7.1)$$

whereas $\Delta x(t_i) = x(t_i) - x(t_{i-1})$, and $\Delta w(t_i) = w(t_i) - w(t_{i-1})$ constitutes the influence of microscopic fluctuations on the deterministic macroscopic process described by x . In order to find a suitable description of the fluctuating forces, one resembles to the framework of statistics, as will be addressed later in this section. Quite often the fluctuations Δw happen to appear jointly with the quantity x . Thus, one has to consider stochastic differential equations of the general form

$$\Delta x(t_i) = K(x(t_{i-1}))\Delta t + g(x)\Delta w(t_i) \quad . \quad (7.2)$$

The notation of the function $g(x)$ in (7.2) leaves the question open at what time the variable x in the argument of $g(x)$ has to be evaluated. It emerges that this time cannot be chosen arbitrarily, whereas two distinct approaches have gained particular scientific recognition - the $\hat{\text{I}}\text{to}$ and Stratonovich interpretation of stochastic calculus. According to $\hat{\text{I}}\text{to}$, x in $g(x)$ is taken at time t_i , which leads to a decorrelation of $x(t_{i-1})$ and $\Delta w(t_i)$. In contrast, Stratonovich proposed to take x at the midpoint between the times t_{i-1} and t_i , i.e., at the time $(t_i + t_{i-1})/2$. While $\hat{\text{I}}\text{to}$'s interpretation simplifies mathematical operations but often does not represent the most natural choice in a physical context, one often resembles to the Stratonovich formalism when formulating specific problems, for instance in the discipline of engineering. Moreover, the Stratonovich formalism allows variables to be transformed in accordance with ordinary calculus applicable to normal differential equations. In order to keep the focus of this thesis, we shall end

the introduction into Itô and Stratonovich calculus here, and we refer the reader to corresponding standard work (Gardiner, 2004; Risken, 1989; Horsthemke and Lefever, 1984). However, it should be noted that both approaches yield the same results if the fluctuating forces are independent of variable x and time t . Then, the corresponding stochastic differential equations represent a special case of the Itô and Stratonovich equations and are called Langevin equations (Haken, 2004). The Langevin equations, which describe the temporal evolution of a stochastic variable \mathbf{x} , possess corresponding Fokker-Planck equations, accounting for the temporal evolution of the conditional probability density distribution p of the stochastic variable \mathbf{x} .

7.1.1 The Langevin and the Fokker-Planck Equation

The approach proposed in Ref. (Gradišek *et al.*, 2000; Siegert *et al.*, 1998; Friedrich and Peinke, 1997b) represents a general method for the estimation of drift and diffusion coefficients of the corresponding Fokker-Planck equation, valid for stationary continuous stochastic processes with Markovian properties. The treatment focuses on an important and wide class of dynamical systems, which can be described in terms of Langevin equations. Thereby, the evolution of a n -dimensional stochastic variable $\mathbf{x}(t)$ in phase space \mathfrak{S} is governed by

$$\frac{dx_i(t)}{dt} = h_i(\mathbf{x}(t)) + \sum_j g_{i,j}(\mathbf{x}(t)) \Gamma_j(t) \quad , \quad i, j = 1, \dots, n \quad , \quad (7.3a)$$

where

$$\langle \Gamma_i(t) \rangle = 0 \quad , \quad \langle \Gamma_i(t) \Gamma_j(t') \rangle = Q \delta_{ij} \delta(t - t') \quad \forall i, j \quad . \quad (7.3b)$$

The quantity Γ_i denotes random noise which is assumed to be uncorrelated and to exhibit vanishing mean value, while Q determines the noise amplitude. Thus, the time derivative of the stochastic vector \mathbf{x} is defined by a sum of a deterministic, \mathbf{h} , and a stochastic part, $\mathbf{g} \cdot \mathbf{\Gamma}$. Apart from (7.3b), no further assumptions on the matrix \mathbf{g} or the vector \mathbf{h} have to be made, and \mathbf{h} may also contain nonlinearities to account for the formulation of deterministic chaos.

The random terms in equation (7.3) generally precludes the identification of distinct solutions to the Langevin equation. An alternative way to model the underlying dynamical system is based on the description of the stochastic process by a conditional probability density distribution, $p(\mathbf{x}, t)$, of the n -dimensional stochastic variable \mathbf{x} in phase space \mathfrak{S} . It can be shown that the temporal evolution of $p(\mathbf{x}, t)$ is governed by the deterministic Fokker-Planck equation reading (Haken, 2004; Gardiner, 2004; Risken, 1989)

$$\frac{\partial p(\mathbf{x}, t)}{\partial t} = \left(- \sum_{i=1}^n \frac{\partial}{\partial x_i} D_i^{(1)}(\mathbf{x}, t) + \frac{1}{2} \sum_{i,j=1}^n \frac{\partial^2}{\partial x_i \partial x_j} D_{ij}^{(2)}(\mathbf{x}, t) \right) p(\mathbf{x}, t) \quad . \quad (7.4)$$

Thereby, $D_i^{(1)}(\mathbf{x}, t)$ and $D_{ij}^{(2)}(\mathbf{x}, t)$ are denoted as drift and diffusion coefficients, respectively. The direct statistical definition of the drift and diffusion coefficients is given by (Risken, 1989)

$$D_i^{(1)}(\mathbf{x}, t) = \lim_{\tau \rightarrow 0} \frac{1}{\tau} \langle x_i(t + \tau) - x_i \rangle_{\mathbf{x}(t)=\mathbf{x}} \quad , \quad (7.5a)$$

$$D_{ij}^{(2)}(\mathbf{x}, t) = \lim_{\tau \rightarrow 0} \frac{1}{\tau} \langle (x_i(t + \tau) - x_i)(x_j(t + \tau) - x_j) \rangle_{\mathbf{x}(t)=\mathbf{x}} \quad , \quad (7.5b)$$

where $\langle \dots \rangle$ represents a suitable average. It has been shown that it is possible to determine $\mathbf{D}^{(1)}$ and $\mathbf{D}^{(2)}$ for stationary continuous Markovian processes with uncorrelated noise directly from the corresponding data by applying definition (7.5) (Friedrich and Peinke, 1997b; Siegert *et al.*, 1998), whereas the limit $\lim_{\tau \rightarrow 0}$ can be reached by interpolation. Using $\hat{\text{Ito}}$'s definition for stochastic integrals, it has been shown in Ref. (Risken, 1989) that the drift and diffusion coefficients $\mathbf{D}^{(1)}$ and $\mathbf{D}^{(2)}$ can be related to the matrix and vector valued coefficients \mathbf{g} and \mathbf{h} of the corresponding Langevin equation using the formulas

$$D_i^{(1)}(\mathbf{x}, t) = h_i(\mathbf{x}, t) \quad , \quad (7.6a)$$

$$D_{ij}^{(2)}(\mathbf{x}, t) = Q \sum_k g_{ik}(\mathbf{x}, t) g_{jk}(\mathbf{x}, t) \quad . \quad (7.6b)$$

It shall be noted that for a stationary process, $p(\mathbf{x}, t)$, and therewith $\mathbf{D}^{(i)}$, $i = 1, 2$, are independent of the time t . If one has already obtained $D_{ij}^{(2)}$ according to expression (7.5), and subsequently aims at recovering g_{ij} to investigate the corresponding Langevin equation, one is disposed to calculate g_{ij} from $\mathbf{D}^{(2)} = Q\mathbf{g}\mathbf{g}^\dagger$ by means of Cholesky decomposition (Zeidler, 1996). Basically the Cholesky decomposition states that a symmetric positive-definite matrix can be decomposed into a lower triangular matrix and the transpose of the lower triangular matrix, indexed by \dagger . The numerical implementation is straightforward and can be achieved by applying standard algorithms. When the drift and diffusion coefficients $\mathbf{D}^{(1)}$ and $\mathbf{D}^{(2)}$ have been computed from a long time series generated by the dynamical system utilizing equation (7.5), one can easily recover the corresponding Langevin coefficients \mathbf{h} and \mathbf{g} via relation (7.6), so that the nature of the intrinsic stochastic process is completely determined.

7.2 Numerical Results of the Stochastic Model

The present section is devoted to the presentation of numerical results concerning the modeling of certain degrees of freedom associated with the ABCDE system by a suitable stochastic process. The scientific objective is to find a stochastic description of the \mathbf{b} variables by dividing the underlying dynamics into a deterministic part, governing the evolution of macroscopic variables, and a stochastic component, representing fluctuations of microscopic degrees of freedom. The algorithm employed is based on the idea to impose a regular $d \times d$ grid onto the b_1 - b_2 plane to divide the area of the phase space which is visited by the projected system trajectory into individual bins. The stochastic treatment rests upon the principle to determine a stationary Langevin equation of the form (7.3) for each of the bins containing enough data points to allow a stochastic interpretation. Hence, the deterministic and stochastic component \mathbf{h} and \mathbf{g} in (7.3) are not explicitly time dependent. At an arbitrary time t_i , when the trajectory visits a certain point \mathbf{x} in phase space, the position at time $t_i + \Delta t$ is being determined by the deterministic component $\mathbf{h}(\mathbf{x})$, as well as the stochastic part $\mathbf{g}(\mathbf{x}) \cdot \mathbf{\Gamma}(t_i)$, according to equation (7.3). In this manner, a whole trajectory can be determined to set up the stochastic process. The size of the grid spacing Δd should be chosen with all due caution since too small sections would not contain sufficiently many data points, while too large grid spacing results in declined resolution

and accuracy. The grid size that has been chosen for our investigations is being reasoned later in this section when we investigate autocorrelation functions of relevant quantities.

Two general attempts have been followed to construct a suitable description in terms of a Langevin equation. In the first case, the variables b_1 and b_2 have been directly consulted to model the deterministic dynamics, whereas in the second case, the dynamics of the transformed hyperbolic variables r and ϕ have been stochastically reproduced. In conclusion, it has become evident that the stochastic modeling of the variables r and ϕ is more favorable due to miscellaneous reasons. One argument emerges from consideration of a projection of the trajectory on either the b_1 - b_2 plane or the r - ϕ subspace as illustrated in figure 7.1. Thereby, we have used the regular parameter values together with $\epsilon = 4.5$. The grid in figure 7.1 represents just a schematic representation and would be increasingly fine structured in an actual simulation. However, evoked by the geometric structure of the attractor, the hyperbolic coordinates allow a more accurate treatment, especially in an area close to the origin which is visited frequently by the trajectory. For the following results of numerical simulations, a Cartesian grid has been chosen to increase efficiency. In a later section of this chapter, it is necessary to refer to particular bins to present corresponding numerical results. Therefore, index numbers (i, j) , whereas i denotes the column and j the row number, satisfying $1 \leq i \leq d$ and $-d/2 \leq j \leq d/2$, are being assigned to all individual bins.

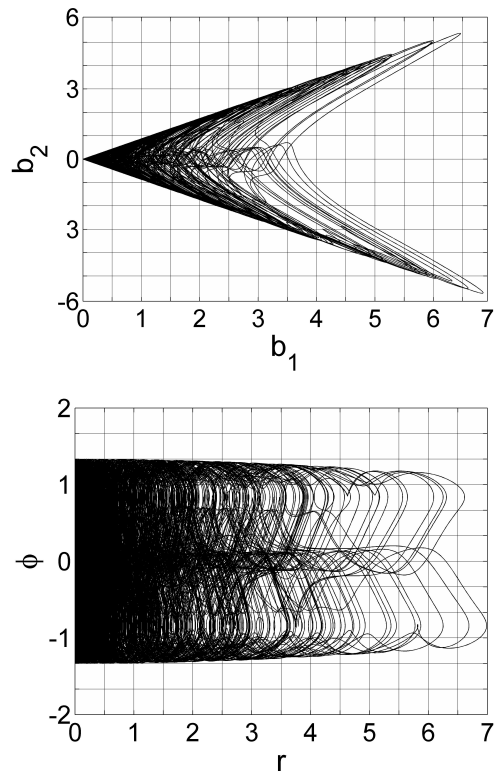


Figure 7.1: Superimposed grid and projection of trajectory onto b_1 - b_2 plane (upper diagram) as well as on r - ϕ subspace (lower diagram)

7.2.1 Determination of Drift Coefficients

The drift coefficients can be obtained directly from a sufficiently long time series of the corresponding variables by applying the statistical definition which has been given in equation (7.5a). When reconstructing the dynamics of the \mathbf{b} variables, we apparently encounter a 2-dimensional vector $\mathbf{D}^{(1)}$, containing two drift coefficients for each of the considered bins. Figure 7.2 shows a vector field representation of numerically computed drift coefficients $\mathbf{D}^{(1)}$, where a 60×60 Cartesian grid with a grid spacing of $\Delta d = 1/6$ has been employed. Furthermore, we have applied standard parameter values and $\epsilon = 4.5$ for the present calculation. The drift coefficients of the Fokker-Planck equation, which can be directly identified with the deterministic part of the corresponding Langevin equation, govern the fundamental dynamics of the sto-

chastic process. Figure 7.2 therefore gives information about the expected principal nature of the stochastic dynamics and furthermore recovers the basic structure of the projected attractor onto the b_1 - b_2 subspace. In turn, a similar diagram can be produced for the drift coefficients in the case of the hyperbolic coordinates r and ϕ . Figure 7.3 shows a vector field of drift coefficients $\mathbf{D}^{(1)}$ for every bin, while the same gridding has been employed. For the sake of clear presentability, the former configuration has also been used to compute the remaining diffusion matrix $\mathbf{D}^{(2)}$, which is being contemplated in the following paragraph. However, for consecutive computations concerning the final setup of a stochastic model, a 100×100 Cartesian grid with grid spacing $\Delta g = 7/100$ was superimposed onto the corresponding subspace.

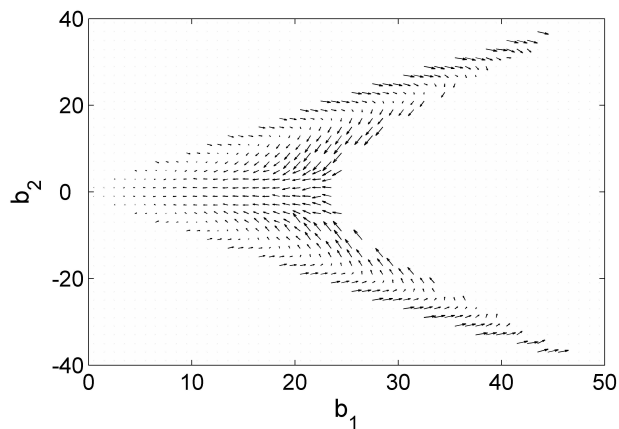


Figure 7.2: Vector field of drift coefficients in the b_1 - b_2 plane

7.2.2 Determination of Diffusion Coefficients

Even though all relevant subsequent calculations have been performed employing the hyperbolic coordinates r and ϕ , results concerning the composition of the diffusion matrix are being presented in terms of the quantities b_1 and b_2 for the sake of consistency and clearness.

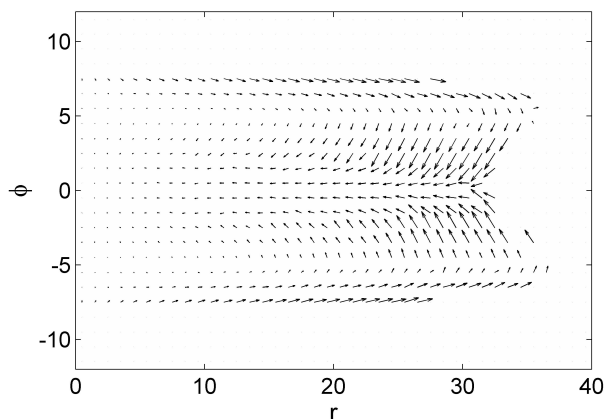


Figure 7.3: Vector field of drift coefficients in the r - ϕ plane

Because of the two-dimensional \mathbf{b} subsystem, a 2×2 diffusion matrix $\mathbf{D}^{(2)}$ emerges in the corresponding stochastic description by a Fokker-Planck equation of the form (7.4). Therefore, for the investigation of the diffusion coefficients it is tempting to examine eigenvectors and eigenvalues of the diffusion matrix $\mathbf{D}^{(2)}$ for each bin. The upper diagram in figure 7.4 monitors the eigenvectors of the diffusion matrices, located at the center of each segment that has been visited stochastically often by the system trajectory. The eigenvectors represent a linear combination of the variables which are biased by the uncorrelated random forces. Since $\mathbf{D}^{(2)}$ is a symmetric matrix, its eigenvectors are orthogonal, and the corresponding eigenvalues strictly real. In the lower part of figure 7.4, we report the eigenvalues of the symmetric diffusion matrices, evaluated by standard methods for every bin that has been visited sufficiently frequent by

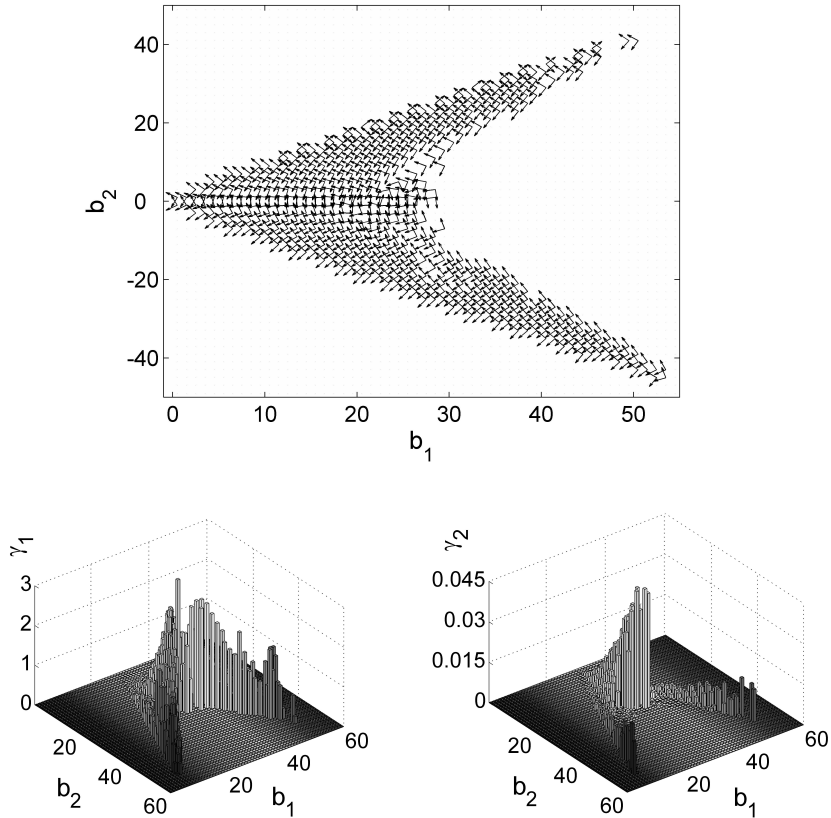


Figure 7.4: Vector field depicting eigenvectors (upper diagram), and bar diagrams showing eigenvalues (lower diagrams) of the diffusion matrices for each bin

the trajectory to allow a statistical interpretation. The significance of the consideration of characteristic roots for the diffusion matrix $\mathbf{D}^{(2)}$ is given by the fact that the eigenvalues determine the strength of independent fluctuating forces in the space of relevant variables (Kuhn *et al.*, 1991). Hence, we can conclude that fluctuations become extremely relevant in the vicinity of the b_1 axis close to the origin. The outcome, concerning the investigation of eigenvalues of the diffusion matrix, takes account of the dynamical property that transitions of the system from one leaf of the attractor with $b_2 > 0$ to the lower half-space determined by $b_2 < 0$, or vice versa, represent an extremely important feature of this chaotic system.

7.2.3 Discussion of Stochastic Force \mathbf{F}

The aim of the present section is to find an applicable stochastic description for the chaotic dynamics of the \mathbf{b} variables. However, it is not clear from the beginning that there exists a suitable description for the case under consideration. Focusing on the stochastic part of the Langevin equation (7.3), it has to be investigated whether the actually deterministic fluctuation can be treated by means of random forces. To this end, it is convenient to introduce a stochastic force \mathbf{F} , defined by the expression

$$\mathbf{F} = \mathbf{b}(t + \Delta t) - \mathbf{b}(t) - \Delta t \mathbf{D}^{(1)} \quad . \quad (7.7)$$

Comparing (7.7) with the Langevin equation (7.3), it becomes evident that \mathbf{F} represents the fluctuating part of the deterministic dynamics which shall be described by random Langevin forces. An essential criterion that indicates whether the ABCDE system is suitable for a stochastic description of the present form is the behavior of the *autocorrelation function* G of the stochastic force \mathbf{F} . The autocorrelation function is a measure for the correlation of a signal with a time-shifted version of itself. Let y_t denote the value of the process under investigation determined at time t , exhibiting the mean μ and variance σ^2 . In the stationary case, when the first and second moments are time invariant, the autocorrelation G is defined as (Gardiner, 2004; Kantz and Schreiber, 2000)

$$G(\tau) = \frac{E[(y_t - \mu)(y_{t+\tau} - \mu)]}{\sigma^2} \quad , \quad (7.8)$$

where τ denotes the lag, and $E(y_t)$ represents the expected value of the quantity y_t . Due to the normalization by σ^2 , the autocorrelation function satisfies the condition $-1 \leq G(\tau) \leq 1$.

Since we assume a δ -correlated noise process with vanishing mean (7.3b), it is essential that the autocorrelation function of \mathbf{F} decreases sufficiently fast. The significance of this becomes evident when taking the bin size into account. Long range autocorrelations of \mathbf{F} would imply the need for larger bin sizes, which would negatively affect the accuracy of calculations; employing too small bin sizes on the other hand, it becomes impossible to draw conclusions based on stochastic arguments. Only when the autocorrelation function decreases sufficiently fast and exhibits features of stochastic nature, a reconstruction of the dynamics by stationary Langevin equations, based on discretization of the b_1 - b_2 phase subspace, is expected to generate satisfactory results.

In order to highlight the advantages of choosing a description based on hyperbolic coordinates r and ϕ , rather than using the \mathbf{b} variables, the following results, which have been obtained utilizing hyperbolic coordinates, shall be compared with the graphs presented in appendix B. In the latter case, we have performed an analogous treatment based on the immediate variables \mathbf{b} . Figure 7.5 presents the one-dimensional autocorrelation functions G of the components F_r and F_ϕ as a function of the delay time τ . As can be seen clearly, the upper diagrams in figure 7.5 highlight a much more rapid decay of the autocorrelation function than shown in the corresponding figure B.1, where quasi periodic oscillations dominate over long periods of time. Moreover, when considering larger lags in time, figure B.1 reveals intermittency leading to significant correlations, while the functions plotted in figure 7.5 fluctuate closely around zero. In this regard, it might be interesting to note that the autocorrelation function of a periodic function is periodic itself with the very same period, while the autocorrelation of a continuous white noise signal exhibits a strong peak when the lag equals zero and vanishes for all other delay values. The investigation of the autocorrelation function of the stochastic force \mathbf{F} also allows a reasoning of the chosen bin size; due to the rapidly decaying autocorrelation functions, it is possible to choose an appropriate bin size, as declared in section 7.2.1, by striking a balance between the prerequisites for a stochastic interpretation and a satisfying spacial accuracy.

In the attempt to describe deterministic dynamical systems by appropriate stochastic model

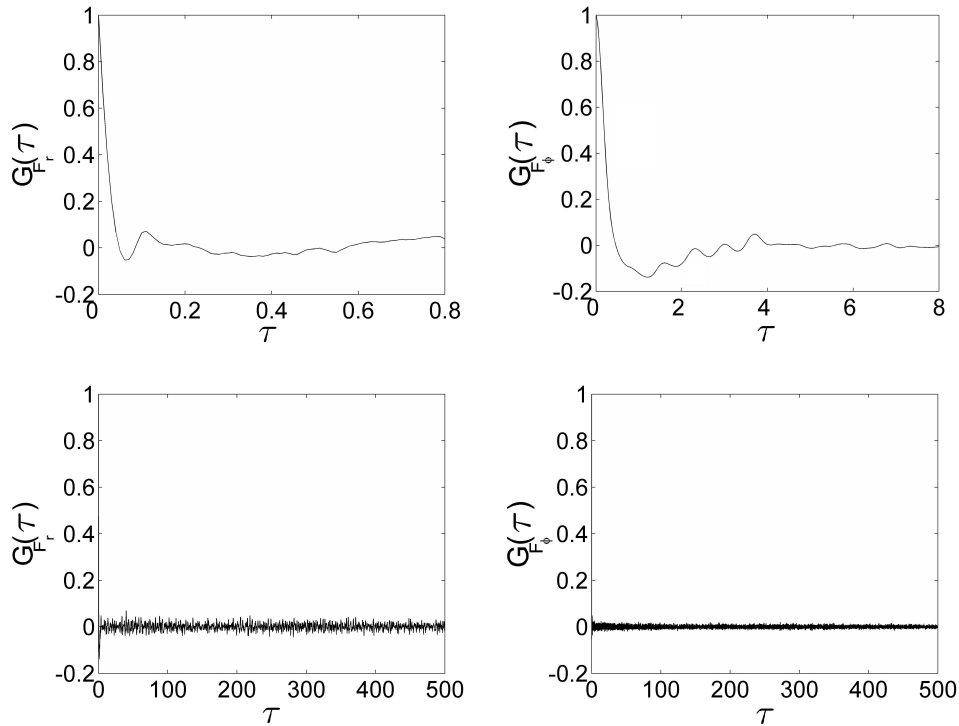


Figure 7.5: Autocorrelation functions of the components F_r (left column) and F_ϕ (right column) in dependence of lag τ for two different time scales

equations, it is crucial to investigate the suitability of the chosen random processes entering the final description. In the case under consideration, we assume that Γ_i in equation (7.3) symbolizes a δ -correlated Gaussian white noise process. To verify if this assumption holds true and is able to account for the characteristic features of the ABCDE system, it is tempting to survey estimates of the probability density functions, f_r , and f_ϕ , of the stochastic force \mathbf{F} for exemplary bins. Figure 7.6 presents probability density estimates f_r , as well as f_ϕ , of the corresponding forces F_r , and F_ϕ , evaluated at certain particular bins, as functions of r , and ϕ , respectively. The numeration of the bins is in accordance with the general notation introduced at the beginning of paragraph 7.2. As can be reasoned from the above diagram, even though the shape of the probability density estimates deviate partially from the shape of a normal distribution, one can expect satisfactory results assuming a Gaussian distributed white noise process Γ in equation (7.3). This argument is mainly based on the fact that we immediately observe the distribution of quantities related to the form $\mathbf{g} \cdot \mathbf{\Gamma}$. In the vicinity of the b_1 axis and close to the origin, fluctuations play a major role, while they become a minute detail in other regions of the b_1 - b_2 plane, as we have concluded from figure 7.4; deviations in the probability density function from Gaussian characteristics are recorded mainly in those regions of less importance. Moreover, the system trajectory visits the critical areas far less frequent compared to the bins, which give rise to satisfactory distributions of the stochastic force \mathbf{F} . In comparison to the above results, the computation of probability density functions obtained by immediately employing \mathbf{b} variables, namely f_{b_1} , and f_{b_2} , as displayed in appendix C, leads to poor results and implies that an

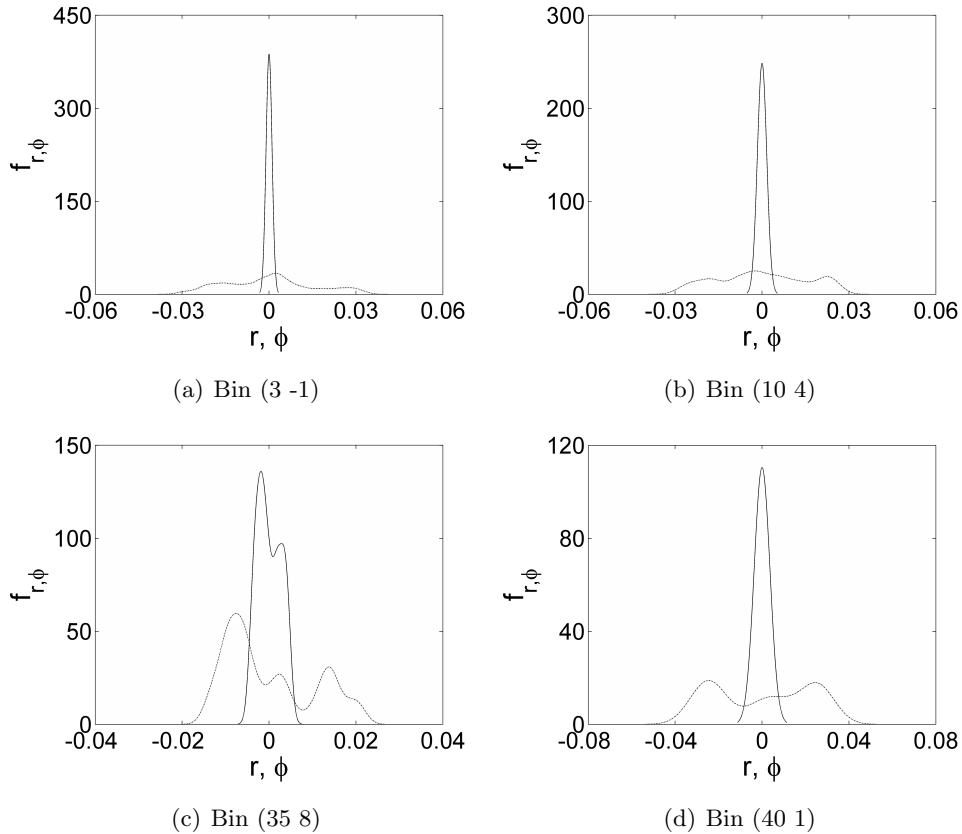


Figure 7.6: Probability density estimates of stochastic force \mathbf{F} for exemplary bins, denoted by f_r (—), f_ϕ (---)

appropriate stochastic description might not be found.

In conclusion, the outcome concerning our assessment of the stochastic force \mathbf{F} underpins the validity of the chosen ansatz. The question, aiming at a mathematically sound and explicit derivation of the optimal choice for the bin size, may serve as motivation for further investigation. Here, it might be crucial to examine the characteristic time scale, which is associated with the system's loss of memory, reflected in the exponentially decreasing autocorrelation function of the stochastic force \mathbf{F} . In a final step, the following section presents detailed results regarding the actual implementation of the stochastic reconstruction.

7.2.4 Reconstruction of Variable \mathbf{b} in Terms of Langevin Process

Having examined the conditions which form a prerequisite for the success of a reconstruction of the dynamics by a suitable stochastic process, the present section aims at discussing the actual implementation and final results of the Langevin approach. Combining the deterministic as well as random terms of the underlying dynamics, it is possible to generate typical stochastic trajectories modeling the process. These trajectories should possess very similar properties compared to the corresponding time series from which they have been generated. In particular, the phase space portraits should exhibit this similarity, and furthermore probability density estimates for the system variables should match qualitatively well. In order to reconstruct a

characteristic stochastic trajectory of the dynamical system, the Langevin equation (7.3) has to be integrated using a conventional Runge-Kutta routine. Figure 7.7 shows a projection of two different trajectories onto the b_1 - b_2 subspace. The original and reconstructed stochastic trajectories match qualitatively very well when comparing the above plot with the phase space diagrams presented in chapter 4. The general topology of the attractor has been recovered meticulously by the stochastic model. Moreover, characteristic features of the original attractor, such as the behavior for different control parameter values ϵ , or dynamical fluctuations in the vicinity of the b_1 axis, can be reproduced to an impressive extent by the stochastic model equations. In contrast, in appendix D we present a reconstructed stochastic trajectory which has been obtained using the \mathbf{b} , rather than hyperbolic coordinates. As can be seen clearly, the dynamics are not reproduced satisfactorily due to the disadvantages of the latter approach, as addressed above in the text.

In conclusion, the reconstructed phase space diagrams are, at least phenomenologically, in close agreement with the original trajectory projections. In order to gather ample evidence confirming our approach, it is tempting to compute probability density estimates of all relevant variables generated by either the original dynamical system or the reconstructed stochastic process. Above, we already qualitatively showed a good conformity of the reconstructed trajectory with the actual path in phase space. However, the following investigation aims at numerically proving the validity of the results in a more rigorous way. To this end, figure 7.8 shows plots of probability density estimates, h_ϕ , and h_r , for the hyperbolic coordinates ϕ , and r , obtained for a control parameter value of $\epsilon = 4.5$. Thereby, the dashed

lines represent the estimates for the original dynamics, while the solid lines denote the probability density estimates obtained from reconstructed time series that have been generated by the stochastic process. Both density estimates compare favorably and show the same specific features; while the function h_ϕ exhibits, as expected, symmetry, and takes on three local maxima, h_r recovers the basic form which has been foremost reported in Ref. (Friedrich and Haken, 1992), owing to the intermittent nature of the corresponding variable r close to the critical threshold.

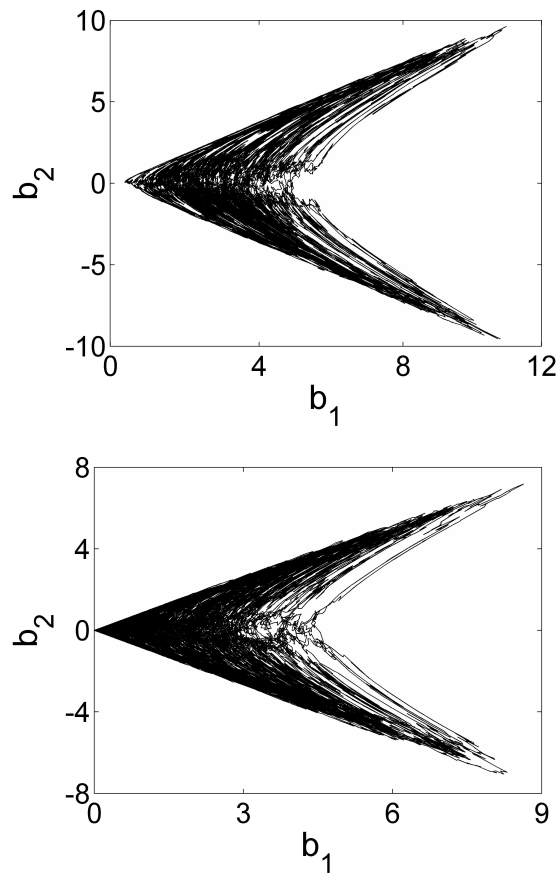


Figure 7.7: Stochastic reconstruction of the variables b_1 and b_2 for $\epsilon = 2.5$ (upper diagram) and $\epsilon = 4.5$ (lower diagram)

Figure 7.9 shows plots of the same quantities using corresponding notation, obtained for a control parameter value of $\epsilon = 2.5$. Thereby, we record three local maxima for the function h_ϕ , while the shape of the density distribution slightly changes compared to the previous calculation. Again, h_r recovers the behavior which has been reported in Ref. (Friedrich and Haken, 1992), reflecting the fluctuations of the corresponding variable r around a certain non-zero mean value. Considering both figures 7.8 and 7.9, the probability density functions obtained from the reconstructed trajectories, represented by the solid lines, lead to slightly asymmetric graphs in contrast to the functions computed from directly obtained data, denoted by the dashed lines. It is being assumed that a longer integration time of the stochastic differential equations would further diminish these deviations from the actual shape. Comparing the upper and left diagram in figures 7.8 and 7.9, respectively, with each other, the general shape persists when decreasing the control parameter, even though the system seems to sojourn in the vicinity of the b_1 axis more frequently.

As can be concluded from the results of our investigation of the probability density estimates and phase space reconstructions for the relevant degrees of freedom, the stochastic description is able to account very well for the characteristics of the underlying dynamical system. The suitability of the studied dynamical system for a stochastic description can be attributed to the separability of the two subspaces \mathbf{x} and \mathbf{b} composing the whole ABCDE system.

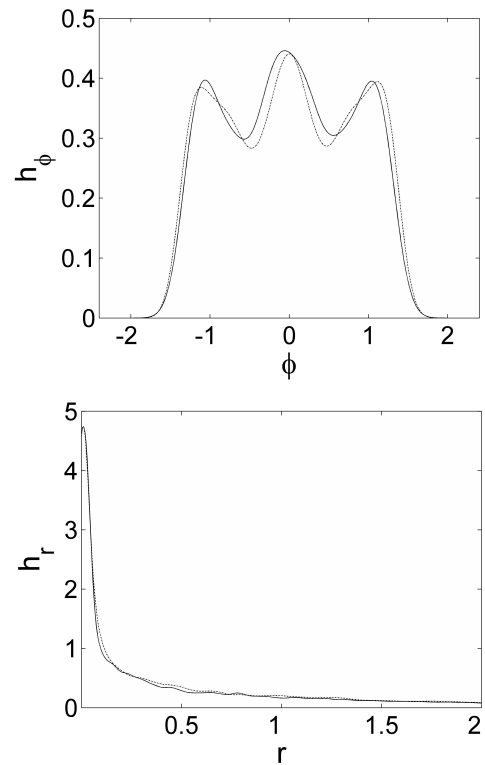


Figure 7.8: Probability density estimates of the quantities r and ϕ for the control parameter value $\epsilon = 4.5$. Estimates obtained from a stochastic reconstruction are denoted by solid lines (-), directly obtained probability densities by dashed lines (-.)

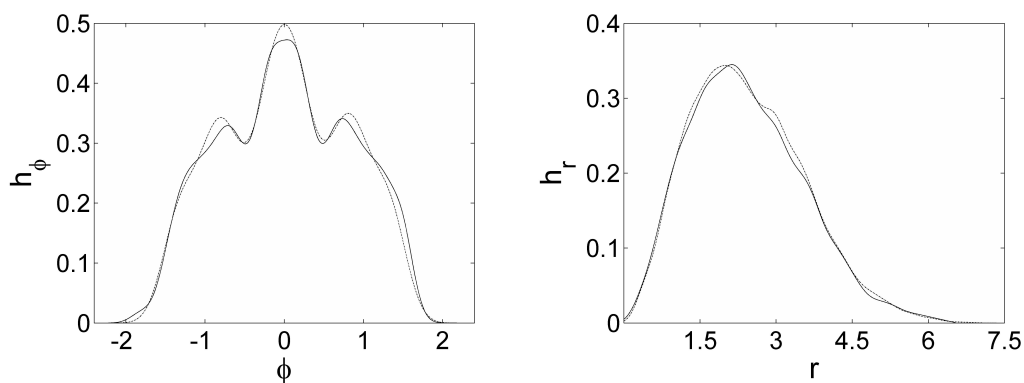


Figure 7.9: Probability density estimates of the quantities r and ϕ for $\epsilon = 2.5$. Estimates obtained from a stochastic reconstruction are denoted by solid lines (-), directly obtained probability densities by dashed lines (-.)

Chapter 8

Conclusion

As can be reasoned from the extent of persistent scientific activity in the fields of theoretical as well as experimental study of dynamo action, there can be no doubts about the need of a substantial understanding concerning the temporal evolution, and generating processes of astrophysical magnetic fields. The practical significance of solar and terrestrial magnetic fields to the past and future development of life on our planet is apparently given by the interrelated level of solar activity and the induced protection against cosmic radiation, respectively. The intermittency close to the threshold to dynamo action may be the key to an understanding of the observation of various minima of the sun's magnetic activity. Besides, geomagnetic excursions and polarity reversals of the earth's magnetic field might become comprehensible, formulating a description based on periods of intermittent magnetic behavior. In general, nonequilibrium phase transitions observed in natural systems are preeminent processes giving rise to extremely relevant phenomena such as spatio-temporal patterns and self-organization. Summing up, the results presented in this manuscript clarify the nature of the transition observed in the ABCDE model by considering various relevant characteristic properties of the underlying dynamical system. After having laid the theoretical foundation for a comprehensive general treatment of deterministic dynamical systems, we have introduced the specific magnetohydrodynamic model equations under investigation. In this context, we have highlighted relevant properties of the ABCDE model and the constituent Lorenz equations. In order to motivate our theoretical interest in the nature of the given transition, we have given a brief introduction into the history of laboratory experiments generating dynamo action. Special attention has been paid to underline recent experimental observations, which remarkably underscore our interest in the intermittent dynamo action revealed in the ABCDE system. Moreover, we have presented evidence that a nonequilibrium phase transition occurs for a critical control parameter value ϵ_c , by reproducing results which have foremost been contemplated in Ref. (Friedrich and Haken, 1992).

The study of further characteristics has led us to various novel results including the determination of stationary solutions, as well as a numerical, and, wherever applicable, analytical discussion of bifurcation routes by means of linear stability analysis. Furthermore, we have presented an extensive investigation of Lyapunov characteristic exponents for the chaotic system

under investigation. Therefore, we have introduced a related low-dimensional model system, and elucidated the anticipated behavior of the critical characteristic exponent in dependence of the control parameter. In addition, the spectrum of Lyapunov exponents has been determined for various control parameter values ϵ , employing ordinary parameter values to characterize the nature of the phase transition. Deviating from the general convention, we have also investigated the deterministic system for high Rayleigh numbers r , leading to the development of stable periodic solutions of the Lorenz subsystem. In this particular regime, we have observed hysteretic behavior, and correspondingly subcritical dynamo action. In addition, it has also been possible to apply Floquet's theory to model corresponding qualitative analytical solutions for the \mathbf{b} variables, using techniques associated with periodic orbit analysis. In a further step, the contribution of periodic orbits to the observed instability up to fundamental period 4, utilizing original parameter values, has been studied. We have been able to show that the basic cycle does not contribute to the observed bifurcation, while other periodic orbits induce the transition with increasing proportion according to their ascending periodicity. In analogy to the previous treatment of high Rayleigh numbers, it has also proved possible to construct explicit analytical solutions describing the temporal evolution of the \mathbf{b} variables. In a final analysis, we have revealed that, close to the critical threshold of the control parameter ϵ indicating the onset of dynamo action, local fluctuations of the corresponding Lyapunov exponent characterize the intermittent temporal behavior of the magnetic field modes.

In the subsequent study, aiming at a stochastic treatment of the nonequilibrium phase transition, we have outlined how to obtain drift and diffusion coefficients from various realizations of the underlying deterministic process. It shall be mentioned that, owing to the reasons outlined in the respective section, it is more suitable to set up the stochastic simulation using hyperbolic coordinates. Proceeding by consulting b_1 and b_2 directly does not lead to satisfactory results, as has been discussed in the relevant paragraphs. Vector field diagrams of drift coefficients $\mathbf{D}^{(1)}$ have depicted the main deterministic drivers governing the temporal evolution of the magnetic \mathbf{b} variables. The diffusion coefficients $\mathbf{D}^{(2)}$, expressed by 2×2 symmetric matrices, have been calculated and investigated with respect to their eigenvalues and eigenvectors. The results have provided important information about the underlying dynamical process and enabled us to specify a promising stochastic description. To this end, the stochastic force \mathbf{F} has been introduced, representing the quantity which describes the fluctuating part of the chaotic process, chosen to be described by means of stochastic random forces. Resulting from the assessment of quantities such as the autocorrelation function and probability density estimates of \mathbf{F} , we have been able to set up a suitable stochastic description of the actual deterministic dynamics employing a Langevin approach. In a final step, we have performed some exemplary simulations of the \mathbf{b} variables by dint of the chosen stochastic description for different parameter values. The obtained phase space portraits, as well as the corresponding probability density estimates for the relevant degrees of freedom, showed very good agreement with the respective values generated by direct integration of the nonlinear dynamical system explored in this work.

Future investigations could broach the issue of systematically performing a parameter study

of the ABCDE model. We believe that there exist additional parameter regimes that lead to significant complex dynamical behavior. In chapter 5, we have, for instance, indicated that we expect to observe qualitative changes for a control parameter value in the vicinity of $\epsilon = \alpha^2 b(R-1)/(a_1 a_2)$. Furthermore, opportunity for advanced investigation might be given by an extended contemplation of the stochastic properties of the underlying dynamics or the corresponding stochastic model system. Thereby, future prospects could involve an examination of the mean first passage time of the dynamical system and its stochastic modeling, as has been carried out in the analysis of stochastic and deterministic time series reported in Ref. (Gradišek *et al.*, 2000). With respect to the present objective, an application might arise when addressing the problem of determining the transition time which the system needs to go from one maximum of the distribution function h_ϕ in figure 7.8 to another one. For an introduction into the first passage time formalism, and an extensive application of the framework to a class of non-Markovian processes, we refer the reader to Ref. (Dienst and Friedrich, 2007). Moreover, we raise the open question regarding a firm mathematical treatment concerning the optimal bin size employed; in this context, a fruitful attempt might involve the study of characteristic decaying times of the stochastic force's autocorrelation function (see figure 7.5).

To emphasize the significance of our results, we would like to mention that the intermittency close to the critical control parameter might be the key explanation of magnetic field reversals, as has been concluded from the outcome of recent laboratory experiments (Nornberg *et al.*, 2006). In contrast to related numerical investigations of dynamo action which are based on the basic magnetohydrodynamic equations, such as those reported in Ref. (Ponty *et al.*, 2005; Sweet *et al.*, 2001; Christensen and Glatzmaier, 1999), our observations are more likely to disclose basic properties and mechanisms leading to the generation of dynamo action. Features such as magnetic intermittency and field excursions can be studied directly as a consequence of the enhanced and immediate mathematical accessibility. In comparison to the recent related work presented in Ref. (Zhou *et al.*, 2007), we have treated a similar, but more complex model system since we do not neglect the back coupling of the additional degrees of freedom on the Lorenz subspace; a feature which is essential for the observed complex dynamics and resulting in self-sustained dynamo action.

There remains the question whether our results are directly reproducible via experimental investigations, owing to the system's geometry and idealized design. However, even though the ABCDE system embodies a low-dimensional model and therefore represents a simplification of the governing fundamental hydromagnetic equations, we believe that our results regarding the general nature and onset of dynamo action can lead to a more profound understanding of the involved processes. In particular, it is highly convincing that theoretical investigations and various dynamo experiments, especially the one carried out in Lyon (Berhanu *et al.*, 2007; Monchaux *et al.*, 2006), have disclosed the same features that we have revealed when studying the ABCDE model, such as intermittency close to the onset of dynamo action, shifts of the critical threshold associated with the level of turbulence, and hysteresis of relevant order parameter.

Bibliography

- Argyris, J., Faust, G., and Haase, M. (1994). *Die Erforschung des Chaos*. Vieweg, Wiesbaden.
- Benettin, G., Galgani, L., Giorgilli, A., and Strelcyn, J. (1980). Lyapunov Characteristic Exponents for Smooth Dynamical Systems and for Hamiltonian Systems: A Method for Computing All of Them. part 2: Numerical Application. *Meccanica*, **15**, 21–30.
- Berhanu, M., Monchaux, R., Bourgoïn, M., Odier, P., Pinton, J.-F., Volk, R., Fauve, S., Mor-dant, N., Pétrélis, F., Chiffaudel, A., Daviaud, F., Dubrulle, B., Marié, L., and Ravelet, F. (2007). Magnetic Field Reversals in an Experimental Turbulent Dynamo. *Eur. Phys. Lett.*, **77**, 59001.
- Bittanti, S. (1991). *The Riccati Equation*. Springer – Verlag, Berlin.
- Bogue, S. and Merrill, R. (1992). The Character of the Field During Geomagnetic Reversals. *Annu. Rev. Earth Planet. Sci.*, **20**, 181–219.
- Chandrasekhar, S. (1981). *Hydrodynamic and Hydromagnetic Stability*. Dover Publ., New York.
- Christensen, U. and Glatzmaier, P. O. G. (1999). Numerical Modelling of the Geodynamo: A Systematic Parameter Study. *Geophys. J. Int.*, **138**, 393–409.
- Dienst, A. and Friedrich, R. (2007). Mean First Passage Time for a Class of Non-Markovian Processes. *Chaos*, **17**, 033104.
- Eckhardt, B. and Ott, G. (1994). Periodic Orbit Analysis of the Lorenz Attractor. *Z. Phys. B*, **93**, 259–266.
- Eddy, J. (1977). Climate and the Changing Sun. *Climatic Change*, **1**, 173–190.
- Franceschini, V., Giberti, C., and Zheng, Z. (1992). Characterization of the Lorenz Attractor by Unstable Periodic Orbits. *Nonlinearity*, **6**, 251–258.
- Frank, T. (2005). *Nonlinear Fokker-Planck Equations*. Springer – Verlag, Berlin.
- Friedrich, R. and Haken, H. (1992). Nonequilibrium Phase Transition in a System with Chaotic Dynamics. *Phys. Lett. A.*, **164**, 299–304.

- Friedrich, R. and Peinke, J. (1997a). Description of a Turbulent Cascade by a Fokker-Planck Equation. *Phys. Rev. Lett.*, **78**, 863–866.
- Friedrich, R. and Peinke, J. (1997b). Statistical Properties of a Turbulent Cascade. *Physica D*, **102**, 147–155.
- Friedrich, R., Peinke, J., and Renner, C. (2000). How to Quantify Deterministic and Random Influence on the Statistics of the Foreign Exchange Market. *Phys. Rev. Lett.*, **84**, 5224–5227.
- Frøyland, J. and Alfsen, K. (1984). Lyapunov Exponent Spectra for the Lorenz model. *Phys. Rev. A*, **29**, 2928–2931.
- Gailitis, A., Lielausis, O., Platacis, E., Dement'ev, S., Cifersons, A., Gerbeth, G., Gundrum, T., Stefani, F., Christen, M., Hänel, H., and Will, G. (2000). Detection of a Flow Induced Magnetic Field Eigenmode in the Riga Dynamo Facility. *Phys. Rev. Lett.*, **84**, 4365–4368.
- Gardiner, C. (2004). *Handbook of Stochastic Methods*. Springer – Verlag, Berlin.
- Gradišek, J., Siegert, S., Friedrich, R., and Grabec, I. (2000). Analysis of Time Series from Stochastic Processes. *Phys. Rev. E*, **62**, 3146–3155.
- Hahn, W. (1967). *Stability of Motion*. Springer – Verlag, New York.
- Haken, H. (1983). At Least One Lyapunov Exponent Vanishes if the Trajectory of an Attractor Does Not Contain a Fixed Point. *Phys. Lett. A*, **94**, 71–72.
- Haken, H. (2004). *Synergetics - Introduction and Advanced Topics*. Springer – Verlag, New York.
- Hartmann, P. (1982). *Ordinary Differential Equations*. Birkhäuser, Boston.
- Hénon, M. (1982). On the Numerical Calculation of Poincaré Maps. *Physica D*, **5**, 412–414.
- Horsthemke, W. and Lefever, R. (1984). *Noise-Induced Transitions*. Springer – Verlag, Berlin.
- Kamke, E. (1967). *Differentialgleichungen-Lösungsmethoden und Lösungen*. Akademische Verlagsgesellschaft Geest & Portig K.-G., New York.
- Kantz, H. and Schreiber, T. (2000). *Nonlinear Time Series Analysis*. Cambridge University Press, Cambridge.
- Kennett, R. (1976). A Model for Magnetohydrodynamic Convection Relevant to the Solar Dynamo Problem. *Stud. Appl. Math.*, **55**, 65–81.
- Kuhn, T., Reggiani, L., and Varani, L. (1991). Coupled Langevin Equation Analysis of Hot-Carrier Transport in Semiconductors. *Phys. Rev. B*, **45**, 1903–1906.
- Letellier, C., Dutertre, P., and Gouesbet, G. (1994). Characterization of the Lorenz System, Taking into Account the Equivariance of the Vector Field. *Phys. Rev. E*, **49**, 3492–3495.

- Lorenz, E. (1963). Deterministic Nonperiodic Flow. *J. Atmos. Sci.*, **20**, 130–141.
- Lowes, F. and Wilkinson, I. (1963). Geomagnetic Dynamo: A Laboratory Model. *Nature*, **198**, 1158–1160.
- Lowes, F. and Wilkinson, I. (1968). Geomagnetic Dynamo: An Improved Laboratory Model. *Nature*, **219**, 717–718.
- Majda, A., Timofeyev, I., and Vanden-Eijnden, E. (2006). Stochastic Models for Selected Slow Variables in Large Deterministic Systems. *Nonlinearity*, **19**, 769.
- Monchaux, R., Berhanu, M., Bourgoin, M., Moulin, M., Odier, P., Pinton, J.-F., Volk, R., Fauve, S., Mordant, N., Pétrélis, F., Chiffaudel, A., Daviaud, F., Dubrulle, B., Gasquet, C., Marié, L., and Ravelet, F. (2006). Generation of a Magnetic Field by Dynamo Action in a Turbulent Flow of Liquid Sodium. *Phys. Rev. Lett.*, **98**, 044502.
- Nornberg, M., Spence, E., Kendrick, R., Jacobsen, C., and Forest, C. (2006). Intermittent Magnetic Field Excitation by a Turbulent Flow of Liquid Sodium. *Phys. Rev. Lett.*, **97**, 044503.
- Oseledec, V. (1968). A Multiplicative Ergodic Theorem. Ljapunov Characteristic Numbers for Dynamical Systems. *Trans. Moscow Math. Soc.*, **19**, 197–231.
- Parker, T. and Chua, L. (1989). *Practical Numerical Algorithms for Chaotic Systems*. Springer – Verlag, New York.
- Pesin, Y. (1977). Characteristic Lyapunov Exponents and Smooth Ergodic Theory. *Russian Math. Surveys*, **32**, 55–114.
- Platt, N., Spiegel, E., and Tresser, C. (1992). On-Off Intermittency: A Mechanism for Bursting. *Phys. Rev. Lett.*, **70**, 279–282.
- Ponty, Y., Mininni, P., Montgomery, D., Pinton, J., Politano, H., and Pouquet, A. (2005). Numerical Study of Dynamo Action at Low Magnetic Prandtl Numbers. *Phys. Rev. Lett.*, **94**, 164502.
- Ponty, Y., Laval, J., Dubrulle, B., Daviaud, F., and Pinton, J. (2007). Subcritical Dynamo Bifurcation in the Taylor Green Flow. *arXiv:0707.2498v2 [physics.flu-dyn]*.
- Ramasubramanian, K. and Sriram, M. (2000). A Comparative Study of Computation of Lyapunov Spectra with Different Algorithms. *Physica D*, **139**, 72–86.
- Reid, W. (1972). *Riccati Differential Equation*. Academic Press, Inc., New York.
- Risken, H. (1989). *The Fokker-Planck Equation*. Springer – Verlag, Berlin.
- Sandri, M. (1996). Numerical Calculation of Lyapunov Exponents. *The Mathematica Journal*, **6**, 78–84.

- Siegert, S., Friedrich, R., and Peinke, J. (1998). Analysis of Data Sets of Stochastic Systems. *Phys. Lett. A*, **243**, 275–280.
- Sparrow, C. (1982). *The Lorenz Equations: Bifurcations, Chaos and Strange Attractors*. Springer – Verlag, New York.
- Stemler, T., Werner, J., H.Benner, and Just, W. (2007). Stochastic Modeling of Experimental Chaotic Time Series. *Phys. Rev. Lett.*, **98**, 044102.
- Stieglitz, R. and Müller, U. (2001). Experimental Demonstration of a Homogeneous Two-Scale Dynamo. *Phys. Fluids*, **13**, 561–564.
- Sweet, D., Ott, E., and and D.P. Lathrop, T. A. J. (2001). Blowout Bifurcation and the Onset of Magnetic Dynamo Action. *Phys. of Plas.*, **8**, 1944–1952.
- Wolf, A., Swift, J., Swinney, H., and Vastano, J. (1984). Determining Lyapunov Exponents from a Time Series. *Physica D*, **16**, 285–317.
- Zeidler, E. (1996). *Teubner – Taschenbuch der Mathematik*. B.G. Teubner Verlagsgesellschaft, Leipzig.
- Zhou, Q., Chen, Z., and Yuan, Z. (2007). On-Off Intermittency in Continuum Systems Driven by Lorenz Systems. *Physica A*, **383**, 276–290.
- Zwillinger, D. (1989). *Handbook of Differential Equations*. Academic Press, Inc., San Diego.

Appendix A

Description of Hénon Trick

Consider the five dimensional system $\mathbf{X} = (\mathbf{b}_1, \mathbf{b}_2, \mathbf{x}, \mathbf{y}, \mathbf{z})$ of differential equations given in expression (2.2) as an example of a more generalized system of ordinary differential equations which can be treated in terms of Henon's approach. Thereby, an application of the Henon method in case of the ABCDE model can be described as follows. An estimate for the period of an oscillatory solution can be obtained by determining successive intersection of the system trajectory with a previously defined Poincaré surface of section Σ , which is usually chosen to be a $(n - 1)$ -dimensional subset of the n -dimensional phase space. Due to the geometric structure of the Lorenz attractor, it is tempting to define the surface of section by $z - r + 1 = 0$ (in the pure Lorenz system, the plane $z = r - 1$ contains the two symmetric unstable fixed points and is transversal to the flow). The difficulty is given by the fact that the relevant quantity $z = z(t)$ is a dependent variable and therefore its variation over an integration step cannot be concluded in advance. To overcome this problem, Henon proposed to invert the one particular equation defining the variable z , and divide the whole set of equations determining \mathbf{X} , excluding the inverted equation for z , by the dependent variable z . By rearranging the system of equations in this form, z becomes an independent variable while t becomes dependent. Now, the rearranged set of equations reads

$$\begin{aligned}x' &= \sigma(-x + y) - b_1 b_2 / (-bz + xy) \\y' &= -y + (r - z)x / (-bz + xy) \\t' &= 1 / (-bz + xy) \\b_1' &= -\epsilon a_1 b_1 + \alpha x b_2 / (-bz + xy) \\b_2' &= -\epsilon a_2 b_2 + \alpha x b_1 / (-bz + xy) \quad ,\end{aligned}\tag{A.1}$$

whereas the prime $'$ denotes the derivative d/dz with respect to the independent variable z .

The practical implementation of the algorithm then demands to numerically integrate the system until the quantity $S = z - r + 1$ changes sign. Subsequently, using the last computed value as initial condition, one has to integrate the newly obtained differential equations (A.1) for one step, using the step size $\Delta z = -S$. This procedure yields to an extremely accurate integration directly into the Poincaré surface of section.

Appendix B

Autocorrelation Functions

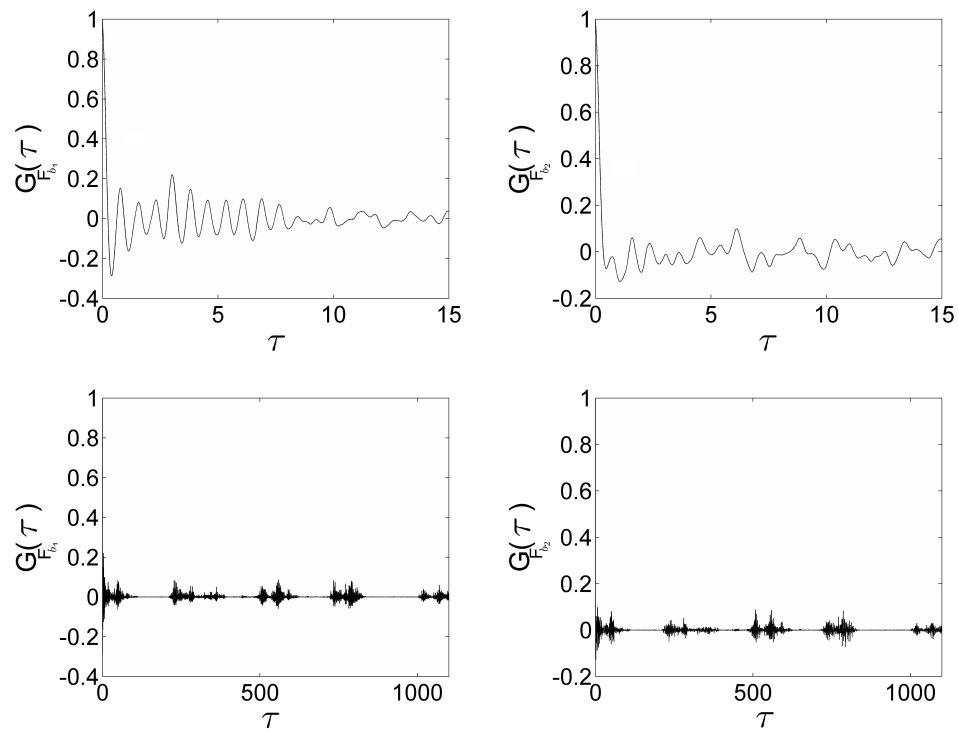


Figure B.1: Autocorrelation functions of the components F_{b_1} (left column) and F_{b_2} (right column) in dependence of the lag τ for two different time scales. The autocorrelation functions decrease slowly and show almost oscillating behavior. On a larger time scale, intermittent bursts can be identified

Appendix C

Probability Density Estimates

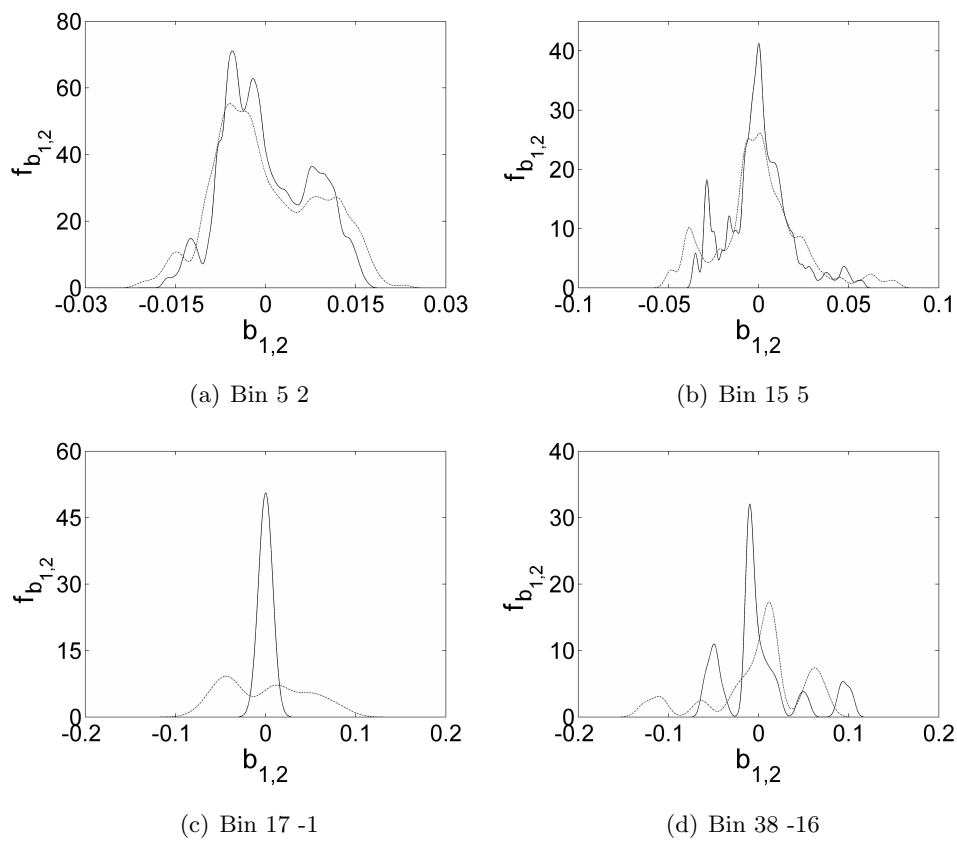


Figure C.1: Probability density estimates of the stochastic force \mathbf{F} for exemplary bins, denoted by f_{b_1} (—) and f_{b_2} (- -). The estimates stem from an investigation of the stochastic force extracted from a time series based on a direct simulation of b_1 and b_2 . Remarkable is the (in comparison to figure 7.6) dramatically deviating shape of the distribution functions, limiting the success of a description in terms of a Gaussian white noise process

Appendix D

Stochastic Reconstructions

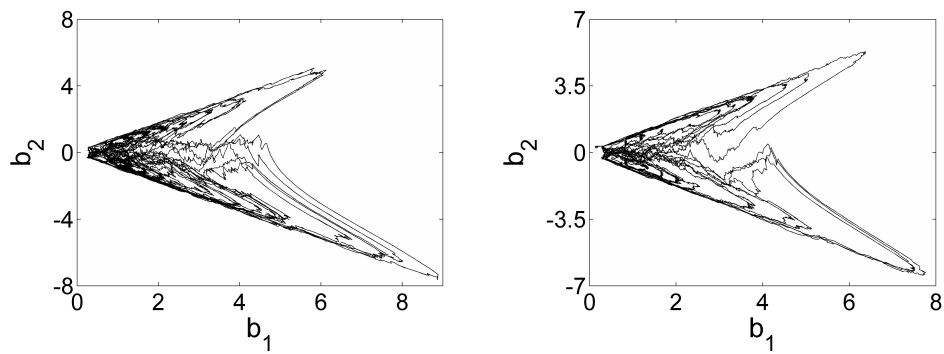


Figure D.1: Two realizations of a stochastic reconstruction of the variables b_1 and b_2 employing $\epsilon = 4.5$. The results were achieved by directly modeling the degrees of freedom b_1 and b_2 by a suitable Langevin process. Comparing the stochastic trajectories above with the results presented in figure 7.7, the major drawbacks of this alternative treatment become apparent